THE EFFECTS OF PULSED CHARGING ON LITHIUM ION BATTERIES

A Thesis
Presented to
The Academic Faculty

by

Daniel William Gaddes

In Partial Fulfillment
of the Requirements for the Degree
Masters of Science in the
George W Woodruff School of Mechanical Engineering

Georgia Institute of Technology
December 2016

THE EFFECTS OF PULSED CHARGING ON LITHIUM ION BATTERIES

Approved by:

Professor Yogendra Joshi, Advisor
George W Woodruff School of
Mechanical Engineering
Georgia Institute of Technology

Professor Cristina Tarin
Institute for System Dynamics
University of Stuttgart

Professor Paul Kohl
School of Chemical and Biomolecular
Engineering
Georgia Institute of Technology

Professor Oliver Sawodny
Institute for System Dynamics
University of Stuttgart

Professor Seung Lee
George W Woodruff School of
Mechanical Engineering
Georgia Institute of Technology

Date Approved: 4 August 2016

To my parents,

for your love, support, and encouragement.

ACKNOWLEDGEMENTS

I want to thank Dr. Oliver Sawodny of the University of Stuttgart and Dr. Paul Neitzel of the Georgia Institute of Technology for developing and accepting me into this joint masters program. By taking part in this, I have been given incredible opportunities and experiences at two great institutions of science.

I also want to thank my advisors at Georgia Tech, Dr. Yogendra Joshi and Dr. Paul Kohl, who took me into their labs and provided a wonderful environment for my year at Georgia Tech and who have continued to provide assistance after I left to complete my masters at the University of Stuttgart.

I would like to thank my supervisor at Bosch, Dr. Andreas Letsch, for taking me on and advising me on my work. Additionally, I want to express my gratitude to Dr. Volker Doege and Dipl.-Ing Raphael Wegmann, who aided me in completing the experiments while at Bosch and answering any questions I had on lithium ion batteries.

A special thanks to my advisor at the University of Stuttgart, Dipl.-Ing Conrad Sagert, and to Dipl.-Ing Frank Bender and M.Sc. Florian Morlock who have aided me in the completion of this program and in my transition to working and studying in Germany.

I would also like to express my appreciation to all the administrators and aids at both institutions who have helped me fulfill all the requirements necessary for this degree and for living in a Germany.

Finally, my deepest gratitude to my parents and brother, whose constant support and encouragement have allowed me to pursue my goals which have taken me across America and now overseas. I will always be grateful for the life you have given me.

TABLE OF CONTENTS

LIST OF TABLES

LIST OF FIGURES

LIST OF ABBREVIATIONS

0.1 Abbreviations

BMS	Battery Management System
$CCCV$	Constant current constant voltage charging
CC	Constant current charging
CV	Constant voltage charging
C-Rate	Normalized current to achieve charge in 1 hr
DE	Differential equation
EIS	Electrochemical Impedance Spectroscopy
I_{mean}	Mean current
I_{rms}	Root mean square current
OCV	Open Circuit Voltage
NCA	Lithium ion cathode chemistry $\text{LiNi}_{0.8}\text{Co}_{0.15}\text{Al}_{0.05}\text{O}_2$
PDE	Partial Differential Equation
SEI	Solid Electrolyte Interface
SEM	Scanning Electron Microscope
SoC	State of Charge
SoH	State of Health
SRC	Sinusoidal-ripple-current
XRD	X-ray Diffraction

0.2 Formula Signs

formula symbol	unit	description
Electrochemical Equations		
a_s	$^{1}/_{\mathrm{m}}$	Specific Interfacial Area
$c_{\mathrm{l},0}$	$^{\mathrm{mol}}/_{\mathrm{m}^3}$	Electrolyte initial concentration
c_0	$^{\mathrm{mol}}/_{\mathrm{m}^3}$	Initial concentration
$c_{\mathrm{s}_{\mathrm{max}},i}$	$^{\mathrm{mol}}/_{\mathrm{m}^3}$	Electrode particle maximum concentration
$c_{\mathrm{s/l},i}$	$^{\mathrm{mol}}/_{\mathrm{m}^3}$	Soild/liquid phase concentration
C_dl	$^{\mathrm{F}}/_{\mathrm{m}^2}$	Double Layer Capacity
D_e^eff	$^{\mathrm{m}^2}/_{\mathrm{s}}$	Electrolyte or Electrode Diffusion Coefficient
$i_{\mathrm{a},i}$	$^{\mathrm{A}}/_{\mathrm{m}^2}$	Current Density
i_dl	$^{\mathrm{A}}/_{\mathrm{m}^2}$	Double Layer Current
i_i	$^{\mathrm{A}}/_{\mathrm{m}^2}$	Current in Solid or Liquid phase
$i_{\mathrm{o},i}$	$^{\mathrm{A}}/_{\mathrm{m}^2}$	Exchange Current Density
j_i^Li	$^{\mathrm{A}}/_{\mathrm{m}^3}$	Transfer Current
k	$^{\mathrm{m}}/_{\mathrm{s}}$	Reaction Rate Coefficient
r_p	m	Reaction Rate Coefficient
t_+^0		Positive Ion Transference Number
$U_{i,\mathrm{ref}}$	V	Reference OCV
$\frac{\mathrm{d}\ln f}{\mathrm{d}\ln c_l}$		Mean Molar Activity Coefficient of Electrolyte

formula symbol	unit	description
Greek Letters		
α		Transfer Coefficient
ϵ		Volume fraction in solid, liquid, or filler phase
η	V	Overpotential
κ	$^{\mathrm{S}}/_{\mathrm{m}}$	Electrolyte Conductivity
ϕ	V	Potential in solid or electrolyte phase
σ	$^{\mathrm{S}}/_{\mathrm{m}}$	Electrode Conductivity
τ		Tortuosity
θ		SoC
Subscripts		
a		Anode
c		Cathode
e		Electrolyte
l		Liquid Electrolyte Phase
s		Solid Electrode Phase or Electrode
Thermodynamic Equation		
c_p	$^{\mathrm{kJ}}/_{\mathrm{kg\cdot K}}$	Specific Heat Capacity
G	J	Gibbs Free Energy
H	J	Enthalpy
h	$^{\mathrm{W}}/_{\mathrm{m}^2}$	Heat Transfer Coefficient
λ	$^{\mathrm{W}}/_{\mathrm{m\cdot K}}$	Thermal Conductivity
Q	$^{\mathrm{W}}/_{\mathrm{m}^3}$	Heat Generation
T	K	Temperature
$\frac{\partial U}{\partial T}$	$^{\mathrm{V}}/_{\mathrm{K}}$	Entropic Coefficient
ρ	$^{\mathrm{kg}}/_{\mathrm{m}^3}$	Density

SUMMARY

As part of this thesis, the effects of pulsed charging on lithium-ion batteries were investigated. Pulsed charging is an alternative method of charging batteries in which the charge current is interrupted by periods of no current and discharge. It has been suggested in past research that this method can both charge the cell faster and improve the lifetime of the cell through improving the internal kinetics. Based on past literature, influential parameters of the pulse protocol were identified. In this thesis these values were tested through both single charge and lifetime measurements to analyze the impact on charge rate and lifetime. Additionally, a mathematical model was developed to analyze the cell under pulsing for internal conditions which cannot be easily measured experimentally.

As part of the single charge testing, the pulse parameters that were determined to be most influential, the frequency of the pulses, the magnitude of the charging current, the root mean squared current value, the discharge capacity, and the ratio of discharge capacity to charge capacity, were analyzed. After this, two pulsing plans were selected to be tested to evaluate the impact on aging mechanisms and the lifetime of the cells. These plans were also analyzed within an electrochemical model, based on the Doyle, Fuller, Newman model to analyze any potential differences on the internal kinetics.

The results of these tests were compared to cells charged under the constant current constant voltage condition, using an equivalent mean current for all tests and one hour to charge the cell. The results indicated that pulses with constant currents and pulse duration do not produce positive effects, as all parameters are dominated by the higher current magnitude required by the pulse method to maintain an equivalent

mean current. Preliminary analysis of a different pulsing plan, in which the current begins high but decreases as the cell charges does result in a greater capacity before reaching the upper voltage limit, as well as a greater capacity within one hour, and is a potential area for further research.

CHAPTER I

INTRODUCTION

Lithium-ion batteries are being increasingly used in industry because they have a higher energy density and power than other secondary cells. This translates to smaller and lighter batteries for the user which is important for portable applications. They are already used in many electronic devices such as computers and cell phones, as well as many power tools, but they are now also increasingly being used in hybrid and fully electric vehicles. Telsa Motors' vehicles, the Nissan Leaf, and the BMW i3 are a few examples of fully electric vehicles which rely on this technology. However, further implementation has been limited due to concerns over safety, high cost, and the time required to recharge a cell. Safety concerns arise primarily from thermal runaway, a process in which elevated temperatures in the cell trigger heat-generating reactions, and potentially triggering a positive feedback reaction in which the cell temperature raises uncontrollably [4]. Thermal affects not only cause safety concerns, but can also increase the rate of cell degradation from both high and low temperature operation. Capacity fade, a process in which the lithium ions transfer from the active phase to the inactive phase, becoming unrecoverable, is the main cost issue. For the Nissan Leaf, the current battery warranty for the United States is 96 months or 100,000 miles [30] and the cost of a replacement battery pack is estimated at about 5000 US dollars, which would be a considerable reinvestment cost in an eight year old vehicle. It is important when developing a charging method to consider causes of this aging and attempt to minimize their impact. The rate of capacity fade is enhanced mostly from allowing high or low cell temperatures, but also other factors such as charge rate, ratio of charge to discharge, discharge rate, and the depth of discharge [38].

The issue of charging time also concerns many potential users; to refill an internal combustion vehicle will take only a few minutes, while a full recharge of a battery can be a matter of hours. Rapid charging is possible, however, as previously stated, this is known to increase the rate of capacity fade in the battery. These limiting issues are expanded upon in a later chapter, but it is clear that developing a method of charging which increases the rate of charge and lowers the rate of aging and temperature rise is important for the greater implementation of battery technology.

Pulse charging, a method in which the charge current is periodically interrupted by rest and discharge pulses, has been proposed as a method that will improve both the time of charge and battery aging against the traditional constant current constant voltage technique, as it is suggested that pulsing will allow the cell reaction process to occur more efficiently and with less cell degradation. However, up to this point the effectiveness of pulse charging has been disputed in the literature and those methods that suggest it is effective do not often expand on how the pulsing parameters were selected, some stating it was through empirical experimentation [9]. The process of pulse charging and constant current constant voltage charge are expanded upon in chapter 2. Due to the time and expense of lifetime battery testing, a mathematical model which could give insight on the electrochemical process and heat generation during charging would be useful. Additionally, due to the limited data that can be measured during charging, a detailed model that could reproduce experimental results would expand on the information gathered from experimentation. A coupled electrochemical-thermal pseudo-2D model is used here based on the original electrochemical model proposed by Doyle et al. and the coupled electrochemical-thermal model proposed by Gu and Wang [14][16].

In this thesis the scientific background of lithium-ion batteries is broadly explained and the work completed in understanding the impact of pulse charging through experimental and mathematical modeling are discussed. Influential parameters of the

pulse charging process were tested through single charge and lifetime testing to analyze their impact on aging and charge rate. Finally, the developed mathematical model is used to analyze these charging methods and the effect of pulse charging on internal cell kinetics.

CHAPTER II

LITHIUM-ION BATTERIES

2.1 The Basics

2.1.1 Lithium-ion Cell Operation

A lithium-ion battery consists of 5 main components: two metallic current collectors, a cathode electrode, an anode electrode, and a separator with an electrolyte. Depending on how the cell is operating, whether charging or discharging, the electrode that is the cathode or anode will change, however it is convention to refer to each electrode in terms of the role it plays during discharge. For a lithium-ion battery, the cathode will be some oxide of lithium, and the anode some carbon material. Each is a layered structure into which ions will diffuse as the cell charges or discharges. The topic of this thesis is pulsed charging, so the charging process will be described in detail.

During charge, a current is applied to the cell causing lithium ions to de-intercalate from the cathode into the electrolyte, travel through the electrolyte to the anode, and then intercalate into the anode. The purpose of the electrolyte is that it has a very low electric conductivity but allows for the transport of ions. As a results ions can transfer from one electrode to the other while the electrons travel through an exterior circuit via the current collectors from the cathode to the anode. This process is described in Fig. 1.

The purpose of the separator is to prevent a short circuit by creating a physical barrier between the two electrodes. In the completely discharged state, the cathode

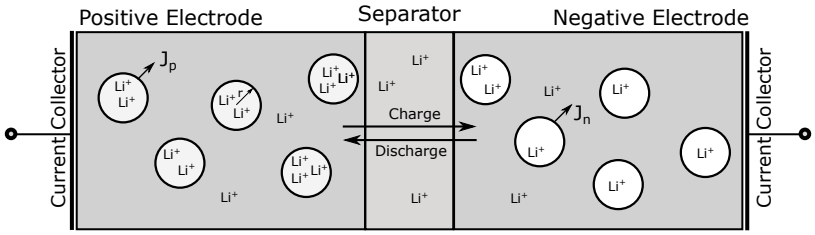

Figure 1: Dual insertion cell. Consists of three regions, the positive and negative electrodes and the separator. All three regions are permeated by the electrolyte, represented here in gray.

is full and the anode empty of lithium ions, as shown below for the $LiCoO_2$ chemistry cathode with graphite anode.

$$\mathrm{LiCoO_2} \underset{Discharge}{\overset{Charge}{\rightleftharpoons}} \mathrm{Li_{1-x}CoO_2} + x\mathrm{Li^+} + x\mathrm{e^-} \tag{1}$$

$$\mathrm{Li_{y-x}C_6} + x\mathrm{Li^+} + x\mathrm{e^-} \underset{Discharge}{\overset{Charge}{\rightleftharpoons}} \mathrm{Li}_y\mathrm{C_6} \tag{2}$$

As can be seen, the cathode is the source of lithium ions and defines the capacity of the cell. The important parameters of the electrode which affect cell performance are particle size distribution, particles shape, specific surface area, and tap density, however the specific roles these parameters play will be described in greater detail when the mathematical model is discussed in chapter 3[26].

2.1.2 Electrochemistry

It is necessary to introduce a few concepts of electrochemistry to understand the details described in later chapters. The first concepts are oxidation and reduction reactions. The process of oxidation (anodic reactions) refers to the release of electrons and the process of reduction (cathodic reactions) refers to the acceptance of electrons. In a cell undergoing discharge, the positive electrode will accept electrons traveling via the external circuit and undergo reduction accepting ions from the electrolyte and the negative electrode will release electrons to the external circuit and undergo oxidation, releasing ions to the electrolyte. Rechargeable lithium-ion batteries are

called secondary batteries, because they can be both charged and discharged. As a result, the reaction at the electrodes will reverse for charging. The half-reactions of a lithium-ion cell are shown in Eq. (1) and Eq. (2).

The rate of energy conversion depends on the kinetics of each half-cell reaction and the material parameters (eg. ionic conductivity) and design parameters (eg. thickness of components) of the cell [41]. The reversible voltage of the cell is determined by the Gibbs Free Energy change of the reaction G_R, where n is the number of moles of electrons and F is Faraday's constant.

$$E_{cell,rev} = -\frac{\delta G_R}{nF} \tag{3}$$

When a metal electrode is brought into contact with a solution of its ions, the half-cell reaction will occur until equilibrium is reached. As either the oxidation or reduction reaction takes place, a charge separation develops which is when a positive and negative charge concentration build up on either side of the electrode/electrolyte layer. This is important, as this charge aspect is what differentiates electrochemical potential, from purely chemical potential which only considers the change in Gibbs free energy from moles of a species being added to a mixture and does not consider the energy of formation associated with the charge separation development. Using the electrochemical potential of each species of the products and reactants from a half-cell reaction, the Nernst equation is developed, which defines the potential of that reaction. The cell voltage is then, the potential of the half-cell reaction of the positive electrode minus the potential of the half cell reaction of the negative electrode

$$E_{cell,rev} = E_{pos,rev} - E_{neg,rev}, \tag{4}$$

where $E_{cell,rev}$ is the reversible cell voltage, $E_{pos,rev}$ is the reversible voltage of the positive electrode, and $E_{neg,rev}$ is the reversible voltage of the negative electrode.

Exchange current density and overpotential are also important concepts and will be described in detail in the modeling equations in chapter 3. When the cell is in dynamic equilibrium, the rates at which the cathodic and anodic reactions occur in a particular electrode are equal. This rate of reaction is referred to as the exchange current density. In this case, no external current is measured. In order to produce an external current, the exchange current densities must be offset, so they are no longer equal, and when this occurs an overpotential is produced. For a cell to discharge, the cathodic reaction rate at the positive electrode must shift to exceed the anodic reaction rate at the positive electrode and the anodic reaction rate at the negative electrode must shift to exceed the cathodic reaction rate. When this happens, an anodic overpotential is produced at the negative electrode, increasing the negative electrode potential and a cathodic overpotential is produced at the positive electrode, decreasing the potential of the positive electrode.

$$\mathrm{E_{cell}} = \mathrm{E_{pos,rev}} - \mathrm{E_{neg,rev}} - \eta_{\mathrm{anodic}} - |\eta_{\mathrm{cathodic}}| = \mathrm{E_{cell,rev}} - \eta_{\mathrm{anodic}} - |\eta_{\mathrm{cathodic}}| \qquad (5)$$

The reverse is then true for a cell being charged.

$$\mathrm{E_{cell}} = \mathrm{E_{pos,rev}} - \mathrm{E_{neg,rev}} + \eta_{\mathrm{anodic}} + |\eta_{\mathrm{cathodic}}| = \mathrm{E_{cell,rev}} + \eta_{\mathrm{anodic}} + |\eta_{\mathrm{cathodic}}| \qquad (6)$$

The exchange current density and overpotential of the electrode is then used in calculating the actual ion transfer current from the electrolyte to the electrode and vice-versa by the Bulter-Volmer equation, which is described later in chapter 3.

It is also important to understand electroneutrality, this is the concept that in a conductor the combined density of all ions is zero and this requires that all charge transfered via external circuit must be balanced by an equal charge transfer by ionic current through the electrolyte [3]. The electrolyte is an electrically insulating but ionically conductive material. Within the electrolyte both anions and cations are

used to transfer the charge, in order to match the external circuit charge transfer. In addition to charge being transferred by migration from an electric field, ions are also transferred via diffusion. Diffusion is a much slower process than migration, resulting from the concentration gradient that develops in the electrolyte rather than the potential gradient, which causes the ion migration. The proportion of charge which is transferred by each is described by the transport number, also called transference number. For superior performance a higher positive ion transport number is desirable. This process is described in Fig. 2 for a $LiPF_6^-$ electrolyte.

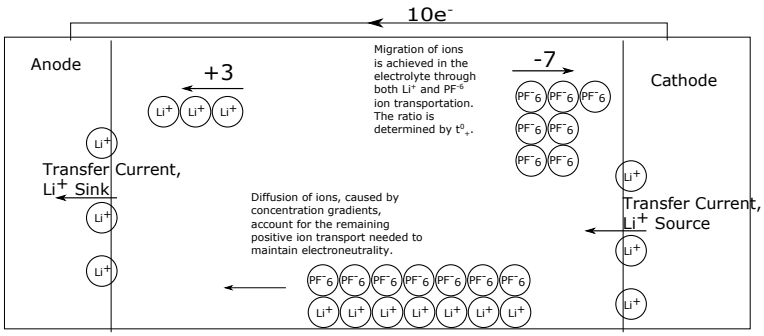

Figure 2: Migration and Diffusion. The anions and cations travel in different directions due to migration, but the same direction due to diffusion. The lithium cations are consumed by the electrode at one end and produced in the other, resulting in a constant concentration gradient in the direction of migration. The anions are not consumed, resulting in a concentration gradient and diffusion opposite the direction of migration.

2.1.3 Intercalation

In lithium-ion batteries, as opposed to lithium metal, the cathode and anode are both made of porous material. This is done to improve the efficiency of the electrode, by providing greater surface contact area between the ions in the electrolyte and the electrode particles to improve the charge transfer reaction. Ideally, the intercalation process is a topotactic reaction which means the lithium ions can be inserted and

removed from the electrodes without causing any significant structural change to the electrode. The intercalation process involves three principled steps [25]

1) Diffusion or migration of solvated Li^+ ions.

2) Desolvation and injection of Li^+ ions into the vacancy structure.

3) Diffusion of Li^+ ions into the host structure.

Positive cathode materials in lithium-ion cells can have either a layered or spinal structure and the graphite anode material has a layered structure. This allows the electrodes to act as "hosts" to the lithium ion "guests" that can be reversibly inserted and removed. Although this process is intended to be reversible and nondestructive, it can causes physical changes to the electrodes as well as, chemical and electrical. As the ions leave and enter the electrodes, a volume change occurs, which can cause strain and fracturing of the electrode particles and lead to decreased cell life. The main parameters which effect the rate of intercalation are particle size, particle diffusivity, and the applied transfer current.

2.2 Panasonic 18650b NCR

The cells used for experiments in this thesis were Panasonic 18650b NCR, which is very similar in properties to cells being used by Tesla and other electric vehicle manufactures. The title 18650 describes the dimensions of the cell, being 18 mm in diameter and 65 mm tall. It is assembled in what is called a jellyroll, in which long strips of the 5 battery components are placed on each other and rolled into a spiral to fit into a cylindrical metal casing.

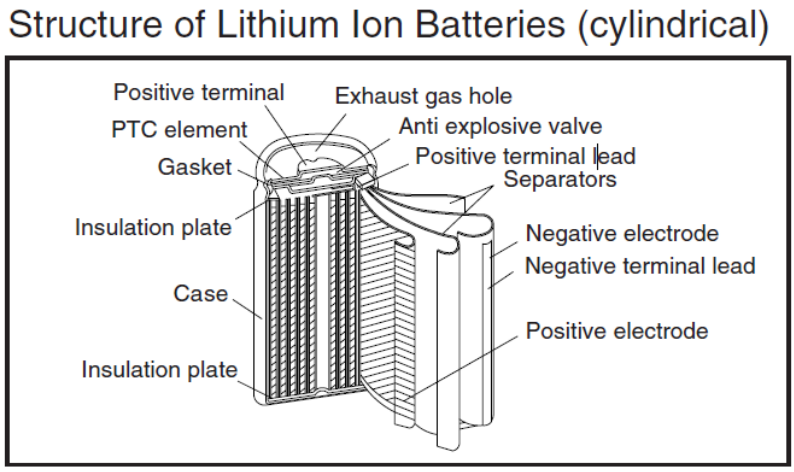

Figure 3: Image from Panasonic detailing the structure of a cylindrical cell and the components of the jellyroll[33].

The dimensions refer to the size of the casing and not the battery components. One of the important parameters in determining cell capacity is the thickness of the individual components, which were measured for the cells used in this study using a scanning electron microscope(SEM), and are listed in Table 1.

Table 1: Thicknesses of the Panasonic 18650B components, as estimated from SEM analysis. These values are used as the component lengths in the mathematical model.

Cell Component	Negative Current Collector	Negative Electrode	Separator	Positive Electrode	Positive Current Collector
Thickness (nm)	10	100	30	75	10

The negative current collector is made of copper and the positive from aluminum. An NCA cathode is used, which denotes the cathode chemistry to be a metal oxide composite, comprised of lithium, nickel, cobalt, and aluminum. The exact composition of the Panasonic cell is proprietary and not disclosed, but the common makeup of the electrode is expected to be $LiNi_{0.8}Co_{0.15}Al_{0.05}O_2$, although the Panasonic cathode will have other additives to improve cell life and operation. This chemistry is used, because high capacity cells are needed, which is achieved through the use of nickel, but this is also very unstable. For this reason, cobalt and aluminum are

also added which will improve cell life. This has similar properties to the LiCoO2 electrode chemistry, which is most commonly used, but the NCA chemistry offers a slightly higher capacity and greater stability [20]. This cathode is considered to have what is called a rock salt-type structure as its layering structure, which means the lithium ions occupy octahedral site in alternating layers [25]. The anode is believed to be made of graphite, Li_xC_6, this choice of material is much more consistent among battery manufactures.

2.3 Constant Current Constant Voltage Charging

Constant current constant voltage charging is a technique in which the cell is charged at a constant current, CC, until an upper voltage limit is reached. This upper voltage limit is put in place to protect the cell electrodes from aging, as is described in Chapter 4. This upper limit for lithium-ion cells is 4.2 V. Once 4.2 V is reached, the charging profile will switch to constant voltage charging, CV, during which the current will continuously decrease to maintain the 4.2 V value. Generally under this type of charging, the charging process is stopped once a low current limit is reached, 55 mA for this cell. This constant voltage period significantly increases charging time; from the testing done here the cell is only charged to about 78 percent capacity (45 minutes) before switching to CV charging which adds about one and a half hours to the charging process. This phase of charging is one of the focus areas which is believed to be improved through pulse charging. The figures Fig. 4 and Fig. 5 show examples of the voltage and current profiles during CCCV charging.

2.4 Pulse Charging

There are a number of different processes which are commonly referred to as pulse charging. In this thesis, pulse charging refers to a process in which the current applied to the cell is periodically halted and a short pause phase or pause and discharge phase

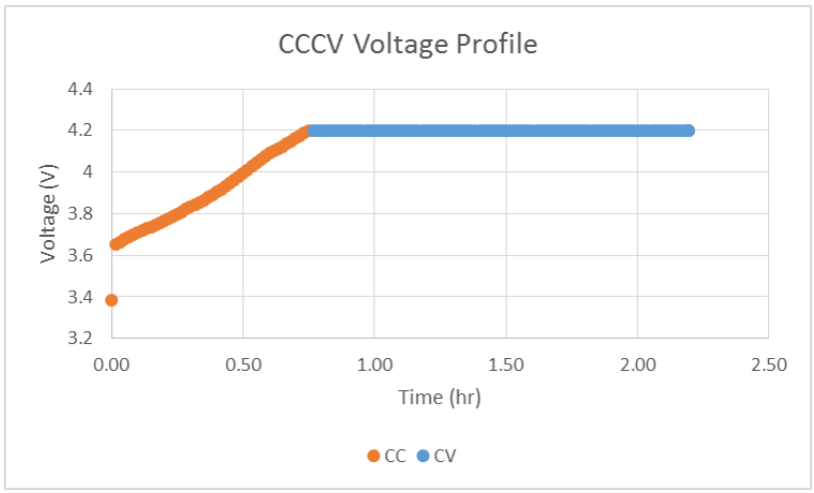

Figure 4: CCCV voltage profile.

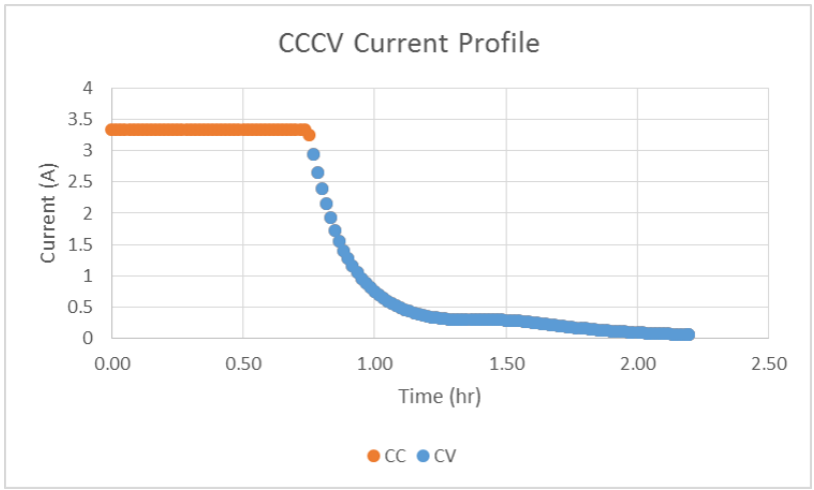

Figure 5: CCCV current profile.

are applied. It is through these series of pauses and discharges that the process is hoped to be improved, by enhancing the ability of lithium ions to transverse the electrolyte and intercalate into the electrodes. To illustrate the application of pulsed charging, examples of the current and voltage profiles of a cell being charged with this technique are shown in Fig. 6 and Fig. 7.

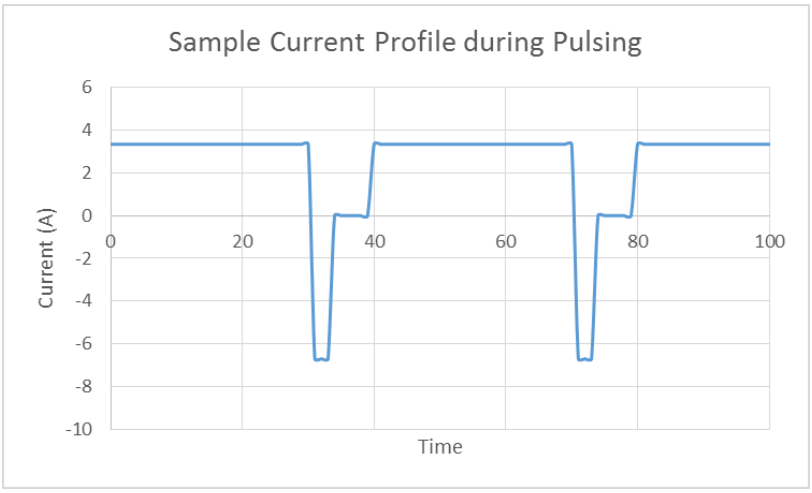

Figure 6: Sample of a current pulse profile. A constant charge current is applied which is interupted by a discharge phase, followed by a rest phase. This cycle is then continued through the charging process at a set frequency.

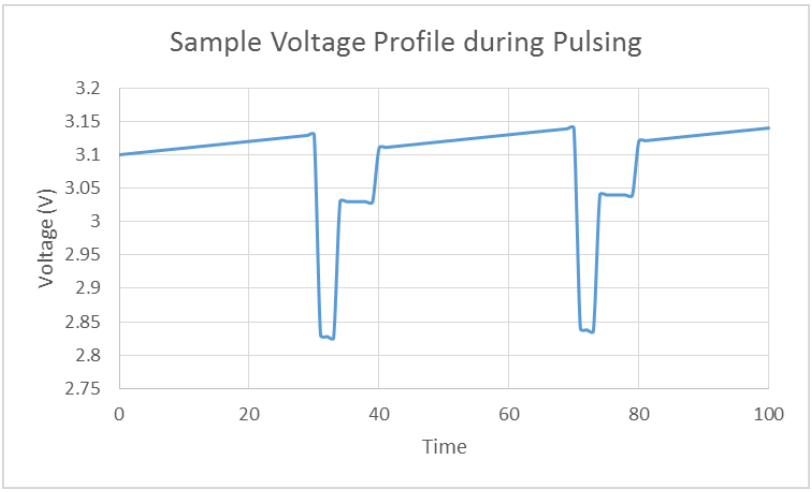

Figure 7: Sample of a voltage profile under pulsed charging. The voltage will increase during the positive charge current, then experiences a sharp drop from the discharge pulse, followed by a rest phase when the cell can equilibrate.

CHAPTER III

MATHEMATICAL MODEL

3.1 Modeling Background

3.1.1 Purpose and Challenges

The main objectives of developing a battery model is to assess cell operation without having to do costly experimentation and to observe parameters which cannot be measured easily through experimentation. One reason researchers are interested in modeling is to optimize the cell through changing various physical parameters, such as the length of the electrodes or particle radius, and they are interested in seeing the effect of how improved diffusivity, conductivity, and other relevant material properties could improve performance and aid in material selection. Another focus of research in modeling assesses how to best estimate the remaining charge in a cell using the limited number of observables that are measured during operation and how to determine the health of a battery. Modeling is also used for developing other features, such as the design of a thermal management system of an entire battery pack, which will consist of many individual cells. Additionally, and as is the case in this thesis, cell modeling is important for analyzing how cells react to certain environmental or operating conditions, in order to optimize things such as charge time, discharge time, cell life, energy management, and how cells will interact when in a battery pack.

A key challenge with modeling batteries, and a reason for why models are necessary, is only two parameters can be easily measured, current and terminal voltage, while the cell is in operation which makes model validation difficult. Cell surface temperature can also be measured, but is generally used to monitor the temperature

of the whole cell for safety conditions, rather than to study the internal dynamics of the cell. There are other experimental techniques, such as three electrode cell tests, which allow for individual analysis of either electrode and can provide additional information, however to conduct these the cells must be disassembled or modified in some way. These are very useful if the researcher is interested in the effects of a specific parameter or of some additive to an electrode, or for measuring the value of a material property of the electrode, however for analyzing a commercial cell and the effect of an applied or environmental condition on it, such techniques are less useful. The best way to assess these effects is to simply run the cell under the conditions of interest.

Another challenge when it comes to modeling commercial cells is a lack of published information on parameters of the cell materials. Most of the parameters necessary to developing a model are considered proprietary to the manufacturer, and must be either estimated or measured through additional experimentation. This experimentation becomes more difficult when considering many of the parameters in the cell experience a considerable change with factors such as aging, temperature, and state of charge (SoC). Due to the scope and time constraints of a masters thesis, the experiments necessary to measure all the relevant parameters were not possible and were instead obtained through an extensive literature review and by adjusting parameters during model validation. Validating the model is made more difficult because only voltage, current, and temperature can be used, and considering the model which is used in this paper is fairly complex, looking at the entire electrochemical and thermal process rather than one specific feature, it is difficult to validate each aspect of the model only using these variables. Parameter selection and model validation is expanded upon in chapter 6.

3.1.2 Types of Battery Models

Multiple different techniques exist for modeling lithium-ion batteries. Some of the most common are analogous circuit techniques, single particle models, and full electrochemical models (the term full electrochemical model is used to describe any model which considers the entire electrochemical process across all elements of the cell). Analogous circuit models are often used in battery management systems (BMS) as a method to obtain information on state of charge and state of health (SoH) of the cell in a method that can be easily implemented on board a car computer [24],[21],[10]. Similar models have also been used for there simplicity by BMS to monitor and estimate cell temperature [15]. From a users prospective, for example a driver of an electric vehicle, the SoC and SoH will be the main values of interest, and from a safety perspective so will cell temperature, which makes analogous circuit methods very useful in practical applications.

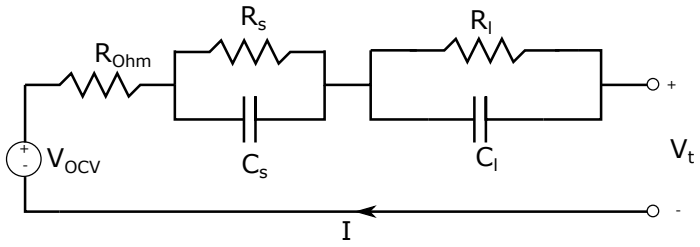

Figure 8: Equivalent circuit model example from a thesis [29] on modeling aging at low temperatures. It accounts for the open circuit voltage which changes with SoC, the Ohmic resistance, then has two sets of resistors and capacitors in parallel to account for two time scales at which voltage changes my occur.

Single particle and full electrochemical models are more often used in battery cell research, as much more data about the cell operation can be obtained, but at greater computation cost and longer solution times. The single particle model solves equations based around a single particle of the cathode or anode material [17], [27]. This gives information about concentration gradients that may exist within the electrode

as well as estimates of the concentration of ions in the solid phase (within the electrode material). It is a simpler technique than a full electrochemical method but provides valuable information. Both the single particle and equivalent circuit methods vary in complexity, some made much simpler to be used on board a car's computer and other more complex to be more valuable in research. The main advantage of each is, however, that aspects of a full electrochemical model have been simplified or left out in order lower the computational complexity.

Full electrochemical models are much more detailed than the other two models previously discussed, considering all aspects of the electrochemical process. The full electrochemical model used here was proposed by Doyle, Fuller, and Newman, sometimes abbreviated as the DFN model [14]. Electrochemical models can vary between 1, 2, and 3 dimensions, depending on the complexity and computation capacity available. They have been used to serve many different types of research, often used to assess the thermal impact on cell operations [40], charging techniques [1] [18], use in hybrid vehicles [43], and analysis of thermal management devices [46].

Each of the cell models described above can be augmented by including thermal dynamics. By coupling the thermal and electrochemical physics, a more accurate model is produced [16]. The open circuit cell voltage has a temperature dependence, as do some material properties, such as the electrolyte conductivity and diffusion coefficient of the negative electrode. By accounting for these changes the cell dynamics can be better represented. Incorporating temperature into the cell model is especially important when analyzing the cell under various operating conditions because, as described in later chapters, temperature has an important effect on both cell efficiency and aging. Depending on the cell model, the thermal model can be an ODE model, as in the case of the analogous circuit model, or a PDE model considering the 1D, 2D, or 3D spatial distribution of the cell.

3.2 Pseudo 2D Electrochemical Model

Implemented in this paper is what is referred to as a pseudo-2D model, in which the cell is modeled based on the thickness of each battery component, and also the radius of the individual particles, with the particles assumed to follow some regular geometric shape. The cell potential distribution and concentration in the liquid phase (within the electrolyte) are calculated along the thickness of the components, while the solid phase concentration is calculated along the radius of the particle, with the particles assumed to be spheres in the model developed here. The coupling factor between the two dimensions comes from the Bulter-Volmer equations which uses the electrolyte ion concentration and the concentration on the surface of the particle to determine the flux of ions into or out of the particles. The particles are represented in a rectangular geometry, with the particle radius being the height and the length of the electrode the width. No diffusion is allowed in the lateral direction, and Fick's Second Law for a sphere is used in the radial direction. The particle concentration at the surface of the particle is calculated from this and then used in the Bulter-Volmer equation of the 1D geometry to determine the transfer current from the electrolyte to the solid phase which is used as the boundary condition in the 2D geometry. This is described in Fig. 9 and made more clear in the following description of equations.

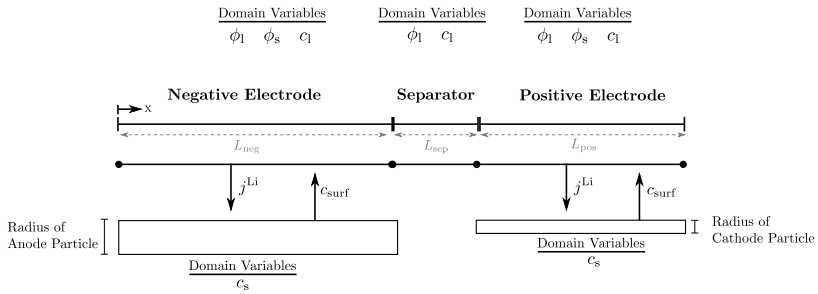

Figure 9: Pseudo 2D Model. The 1D cell length is described above with the relevant dependent variables listed. The 2D domain which considers the particle radius and electrode length are defined by the two rectangles.

The electrochemical model is based around four dependent variables, the potential in the electrode and electrolyte, ϕ_s and ϕ_l respectively, and the concentration in the electrode and electrolyte, c_s and c_l respectively. The differential equations which yield for these values are applied to the positive and negative electrodes, and because the electrodes are porous, the differential equations for the solid electrode and liquid electrolyte phases must both be solved in the electrode domain. Only the electrolyte portions are applied to the separator domain. The first to be introduced here are the PDEs for species conservation. These equations must be solved in the electrolyte phase in all three domains, and in the solid phase within the 2D rectangular domains for the electrodes. The particles which comprise the electrode and into which the ions will diffuse are treated as spheres and, as a result, the spherical form of the diffusion equation is used when solving for the species concentration. The geometric representation of this is described in Fig. 10.

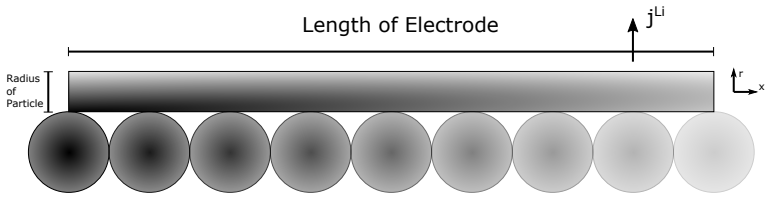

Figure 10: 2D geometric representation of ion concentration within the electrode particles. In this example, the darker areas represent greater ion concentration.

Species conservation: The species conservation equations are both primarily based around Fick's second law of diffusion, with the electrode species conservation as given in (7), applied to a spherical geometry, as previously noted. This equation is solved within the domain of the rectangular geometry described in Fig. 9. The electrolyte species conservation, see (8), also accounts for diffusion, but has an additional term included to account for the effect of migration on ion concentration. Within the

electrolyte, ions move both as a result of the electric field, migration, and the concentration gradient that exists, diffusion [28]. Ions traveling via migration will travel faster, while those traveling via diffusion are slower and cause the concentration polarization resulting in greater overpotential. The transference number, t_+^0, given in (8), relates the proportion of charge which is transferred by the positive Li^+ ion by migration. The higher the transference number, the greater the number of positive ions transferred by migration and the lower the concentration gradient, as a result higher transference numbers are preferred. However, for lithium-ion batteries this number is general measured to have a value around 0.3 [16].

The electrode species conservation is described as:

$$\frac{\partial c_{\mathrm{s}}}{\partial t} = \frac{D_{\mathrm{s}}}{r^2} \cdot \frac{\partial}{\partial r}(r^2 \frac{\partial c_{\mathrm{s}}}{\partial r}), \tag{7}$$

where D_{s} is the electrode diffusivity, r is the particle radius and ϵ_{s} is the solid phase volume fraction. The electrolyte species conservation is described as:

$$\frac{\partial \epsilon_{\mathrm{l}} c_{\mathrm{l}}}{\partial t} = \underbrace{\nabla(D_{\mathrm{e}}^{\mathrm{eff}} \nabla c_{\mathrm{l}})}_{\text{Diffusion}} + \underbrace{\frac{(1 - t_+^0)}{F} j^{\mathrm{Li}} - \frac{i_{\mathrm{l}} \nabla t_+^0}{F}}_{\text{Migration}} \tag{8}$$

where i_l is the current density in the liquid phase, $D_{\mathrm{e}}^{\mathrm{eff}}$ is the effective electrolyte diffusivity, and ϵ_{l} is the liquid phase volume fraction

The transference number is generally considered to be constant, therefore the final term in (8) is considered to be zero.

In the electrolyte species conservation equation the effective diffusivity is used, see (10). This is done to account for the porosity of the electrode material. Tortuosity, τ, corrections are applied to the electrolyte diffusion coefficient, ionic conductivity, and electrode conductivity in order to account for the tortuous path through the electrode. Tortuosity is the ratio of the distance that must be traveled in free space

compared to the distance in the porous media. As a result of the porosity, the area for diffusion is less than what it would be for a free fluid, this results in a higher gradient developing, as diffusion is impeded. The Bruggeman relation for tortuosity, see (9), is used to calculate these effective values as shown in (10) to (12):

$$\tau = \frac{1}{\epsilon^{0.5}} \tag{9}$$

$$D_{\mathrm{e}}^{\mathrm{eff}} = D_{\mathrm{e}} \frac{\epsilon}{\tau_{\mathrm{l}}} = D_{\mathrm{e}} \cdot \epsilon_{\mathrm{l}}^{1.5} \tag{10}$$

$$\kappa_{\mathrm{e}}^{\mathrm{eff}} = \kappa_{\mathrm{e}} \cdot \epsilon_{\mathrm{l}}^{1.5} \tag{11}$$

$$\sigma_{\mathrm{s}}^{\mathrm{eff}} = \sigma_{\mathrm{e}} \cdot \epsilon_{\mathrm{s}}^{1.5} \tag{12}$$

where $\kappa_{\mathrm{e}}^{\mathrm{eff}}$ is the effective ionic conductivity of the electrolyte and $\sigma_{\mathrm{s}}^{\mathrm{eff}}$ is the effective electrode conductivity. These corrections are often used in modeling lithium ion cells, it is also included in the Comsol module, and was used by Doyle in his original model [13].

At the center of the particle, there is no flux, and there is assumed to be symmetry so only the radial direction is considered. The concentration in the solid (electrode) phase is related to the concentration in the liquid (electrolyte) phase by the Bulter-Volmer equation. The equations will also be subject to initial conditions for electrode and electrolyte potential across the battery, initial electrolyte salt concentration across the battery, and initial concentration in the electrode particles. Within the 2D geometry, which is representative of many individual particles, solving for their radial concentration profile, it is assumed that no diffusion can occur between particles and therefore the diffusion constant for the x direction is set to zero.

In the following, the boundary conditions applied to the species concentration equation are discussed.

At the center of each particle, the flux is zero and subsequently:

$$\frac{\partial c_{\mathrm{s}}}{\partial r}|_{r=0} = 0. \tag{13}$$

At the outside of the particle, the flux is given by the transfer current j^{Li} as follows:

$$-D_{\mathrm{s}}\frac{\partial c_{\mathrm{s}}}{\partial r}|_{r=r_{\mathrm{p}}} = \frac{j^{\mathrm{Li}} r_{\mathrm{p}}}{3\epsilon_{\mathrm{s}} F}, \tag{14}$$

where r_{p} is the radius of the particles. There is no mass flux in the liquid phase at both ends of the cell, which results in:

$$\frac{\partial \epsilon_{\mathrm{l}} c_{\mathrm{l}}}{\partial x}|_{x=0, x=L_{batt}} = 0. \tag{15}$$

The continuity of the mass flux in the liquid phase at the interface of both electrodes and the separator is ensured by:

$$c_{\mathrm{l}}\big|_{x=L_{\mathrm{neg}}^{-}} = c_{\mathrm{l}}\big|_{x=L_{\mathrm{neg}}^{+}}, \tag{16}$$

$$c_{\mathrm{l}}\big|_{x=(L_{\mathrm{sep}}+L_{\mathrm{neg}})^{-}} = c_{\mathrm{l}}\big|_{x=(L_{\mathrm{sep}}+L_{\mathrm{neg}})^{+}}, \tag{17}$$

$$D_{\mathrm{e}}\frac{\partial \epsilon_{\mathrm{l}} c_{\mathrm{l}}}{\partial x}|_{x=L_{\mathrm{neg}}^{-}} = D_{\mathrm{e}}\frac{\partial \epsilon_{\mathrm{l}} c_{\mathrm{l}}}{\partial r}|_{x=L_{\mathrm{neg}}^{+}}, \tag{18}$$

$$D_{\mathrm{e}}\frac{\partial \epsilon_{\mathrm{l}} c_{\mathrm{l}}}{\partial x}|_{x=(L_{\mathrm{sep}}+L_{\mathrm{neg}})^{-}} = D_{\mathrm{e}}\frac{\partial \epsilon_{\mathrm{l}} c_{\mathrm{l}}}{\partial r}|_{x=(L_{\mathrm{sep}}+L_{\mathrm{neg}})^{+}}. \tag{19}$$

From the initial conditions and supplemental equations, with emphasis on the concentration flux equation (transfer current) that is dependent on Bulter-Volmer, the boundary conditions of the pdes can be determined. The Bulter-Volmer equation, see (20), is of particular importance in electrochemistry, describing the electrical current that is produced based on the potential difference between an electrode and the electrolyte solution. It is derived from the reaction rate equation, using the overpotential. Within each electrode there are both anodic and cathodic reactions, the reaction rate of the electrode is dependent upon which reaction is dominant. Within the Bulter-Volmer equation is the transfer coefficient, also known as the symmetry factor, which is the ratio of the anodic reaction and cathodic reaction rate values.

For this type of modeling, the value is generally assumed to be 0.5, which is termed symmetric electron transfer, meaning for anodic reactions the anodic reaction rate is twice the cathodic, and vice-versa for a cathodic reaction [19]. When the overpotential, defined as the additional voltage difference above equilibrium between the electrode and solution, see (21), and which drives current, is applied to the reaction rate equation, it takes the form of the Bulter-Volmer equation and the transfer current can be determined. The concentration within the electrodes is not explicitly seen within the Bulter-Volmer equation, but does appear through the calculation of exchange current density, as see in (22), and through its effect on overpotential.

The current density $i_{\mathrm{a},i}$ is used to calculate the pore wall flux (transfer current) at the electrode/electrolyte interface, forming the second boundary condition for the PDE of the electrode concentration. Using the Bulter-Voler Equation, the density of the transfer current at the interface of liquid and solid phase is given by

$$i_{\mathrm{a},i} = i_0 \left(\exp\left(\frac{\alpha_{\mathrm{a},i} F}{RT} \eta_i \right) - \exp\left(-\frac{\alpha_{\mathrm{c},i} F}{RT} \eta_i \right) \right), \tag{20}$$

where η_i is the overpotential in electrode i and α is the transfer coefficient of either the anodic, a, or cathodic, c, reaction in the electrode. The overpotential is given as

$$\eta_i = \phi_{\mathrm{s}} - \phi_{\mathrm{e}} - U_i, \tag{21}$$

with the potentials ϕ_{e} and ϕ_{s} of the liquid and solid phase as well as the open circuit voltage U_i, all to be computed later on. i_0 denotes the exchange current density which yields

$$i_0 = F k_{\mathrm{a}}^{\alpha_{\mathrm{a},i}} k_{\mathrm{c}}^{\alpha_{\mathrm{c},i}} \left(c_{\mathrm{s,max}} - c_{\mathrm{s}} \right)^{\alpha_{\mathrm{a},i}} \left(c_{\mathrm{s}} \right)^{\alpha_{\mathrm{c},i}} \left(c_{\mathrm{l}} \right)^{\alpha_{\mathrm{a},i}}, \tag{22}$$

where k is the reaction rate coefficient and $c_{\mathrm{s,max}}$ is the maximum concentration the electrode can accept.

The exchange current density is the rate of transfer which occurs when there is no overpotential. In this equation, the coupling of the radial diffusion and electrolyte is most apparent, the exchange current density depends on the solid phase concentration on the surface of the particle, and the local concentration of the electrolyte. Additionally, it is dependent on the reaction rate coefficient of the anodic and cathodic reactions occurring in the electrode and the difference between the maximum concentration and current concentration in the particle, which is equivalent to the concentration of ions transferred to the opposite electrode.

By considering the specific surface area of the particles a_{s}, the transfer current can be determined from the value derived, see (24), from the Bulter-Volmer equation.

The specific interfacial area is determined by

$$a_{\mathrm{s}} = \frac{4\pi r_{\mathrm{p}}^2 \epsilon_{\mathrm{s}}}{\frac{4}{3}\pi r_{\mathrm{p}}^3} = \frac{3\epsilon_{\mathrm{s}}}{r_{\mathrm{p}}} \tag{23}$$

with transfer current

$$j_i^{\mathrm{Li}} = a_{\mathrm{s}} \cdot i_{\mathrm{a},i}. \tag{24}$$

Within these equations is also the open circuit potential (voltage), OCV, which is very important in producing the voltage profile within the model. The OCV value is derived from an experimentally measured voltage profile of each electrode, produced from charging (or discharging) the electrode at a very slow current which is assumed to produce very little additional ohmic or polarization voltage. Using this measured profile, the OCV in the model is calculated based on the SoC in the electrode, defined in the model as the concentration of ions in the electrode over the maximum concentration of ions the electrode can hold. This value is one of the most dominant factors on the voltage profile. The model equations mainly calculate the rate at which ions are transferred into and out of the electrodes and to calculate some

additional voltage to account for polarization and ohmic voltage. The general shape of the voltage profile is controlled by the experimentally measured OCV value, with the voltage magnitude offset by the calculated ohmic and polarization voltages. Since the OCV value is only dependent on SoC, the rate of ion transfer then also impacts the profile shape by expanding or contracting the voltage profile with time. While the concentration of ions in both electrodes play an important role in determining the exchange rate of ions, the OCV, and therefore concentration of ions, in the positive electrode tends to play a more dominant role in the voltage profile, as the voltage in the positive electrode is an order of magnitude higher than that in the negative electrode for the majority of the SoC range.

The open circuit potential equation when considering the temperature dependence is described by

$$U_i = U_{i,\text{ref}} + (T - T_{\text{ref}}) \cdot \frac{\partial U_i}{\partial T}, \tag{25}$$

where T is the temperature and T_{ref} is the reference temperature at which the reference OCV, $U_{i,\text{ref}}$, was calculated.

Charge conservation: The next set of differential equations solve for charge conservation, which only apply to the 1D geometry domains. The electrode charge balance, see (28), applies only to the positive and negative domains, while the electrolyte charge balance, see (29), applies to all three domains. Within the model, these charge balances are used to represent the flow of charge through the electrodes; the current is applied (positive for charge, negative for discharge) at L_{batt}, as shown in (31), no charge transfer is assumed at the electrode/separator boundary for both electrodes, and the x=0 boundary of the negative electrode is treated as ground. For the solid phase equation there is only charge transfer due to potential difference, while in the liquid electrolyte phase equation there is charge transfer due to both potential difference and concentration gradient. First, the equations for current in the solid phase,

(26), and liquid phase, (27), are shown

$$i_{\mathrm{s}} = \sigma_{\mathrm{s}}^{\mathrm{eff}} \nabla \phi_{\mathrm{s}} \tag{26}$$

$$i_{\mathrm{l}} = \underbrace{\kappa_{\mathrm{e}}^{\mathrm{eff}} \nabla \phi_{\mathrm{l}}}_{\text{Ohm's Law}} + \underbrace{\kappa_{\mathrm{D}}^{\mathrm{eff}} \nabla \ln c_{\mathrm{l}}}_{\text{Concentration Difference}} . \tag{27}$$

The charge balance is then derived by including the current transfer from the pore wall flux between the solid electrode and the liquid electrolyte. Since there is no net change in charge in either electrode, these equations do not require a time derivative. The applied current and resulting potential gradient produce the transfer current, resulting in electrons leaving the positive electrode through an external circuit and positive charged ions entering the electrolyte, in the case of charging. Within the electrolyte the ions then migrate to the negative electrode, the boundary between the electrodes and separator are again considered continuous. Once inside the separator, the pore wall flux is zero, so the liquid phase transfer current is constant. In the negative solid phase, the boundary condition of ground deviates slightly from reality, where electrons would enter the negative electrode to combine with the incoming positive charged lithium ions to maintain a neutral charge. In the model, treating the boundary as ground and not having a time component within the charge balance equation removes the need to consider electrons entering the negative electrode, without producing an overly positive charged electrode.

The charge balance for the electrode is described as

$$\nabla i_{\mathrm{s}} = j^{\mathrm{Li}} \tag{28}$$

and the charge balance in the electrolyte as

$$\nabla i_{\mathrm{l}} = -j^{\mathrm{Li}}. \tag{29}$$

The diffusional conductivity is calculates by

$$\kappa_{\mathrm{D}}^{\mathrm{eff}} = \left(\frac{2\kappa_{\mathrm{e}}^{\mathrm{eff}} RT}{F}\right)\left(1 + \frac{\mathrm{d}\ln[f]}{\mathrm{d}\ln c_{\mathrm{l}}}\right)\left(t_{+}^{0} - 1\right) \tag{30}$$

where f is the mean molar activity coefficient of the electrolyte. The boundary conditions for charge conservation are shown below. At the positive end of the battery geometry the applied current is set

$$\left(\sigma_{\mathrm{s,p}}^{\mathrm{eff}} \nabla \phi_{\mathrm{s,p}}\right)\Big|_{x=L_{\mathrm{batt}}} = i_{\mathrm{app}}. \tag{31}$$

At the separator boundaries, the solid phase current is set to zero

$$\left(\sigma_{\mathrm{s},i}^{\mathrm{eff}} \nabla \phi_{\mathrm{s},i}\right)\Big|_{x=L_{\mathrm{neg}}+L_{\mathrm{sep}}, x=L_{\mathrm{neg}}} = 0 \tag{32}$$

and at the negative terminal the voltage is set to zero

$$\phi_{\mathrm{s,n}}\big|_{x=0} = 0. \tag{33}$$

At the positive and negative terminals, the liquid phase current is set to zero:

$$\kappa_{i}^{\mathrm{eff}} \frac{\partial \phi_{\mathrm{l},i}}{\partial x}\bigg|_{x=0, x=L_{\mathrm{batt}}} = 0. \tag{34}$$

As with the liquid phase concentration in the electrolyte mass balance, the liquid phase potential and potential flux are continuous across the boundary of the electrodes and separator.

3.3 Electric Double Layer Capacity

In addition to the standard model, the model has been extended to include the dynamics of the double layer capacity, based on an equation proposed by Ong and Newman [32].

The change in current density from the inclusion of the double layer is:

$$i_{\mathrm{dl}} = \left(\frac{\partial \phi_{\mathrm{s}}}{\partial t} - \frac{\partial \phi_{\mathrm{l}}}{\partial t} \right) \cdot a_{\mathrm{v}} \cdot C_{\mathrm{dl}}, \tag{35}$$

where C_{dl} is the double layer capacitance and which results in the following change in the transfer current:

$$j^{\mathrm{Li}} = j^{\mathrm{Li}}_{\text{pre-DL}} + i_{\mathrm{dl}}. \tag{36}$$

3.4 Heat Generation and Thermal Modeling

As stated, modeling the thermal state of the cell is very important for research because it can give insight into what conditions produce optimal charging conditions and what conditions are causing increased rate of aging by producing a significant temperature rise. The most important aspect of this is determining the source of heat generation, which is shown in (37). A detailed explanation of the energy balance of a cell was produced by Bernardi et al. [5]. In this description it details the various sources of heat generation within a battery, including enthalpy of reaction, enthalpy of mixing, phase change, and heat capacity. For the majority of lithium-ion battery models the enthalpy of mixing and phase change terms are assumed very small and not considered. The heat generation terms used here are from the Comsol literature, and of those sources previously described only the enthalpy of reaction is considered. In addition to the enthalpy of reaction, Joule heating is also accounted for.

Heat generation is described by the following equation, which accounts for the two main sources of heat:

$$q = \underbrace{j^{\mathrm{Li}} \cdot \left(\phi_{\mathrm{s}} - \phi_{\mathrm{l}} - U_i + T \cdot \frac{\partial U_i}{\partial T} \right)}_{\text{Enthalpy of Reaction}} + \underbrace{\sigma_{\mathrm{s}}^{\mathrm{eff}} \nabla \phi_{\mathrm{s}} \cdot \nabla \phi_{\mathrm{s}} + \left(\kappa_{\mathrm{e}}^{\mathrm{eff}} \nabla \phi_{\mathrm{l}} \cdot \nabla \phi_{\mathrm{l}} + \kappa_{\mathrm{D}}^{\mathrm{eff}} \nabla \ln c_{\mathrm{l}} \cdot \nabla \phi_{\mathrm{l}} \right)}_{\text{Joule heating}}. \tag{37}$$

The first term in the heat equation is the irreversible and reversible heat generation equations for the electrode reaction. They are developed as the difference from the

total reaction enthalpy and the electrical energy which is leaving the system. The derivation of this heat source is shown in (38) to (42).

The total heat generation from electrochemical conversion, Q_{EC} can be described as the heat from the enthalpy of reaction minus the total electrical energy leaving the system

$$Q_{\mathrm{EC}} = \left(\triangle H_{\mathrm{i}} - \left(\triangle G_{\mathrm{i}} - \eta\left(nF\right)\right)\right) j^{\mathrm{Li}} \left(\frac{1}{nF}\right), \tag{38}$$

where H_i is the enthalpy and n the number of electrons. The change in Gibbs free energy, G_{m}, is defined as:

$$\triangle G_{\mathrm{i}} = \left(\triangle H_{\mathrm{i}} - T\triangle S\right) \tag{39}$$

and the reversible cell voltage has a temperature dependance described by:

$$\frac{\triangle S}{nF} = \frac{\partial U}{\partial T} \tag{40}$$

where S is the entropy. By substituting (39) and (40) into (38) the following equations is produced:

$$Q_{\mathrm{EC}} = \left(\triangle H_{\mathrm{i}} - \left(\left(\triangle H_{\mathrm{i}} - T\frac{\partial U}{\partial T}nF\right) - \eta\left(nF\right)\right)\right) i_{\mathrm{i}} \left(\frac{1}{nF}\right) \tag{41}$$

which reproduces the enthalpy of reaction equation described in (37)

$$Q_{\mathrm{tot}} = \left(\underbrace{\eta}_{\text{Irreversible}} + \underbrace{T\frac{\partial U}{\partial T}}_{\text{Reversible}}\right) j^{\mathrm{Li}}. \tag{42}$$

At this point, the literature generally describes the two terms, shown in (42), as irreversible and reversible. The irreversible term is from the overpotential of the cell, the difference between the actual voltage and the voltage of a completely reversible process, which is attributed to ohmic losses, charge-transfer overpotentials, and mass-transfer limitations [5]. The reversible term is from the entropic heat, related to the entropy change in the cell that occurs with SoC and temperature.

This term then creates the total heat developed from the electrochemical reaction. The second and third terms in the heat generation equation correspond to Joule heating, derived from the electrical conduction.

$$Q_{\text{Joule}} = i_{\text{s}} \nabla \phi_{\text{s}} + i_{\text{l}} \nabla \phi_{\text{l}} \tag{43}$$

where

$$i_{\text{s}} = \sigma_{\text{s}}^{\text{eff}} \nabla \phi_{\text{s}} \tag{44}$$

and

$$i_{\text{l}} = \kappa_{\text{e}}^{\text{eff}} \nabla \phi_{\text{l}} + \kappa_{\text{D}}^{\text{eff}} \nabla \ln c_{\text{l}}. \tag{45}$$

$$\tag{46}$$

These sources of heat generation are applied to the electrochemical model and used to estimate the heat generated from each component of the cell. The spatial average of the heat generation is then used as the heat source in the temperature calculation. From the model it can be seen that the reaction heat generation that is irreversible is the largest source of heat generation. This is a result of the overpotential created during charging and the profile of this heat generation is largely dependent on the open circuit potential of the positive and negative electrode. The entropy coefficient

$$\frac{\partial U}{\partial T} \tag{47}$$

which is used to calculate the reversible heat generation is determined from experimentation. One of the proposed benefits of pulse charging is that it can be used to lower the overpotential in the cell by lowering the concentration gradient. This is suggested to lower strain damage to the electrodes, but will also lower the heat generated in the cell by lowering overpotential, because it is the dependent feature

of the reaction heat. Since temperature is a known cause of cell life degradation and can be modeled easily, this is one possible way to analyze the effectiveness of a pulse charging profile. Another important takeaway from these equations is that all three sources of heat generation are dependent on the current. Since pulse charging will require a higher current than CCCV to maintain the same average current, whatever benefits which are produced from pulse charging in terms of lowering heat generation must offset the negative impact of the higher current. This is particularly true in Ohmic heating, were the heat generation is proportional to i squared.

With the heat generation terms known, the heat equations, see (48), can be solved.

$$\rho C_{\mathrm{p}} \frac{\partial T}{\partial t} = \lambda \frac{\partial^2 T}{\partial x^2} + Q_{\mathrm{irrev}} + Q_{\mathrm{rev}} + Q_{\mathrm{Joule}} \tag{48}$$

where ρ is the density, C_{p} is the specific heat, and λ is the thermal conductivity.

The boundary conditions are simple convection using an estimated heat transfer coefficient for natural convection, h, and described as

$$-\lambda \frac{\partial T}{\partial x}|_{x=L_{\mathrm{batt}}} = h\left(T - T_{\mathrm{inf}}\right) \tag{49}$$

$$-\lambda \frac{\partial T}{\partial x}|_{x=0} = h\left(T_{\mathrm{inf}} - T\right). \tag{50}$$

CHAPTER IV

AGING MECHANISMS

4.1 Introduction to Aging

To understand how pulsed charging is beneficial to cell lifetime, it is necessary to introduce the methods of cell aging. There are many mechanisms which contribute to the aging of lithium-ion cells, which are characterized as either capacity fade or power fade. Power fade is a loss in the ability of the cell to rapidly supply energy and is directly related to impedance growth, while capacity fade is a loss in the total energy storage and results from active material becoming inactive [7]. For this thesis, capacity fade is of greater interest. The two largest sources of capacity fade typically cited are deterioration of the positive electrode active material and the formation of the solid electrolyte interphase (SEI) layer on the negative electrode surface (impedance growth at the negative electrode). The critical area where the side reactions take place that are associated with aging is at the electrode/electrolyte interface [7]. Other aging mechanisms that occur during typical operation are loss of contacts at both positive and negative electrodes, changes in active material of the negative electrode, chemical decomposition of the electrodes, and surface film modification at the positive electrode [44]. In addition to these mechanisms which will always occur, batteries operating under certain conditions will also be subjected to lithium plating and dendrite growth [44]. These sources of aging will be affected by the environment in which the cell operates, as well as the operating conditions such as rate of charge and discharge, extent of discharge, and the ratio of charge to discharge rate.

Another distinction that must be made when studying cell aging is between calender aging and cycle aging. Calender aging is a result of the cell sitting, not during operation. As a cell sits there is a measurable loss in the capacity, and this will depend on the SoC and storage environment. Cycle aging is an irreversible loss of capacity due to the operation of the cell, and will be the main focus of this thesis, as this is what is intended to be reduced by pulsed charging. Aging is monitored during cell operation through capacity fade, impedance rise, which can be done through simple DC resistance measurements or through electrochemical impedance spectroscopy (EIS), and changes in the overpotentials. The following will be a review of these aging mechanisms and the parameters which impact them.

4.2 Aging at the Anode

4.2.1 Aging from SEI Formation

One of the largest forms of cycle aging occurs at the interface between the negative electrode and the electrolyte. The voltage operating range of lithium-ion batteries is known to be outside the stability range of the electrolyte components and causes the reduction of the electrolyte at the electrode/electrolyte interface [44]. When the electrolyte is reduced, it decomposes and interacts with the anode material and lithium ions forming a solid film which covers the particles of the anode, termed the SEI layer. This layer is beneficial to the lithium-ion battery because it separates the anode and electrolyte, preventing further decomposition, but in the process also consumes lithium ions and impacts the performance of the anode by adding some small resistance to the intercalation of lithium ions, as they must then diffuse through this layer. The majority of this formation occurs within the first couple of cycles when the most capacity is lost, however, the layer does not entirely prevent all electrolyte particles from passing through and the thickness of this layer will increase with cycling,

although at a much lesser rate [44]. Additionally, the SEI layer will crack as a result of volume changes in the anode from the intercalation of lithium ions. When this occurs, the SEI layer is immediately repaired as the anode surface becomes exposed, but in doing so additional lithium ions will be consumed resulting in further capacity fade [7].

The formation of the SEI is affected by both the current rate applied and the temperature at which the cell operates. Increased temperatures cause changes in the morphology and composition of the SEI layer, which will cause it to breakdown or dissolve [44]. The choice of electrolyte material and anode material is important, as this will change the way they interact. Optimized choice of materials and additives will improve SEI stability. This is also an area where cathode and anode interaction is important; previous studies have found transition metals from the cathode in the anode SEI layer, changing the SEI stability [44]. As mentioned, this stability is important as any degradation of the SEI layer will result in further lithium consumption and capacity loss as it is repaired.

4.2.2 Additional Mechanisms at the Anode

Other sources of aging which occur at the anode have a much lesser effect on the aging process. The electrode composite itself can be damaged due to volume changes, resulting in the interconnects becoming separated and leading to increased impedance. The effects of this are expected to be small, as volume change is generally less than 10 percent. The greater sources of aging from the anode active material is due to graphite exfoliation (layers become completely separated, under extreme intercalation conditions), which results when the electrolyte reduction occurs within the anode material. This, along with when gas evolution occurs inside the anode can causes particles to crack and rapid capacity fade to occur [44]. Other studies have shown that by changing the chemistry of the negative electrode, the capacity fade can be influenced

significantly, which shows that the choice in negative electrode is also important for battery aging, not just the formation of the SEI layer. Additionally, lithium corrosion can occur at the anode which causes it to become immobile and results in further capacity loss.

4.3 Aging at the Cathode

Describing the aging mechanisms from the cathode is more difficult, as they will heavily depend on the chemistry. While the graphite anode will be relatively similar between manufactures, the cathode chemistry will vary widely both in overall chemistry and what additives are included to improve stability. In the case of the Panasonic NCA cell, which consists of lithium, nickel, cobalt, and aluminum, each metal plays a particular role. The most apparent metal is the nickel, which is generally about 80 percent of the metal composition, and is used to give the cell a higher capacity. However, nickel produces a very disordered reaction during lithium intercalation. As a result, cobalt is added, which is generally about 15 percent of the metal composition, to stabilize the layer structure, as the transition that would occur without it leads to large anisotropic voltage jumps and as a result capacity fade. Aluminum, which comprises the remaining 5 percent of the composition, is added to reduce volume changes [44]. Most aging research seems to be based around the $LiCoO_2$ chemistry, which is the most popular chemistry, but today NCA is becoming much more used for its role in electric vehicles due to its higher capacity capability. What follows is a general review of cathode aging mechanisms and when possible, the specific affects from the NCA chemistry.

There are considered to be three principle forms of aging from the cathode material, first is structural damage that results from cycling, second, chemical decomposition and dissolution reactions, and third, surface modification [45]. Beginning with structural damage, volume variations in the positive electrode contribute to aging by inducing loss of electrode contacts between particles of active material and the conductive additive network [7]. This is expected to play less of a role for this particular chemistry as volume changes are expected to be kept fairly low and past studies have shown that $LiNi_{0.85}Co_{0.15}O_2$ chemistries do not experience phase transition during lithium ion extraction and insertion [12]. Still, many sources have cited cracking of cathode particles and a loss of interparticle contact as an important source of aging in the cathode [38]. When a particle cracks or a chemistry becomes disordered, lithium ions can become inactive and diffusion channels can be cutoff which will limit the utilization of the active material and increase aging.

Another cause of aging which is widely suggested is the formation of a SEI layer on the cathode, as impedance measurements have shown considerable increases in the cathode and changes in the composition of the surface of active material have been noted [38]. One study which noticed the formation of the SEI layer on a $LiCoO_2$ chemistry claimed that this formation occurs due to high potentials between the cathode and electrolyte in a fully charged cell, and during this, the electrolyte decomposes on the surface [22]. Many of these studies have mentioned the impact of high SoC, as well as high voltage and high temperature, on the formation of the SEI layer and on the appearance of phase changes in the chemistry. This is what causes there to be an upper voltage limit in the charging of lithium-ion batteries and also resulted in the suggestion by many of these sources, that lowering the cutoff voltage will decrease capacity fade [38]. If overcharged, metal ions will migrate into the delithiated layer of the host structure [45].

While it is less clear which sources of aging will be apparent in the cathode, it is an important area of focus. Many studies which have analyzed the electrode in postmortem analysis have found the impedance increase in the positive electrode to be greater than that of the negative electrode, suggesting that the deterioration of the positive electrode was more severe and as a result made a greater contribution to capacity decay [44] [36].

4.4 Cycle Fade Profile

Capacity fade does not occur linearly with cycle number, from the cells tested in this thesis initial capacity loss is very low but, about two-thirds the way through the cycle life, a sharp increase in capacity fade occurs after which the cell will quickly reach the 80 percent cutoff. Lifetime capacity plots of lithium ion cells will tend to have 4 distinct regions of capacity fade. The first region is very short, only lasting the first few cycles as the SEI layer is initially formed. After that two very flat regions form with very slow capacity fade, followed by a fourth region of rapid capacity loss. Not all cells see the fourth region, as the 80 percent capacity cutoff has often already occurred [38]. One potential cause of this sharp increase in capacity fade is attributed to heavy deposits of lithium metal on the surface of the electrode through a process called lithium plating [7]. In lithium plating, the diffusion rate in the electrode is too slow and lithium builds up on the surface, eventually reacting and becoming inactive. As the cell ages and the SEI layer on the anode becomes thicker, the micropores of the particles can become clogged reducing the surface area for current to flow. This can increase the reaction rate above the diffusion rate which increases the possibility of dendrite growth and lithium plating. Another possible reason for increased capacity fade with cycling is, as the Ohmic resistance of the cell increases, the voltage drop increases which will result in the voltage cutoffs in charge and discharge being

reached faster, resulting in lower capacity measurements. These will also be chemistry dependent properties, as another study which focused on the regions of capacity fade attributed the early stages to SEI growth, but the sharp increase was attributed to deterioration of the electrode, and it was stated that reference electrode analysis showed no lithium deposition occurred [31].

Other factors which can influence the rate of capacity fade are the environmental and operating conditions described previously. To save time in experimentation of battery cycling, methods are desired to increase the rate of capacity fade without altering the mechanisms of aging [38]. The most influential way to do this is through increasing the temperature which has been shown to increase the rate of aging by 8 times. Other methods used are selecting higher charge current (four time faster capacity fade), increasing the ratio of charge to discharge rate and the discharge rate (three time faster capacity fade each), and increasing the depth of discharge the cell is cycled to (two times faster capacity fade).

4.5 Summary

From the literature review, many causes of aging have been proposed, although the exact sources and contribution of each is still a topic of much research. These mechanisms are heavily dependent on battery chemistry, but since most cells use graphite as the anode the sources of aging attributed to the negative electrode are better known, and the positive electrode will be the source of most variation between cells. The most significant source of aging at the anode is through the formation of the SEI layer and while the anode will also experience volume changes, this will be more likely to cause aging through destruction of the SEI layer than the anode itself. The bigger challenge comes when determining the source of aging at the positive electrode, particularly since numerous studies have found the cathode to be the larger source of

aging. Making it even more challenging to match the sources of aging to a particular battery, many of the issues associated with aging at the cathode can be mitigated by selecting an optimized chemistry, however, the exact chemistry and additives are rarely known [45]. The most common cause of aging of the cathode material is deterioration of the electrode, which will cause the active material to become inactive and as a result increase in capacity fade. It will also cause the internal stability of the battery to breakdown and increase Ohmic overpotential. It is necessary to optimize the choice of charging parameters, as all of these aging mechanisms can be increased through environmental and operational conditions.

CHAPTER V

PULSED CHARGING LITERATURE

5.1 Introduction

To begin analyzing the effectiveness of pulse charging, a review of previous publications on pulse charging was conducted. Multiple papers have been published analyzing the effects of pulse charging on lithium-ion batteries with varying results as to whether the pulse charging is beneficial or detrimental when compared with conventional constant current constant voltage (CCCV) charging. The proposed benefits of pulse charging are faster charge and longer life. These are thought to be achieved by decreasing the concentration gradient within the electrode and electrolyte by applying reverse current or resting periods in which the cell can equilibrate. Additionally, it is believed that the decreased concentration gradient allows lithium ions to insert more uniformly throughout the electrode, more effectively packing and utilizing the active material. In addition to lowered overpotential, this causes less physical stress on the electrode. Other proposed benefits have been that cell life and efficiency can be improved through preventing lithium plating and dendrite growth [2] [37]. No clear method was developed to produce the optimal results and in past papers the choice of pulse parameters have been largely from guess and check [9].

5.2 Review of Past Studies

5.2.1 Studies using Enrev charging

Studies have been conducted experimentally and computationally to analyze whether pulse charging will be effective producing conflicting results. Here we will discuss two studies which used a pulse charge developed by the Enrev Corporation. One study

conducted using the pulse charging technique found that the cell life and charging time where both considerably improved when compared with CCCV charging [23]. They concluded that short discharge and rest periods included in a constant current (CC) charging routine produced a quasi-equilibrium state during charging, resulting in lower overpotential from concentration gradient. This allows the cell to be fully charged once reaching the cutoff voltage and eliminating the need for a constant voltage (CV) charge section, considerably reducing charge time. They also found that the pulse charged battery produced a higher capacity indicating the active material was more thoroughly utilized than when under CCCV conditions. Finally, they concluded that the capacity fade from pulse charging was improved, although starting out slightly higher, as cycling continued the fade became more stable, charging the cell for 1600 cycles, compared with only 700 for CCCV. They also analyzed the aging mechanisms through cyclic voltammetry (CV), SEM, and X-ray diffraction (XRD). Through this, they had some unexpected results but ultimately concluded that aging was improved by pulsing. The pulse charging routine, which charged at 0.5C, had the longest lifetime, but also the highest interfacial resistance. They attributed this to the higher discharge capacity it produced, which resulted in more cations forming at the positive electrode surface during the fully charged state, and as a result was more likely to react with the electrolyte to form a passive layer. Through the CV analysis they found the 0.5C pulse charged cell to have the lowest deterioration of the electrode material and electrode/electrolyte interface. Through XRD analysis, they concluded the 1C pulse charge cell had the best ordered cathode and least inactive cathode material, which they attributed to the pulsing lowering the polarization and allowing the ions to more uniformly extract and reinsert into the electrode. Through SEM analysis of the anode, they determined that no process considerably altered the structure of the graphite but a thicker SEI layer was formed on the CCCV charged anode.

Another study which used the Enrev charging protocol claimed the pulse charging method prevents the reduction to metallic lithium and oxidation of the electrolyte under overcharging conditions [36]. Additionally, they claimed that the pulse charging technique will improve charging kinetics by lowering ohmic drop and polarization resistance, as well as enhancing capacity and preventing increases to internal resistance. They had somewhat conflicting analysis from the previous study, in that both used a Sony US18650S cell but the previous study claimed that lithium diffusion into the anode was the rate limiting step, where as this study claimed through CV analysis, diffusion is only limiting in the discharge direction. Additionally, the previous paper showed the electrode charged under pulse had the greatest resistance increase. However, both make the same claims of enhanced capacity and improved concentration polarization. This study showed that pulsing reduced the capacity fade to a rate of 0.009 percent per cycle from the rate of 0.04 percent per cycle using DC charging after 800 cycles. A comparison of cathode and anode data showed that the cathode was the main source of resistance in the cell and that the increased resistance was a result of electrode interaction with the electrolyte. The authors suggested the ENREV technique is shown to decrease oxide layer formation, which is in agreement with the other study, although these authors also mention SEI formation on the cathode, which is not included in the previous work.

5.2.2 Alternative Studies

Other studies have found conflicting results as to whether pulsed charging can be effective. One study conducted by Savoye et al. found that pulse charging is detrimental to the cell efficiency and, due to increased overpotential caused by the higher magnitude charge current necessary for pulsing, results in reaching the upper voltage limit prematurely and, therefore, lower charge capacity during the CC phase [39].

The parameters most strongly influencing these results were the form factor, which is defined as the root mean square current (I_{rms}) divided by the time averaged current (I_{mean}), and the signal period. When comparing the pulse charging method to the CCCV method on the basis of equivalent I_{mean}, the I_{rms} is higher for the pulse charge. A higher I_{rms} requires a greater energy throughput than an equivalent time charged with CC, and was therefore less efficient, and results in a higher overpotential, as mentioned above. The study did not find pulse charging able to more effectively utilize the active material or produce greater capacity than the CCCV method, in direct opposition to the results found with the Enrev method. As mentioned, they also found the pulse method to produce a greater overpotential, another conflicting point, and further stated that a higher I_{rms} could produce a higher temperature, directly resulting in a faster loss of capacity. Additionally, the study concluded that the longer the pulse and the less frequent, the more detrimental to cell efficiency and overpotential.

The method of pulse charging is also an important factor which could cause the conflicting results. Other studies have been conducted around modeling the cell under pulse charging conditions. Using these models, various parameters of the pulse charging profile were able to be analyzed. One article used an electronic network model, in which the cell is represented using analogous electronic circuit elements. This study found some similar results to the Savoye study [39], that the higher current can cause higher temperature and that the overpotential can be slightly increased under pulse charging [11]. Their concern was that the higher overpotential from pulse charging would exceed the upper voltage limit and cause detrimental side reactions, but they found this to be a negligible effect. Through their analysis, they determined that pulses shorter than the millisecond range are almost completely buffered and effects on the concentration gradient within the battery started changing on the time scale

of seconds.

In a study by Purushothaman and Landau [37], they attempted to better understand the effect of pulse charging through an electrochemical model.They developed a model for the lithium concentration in the negative electrode, considering diffusion through the SEI layer into the graphite anode. Only the negative electrode was analyzed because the ability of lithium to diffuse through the graphite was considered the rate limiting factor during charging and necessitates the CV stage. In this study it was determined that no benefit was produced for the concentration gradient from pulse charging when the amplitude of the current and length of the pulses were constant. However, when the pulse duration and current amplitude were not held constant, the concentration overpotential was decreased. Two different methods were applied, the first in which the battery would charge under CC phase but with varying pulse durations. Charging occurred until the lithium reached near saturation at the anode-SEI boundary, when a rest period would begin until the boundary concentration dropped to some preset value. The higher the concentration value, the faster the cell completed charge. Maintaining the boundary concentration near saturation provides a higher driving force for lithium diffusion into the electrode (it is allowed to lower under rest period to decrease the concentration gradient and overpotential). This method is difficult to implement however, as it is difficult to measure the concentration level of lithium at the boundary during charging. The second method implemented attempted to produce the same results by holding constant the pulse duration but lowering the current amplitude for each charge pulse at a linear rate. This was also found to be successful at lowering overpotential and charging faster (0.85h vs 3h) than CCCV. Another method which was applied in this study, and supported by a study from Notten et al. [31], found not pulsing and beginning charge from a low SoC at a very high rate and gradually lowering was effective. In the Notten

paper, cycling was started with CV phase charging at a preset value for the first 5 to 10 minutes, at which point the charging method changed to CCCV charging. In lifetime studies they conducted, no difference in aging was noticed between the faster charge, which they termed boost charging, and the CCCV method, which indicates that aging mostly occurs in the high SoC region when the boost charging method would have changed to CCCV charging.

One study attempted to find the optimal frequency through ac-impedance measurements [9]. The cell impedance is dependent on the frequency of the current applied. Through using a frequency that minimizes the impedance, the energy lost in converting electrical energy to chemical is also reduced. Using the minimizing frequency the study found the cell could be charged faster, more efficiently, and with lower heat generation when compared with a CCCV method. This study also used the method of sinusoidal-ripple-current (SRC) instead of pulse current, which consisted of charging the cell with a current of a sinusoidal wave, with minimum current 0 and peak-to-peak difference I_{max}. They found the SRC method more effective than pulse charging, but also used the pulse method at this frequency and found it more effective than CCCV. The duty cycle was not optimized, but used at 50 percent to match the sinusoidal charge method. The SRC method also resulted in lower capacity fade than CCCV, the pulse lifetime data was not reported.

5.3 Summary of Pulse Charging

From these studies it was determined that the effectiveness of pulse charging will most depend on duty cycle, pulse amplitude, reverse pulse application, and pulse duration. Numerous studies have been conducted to analyze the effectiveness of pulse charging producing varying results and few listed the reasoning behind their choice of pulsing

parameters. The objectives of these papers have also been mixed, some attempting to charge the cell faster with no increased rate of capacity fade and others attempting to extend the life of the cell. The positive benefit of pulsed charging are claimed to be that the overpotential can be lowered through improving cell kinetics, and that the aging mechanisms can be reduced by more effective utilization of the active material and reduced thickness of the SEI layer.

CHAPTER VI

MODEL DEVELOPMENT

6.1 Introduction

Using Comsol Multiphysics the equations detailed in chapter 3 were implemented into a 1D geometry of 3 domains, for the negative electrode, separator, and positive electrode, and two 2D geometries of length of the electrode and radius of the electrode particles, as described in Fig. 9. As previously described, the intention of this model was two fold. First, by reproducing the experiments that were being conducted, additional information about the internal dynamics of the cell were able to be analyzed which could not be through experimentation alone, as only voltage, current, and temperature are observable during testing. Second, using the model, predictions could be made about pulse charging effectiveness before testing needed to be conducted, making experimentation more effective. In order to develop the model, material parameters were collected for the Panasonic cell and testing results were compared with experimental values to validate the effectiveness of the simulations.

6.2 Parameter Selection

The Panasonic NCR 18650b cell is believed to be a NCA cathode and graphite anode, however detailed material parameters of the cell are not published, as this is proprietary information. Therefore, the model parameters were selected from a literature review of prior research from authors that developed models using similar cell chemistry. Ultimately, a few different sources were used to estimate the relevant parameters for the model and some parameters were altered in order to fit the experimental data for charge and discharge. For the electrolyte and negative electrode, the parameters

were very consistent amongst publications dealing with lithium-ion battery modeling, as these are fairly consistent for most manufacturers and battery chemistries. Most of the parameters used for the graphite electrode and separator were taken from a publication on electrochemical-thermal modeling for a $LiFePO_4$ cathode battery, with a graphite anode, by Saw et al. [40]. For the electrolyte parameters and most SoC dependent parameters (κ, $U_{\text{pos,ref}}$, $U_{\text{neg,ref}}$, $^{\partial U}/_{\partial T_{\text{neg}}}$), the built-in Comsol material library was used. As a result of this, the Comsol values were also used for the maximum concentration of the electrodes, as the SoC is directly dependent on this value.

The cathode material parameters were much more difficult to determine, as these vary widely with chemistry and battery manufacturer. Additionally, NCA chemistry was not as popular to model as other cathode materials, such as $LiCoO_2$ or $LiFePO_4$. For the cathode material parameters used in this thesis, most values were taken from a publication by Bernardi et al. in which a proprietary cell was being tested and modeled by the Ford Motor Company [6]. To supplement this information, some parameters were taken from the Comsol library and another publication by Shadman Rad et al [42]. The publication by Shadman Rad was particularly useful for the entropic coefficient, $^{\partial U}/_{\partial T_{\text{pos}}}$, necessary for reversible heating and OCV temperature dependence, which is rarely published and was necessary to most accurately model the thermal profile.

In addition to parameters which were collected from literature review, some values were also measured directly or an estimate was determined from literature or measurement values, then altered to best fit the experimental data. SEM measurements were used to analyze the positive electrode, negative electrode, and separator; from this the thickness was determined and an initial estimate for the particle radii were

made. The other parameters which were altered to fit the data where the heat transfer coefficient h, the applied current density $i_{a,i}$, the initial concentration for each electrode c_o, and the reaction rate coefficient k. The same k value was used for both the cathode and anode, as this value varies by orders of magnitude in literature and is mainly used to improve the data fit. The heat transfer coefficient used was h=0.45 $^{W}/_{m\cdot K}$, which is slight low, as most papers published values between 1 to 10 $^{W}/_{m\cdot K}$ for natural convection conditions [8].

6.3 Model Validation

In order to validate the model, the voltage and temperature profiles produced by Comsol and from experimental charging were compared. Due to the lack of knowledge of the parameters for the Panasonic cell and from the lack of observables during testing, producing a very accurate model was difficult. However, the main purpose of the model was to examine the effects of pulsing which can be done without the exact parameters, since pulses can still be applied and the internal effects realized. The main issue is then, the values that could produce effective results in the simulation may not be the same values to produce effective results in experimentation, but will still give an idea of how pulsing effects the internal dynamics of the cell.

When validating the model, the 1C CCCV voltage profile was considered the most important to match, followed by the 1C CCCV temperature profile and 1C mean pulse voltage and temperature profiles. In this case pulse profile 7 (PP7) was used, the particulars of which are described in greater detail in chapter 7. In addition to the data which was used to validate the parameters selected, the results were also compared to experimental data collected at the C/3.33 rate to assess how the model compares outside of the desired charging rate range.

The 1C CCCV voltage profile comparison is shown in Fig. 11. From this it is apparent that the voltage profile matched well with the experimental results. Several factors affected this, however, most of the values gathered from the literature mentioned above were unchanged. The main parameters altered to improve the voltage profile were the initial concentration, which was important for fitting the first 600 seconds of charging when the voltage profile experiences the greatest change, and for matching the time to charge. The applied current density and reaction rate were also altered, these were used to ensure the voltage magnitude was accurate.

Since the electrochemical area of the electrode is unknown, the true current density was unable to be determined. As a result, the current density initially applied to produce a 1C current was based on an estimate from the following equation

$$i_{1\mathrm{C}} = F\epsilon_{\mathrm{s,pos}}L_{\mathrm{pos}}\left(c_{\mathrm{s_{max},pos}} - c_{\mathrm{s_{min},pos}}\right)/3600\,[s]\,, \tag{51}$$

however, to fit the data the applied current density needed to be increased, which resulted in a C-Rate of 1.14. This change is rather large, however, it is considered acceptable here because many of the unknown parameters are interrelated, particularly k, r_p, and i_{app}, and errors made in estimates to one of these parameters will also cause error in the others. This makes the model less accurate, but by using best estimates and validating the model, the concept of pulsing can still be analyzed using it. The value for $c_{\mathrm{s_{min},p}}$ was estimated to be 0.3, the Bernardi estimate was 0.36 and the Comsol estimate 0.23. The initial SoC values for the positive and negative electrode, which were used to determine the $c_{0,i}$ values, were 0.93 and 0.2 respectively.

The temperature profile was also compared, which was not quite as accurate. The overall temperature rise was made to match well, however, as mentioned previously, to achieve this a convective heat transfer rate of h = 0.45 was used, which is slightly low. This suggests the heat generation calculated was lower than experienced in the

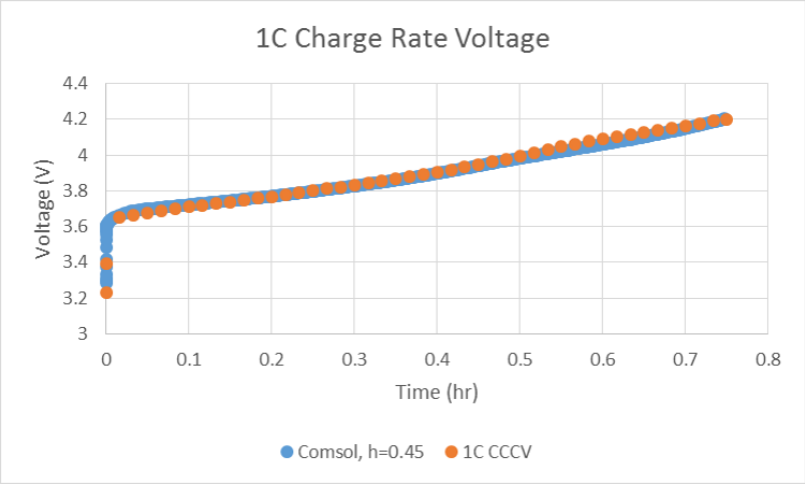

Figure 11: Voltage profile validation of Comsol model at 1C charge rate.

cell. However, the overall shape of the temperature plot is accurate, although the experimental results produced a more wavy profile, shown in Fig. 12. This could be caused by changing environmental conditions, or certain material parameters that change with temperature or SoC which were not realized in the simulation.

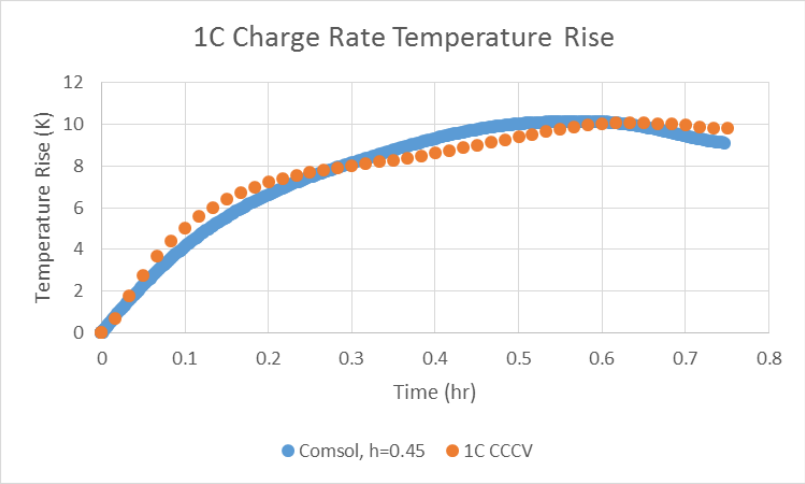

Figure 12: Temperature profile validation of Comsol model at 1C charge rate.

Once a reasonable 1C CCCV model was produced, validating the results to match the pulsing profile was conducted. This was considerably more difficult for a number of reasons. One issue had to do with the computation complexity of the model and the time scale needed to model the pulses. Within Comsol, the Events physics was

used to account for the sudden boundary condition shifts. Without this, the model would reach tolerance errors whenever the pulse changed. This also allowed for a different time step to be applied to the charge section than was applied for the discharge and rest sections, which needed to be much smaller due to the short time the pulses were applied, generally on the millisecond scale compared to the seconds time scale for charging. Through this the solution time was also made considerably faster. Still, the largest time steps were limited to 0.1 seconds, with most being much smaller, which required a considerable solution time, as the model simulated about 2700 seconds. This also created memory issues, which required the model to be segmented into smaller time scale models, generally in the range of 600 second intervals.

Due to these solution difficulties, and the lack of material properties, the pulsing model was never quite as accurate. As it can be seen in Fig. 13 the pulsing voltage is fairly accurate in the early stages, but becomes less accurate at high states of charge, when the voltage change from the discharge pulses in the simulation were overestimated. Fig. 13 needs greater description to fully understand. Due to the way the pulses were implemented in the model, when the sudden boundary condition change would occur, it would take numerous steps to calculate the new voltage, and as a result every small voltage step that occurred was recorded. There was no effective way to remove they values from the solution, and as a result what appears as a very thick voltage profile is produced. What is important from Fig. 13 is the top and bottom of the thick blue voltage profile, which will correspond to the charging voltage, and discharge pulse voltage respectively. The data points in between correspond to the solution steps, described above, and unfortunately as a result of this the rest pulse voltages become lost in this data. The experimental profile also needs further description; in this case it appears three separate voltage profiles were plotted. The three lines correspond to the voltage recorded during charge current (highest voltage),

the voltage recorded during the rest pulse (middle voltage), and the voltage recorded during the discharge pulse (lowest voltage). To keep the plots as clear as possible, this is described in Fig. 19 instead of Fig. 13.

To improve the accuracy of these pulses, the particle radius were altered. The values estimated from the SEI measurements were 5 and 10 μm for the positive and negative electrode respectively, although a wide range of particle radii were observed. From the Comsol material library the estimates were 5 and 12.5 μm respectively, and from various other sources the 12.5 μm estimate for the anode was frequently cited. The values which were chosen for the best fit were 2.5 and 8 μm for the positive and negative electrodes respectively. When these changes were made, it was also necessary to alter the reaction rate, k, again and refit the initial voltage profiles. The plots shown in Fig.11 and Fig.12 were produced after these corrections were made. No additional changes were required to fit the temperature profile produced from the PP7 charge profile. The results were slightly less accurate than for the 1C simulation, but still matched the peak temperature rise well, as seen in Fig. 14.

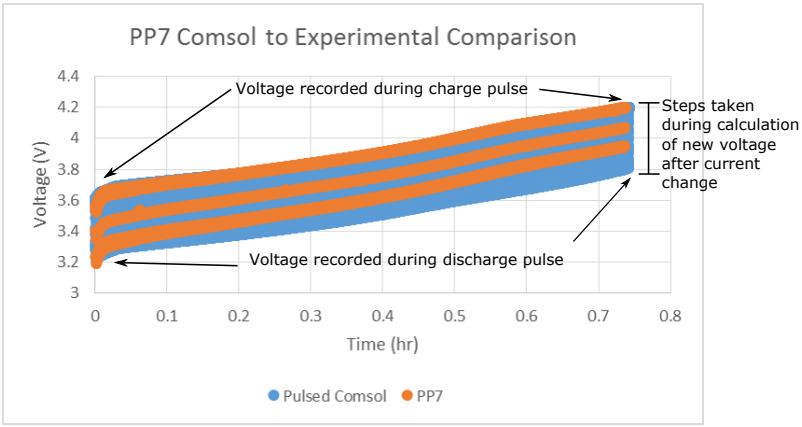

Figure 13: Voltage profile validation of Comsol model for PP7 pulse profile. The relevant data from the pulsed Comsol profile is the upper limit and lower limit of the voltage plot. The points in between were the steps taken by the solver in calculating the new voltage during the change in boundary conditions.

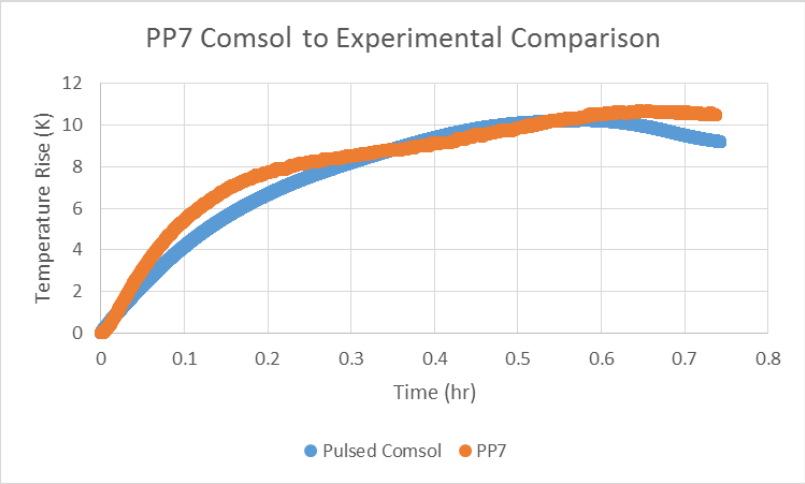

Figure 14: Temperature profile validation of Comsol model for PP7 pulse profile.

The applied current was divided by 3.33 to compare with experimental results at C/3.33 charging. The voltage profile was not as accurate as for 1C, underestimating the initial voltage and reaching 4.2 V in 2.84 hours, while the experimental results ended in 2.88 hours, as seen in Fig. 15. The temperature profile produced for these results was less accurate, estimating a 2 Kelvin temperature rise compared to the 1 Kelvin recorded experimentally, as seen in Fig. 16.

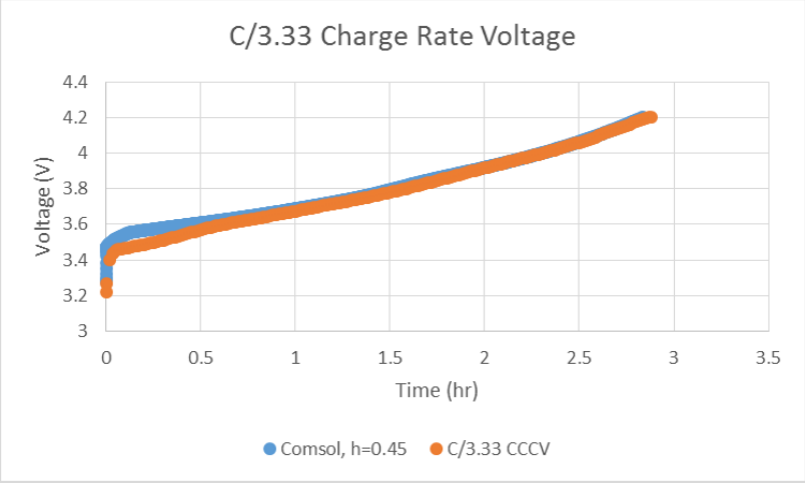

Figure 15: Voltage profile validation of Comsol model at C/3.33 charge rate.

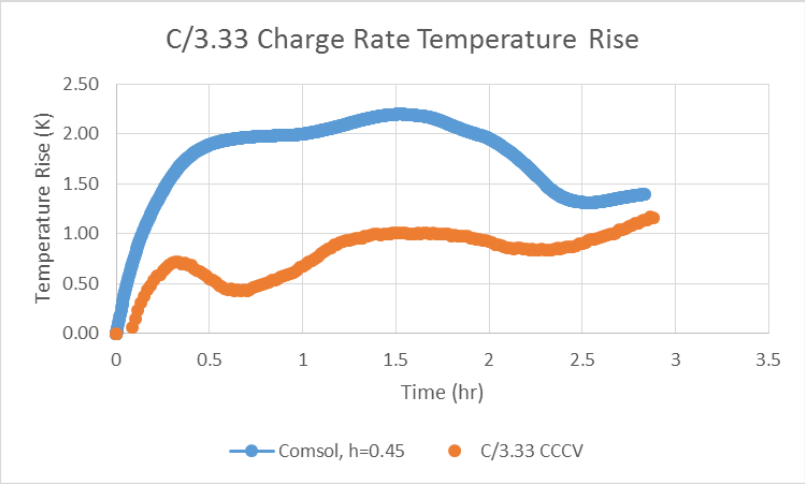

Figure 16: Temperature profile validation of Comsol model at C/3.33 charge rate.

6.4 Summary of Modeling Analysis

Due to the lack of data on material parameters for the cell, parameters had to be estimated from previously published literature, the Comsol material library, SEM analysis, and through alterations of various values made to fit the data. While the 1C charge temperature and voltage profiles were able to fit the experimental results well, the model was less accurate at simulating the cell under conditions of pulsed charging and charge rates outside the 1C range. One of the main factors missing in the simulation is how parameters change with temperature and SoC, with the simulations accounting for only the voltage and entropic heat coefficient being dependent on both, and the electrolyte ionic conductivity being dependent on SoC only. However, these errors were considered small enough to use the model to analyze the effectiveness of pulse charging and gain information on the internal dynamics of the cell. For a detailed description of the parameters used, all values and relevant graphs are included in the appendix.

CHAPTER VII

RESULTS

7.1 Introduction

In order to test the theory of pulsed charging as an effective method of improving battery aging and charging performance, various pulsing methods were investigated, both experimentally and through running the Comsol model. Using the literature review of previous works covering pulse charging, important parameters were identified which would most effectively charge the cell. The paper which showed positive results conducted by Li et al was most heavily focused on as a source to identify a pulse profile which would lead to faster charging and longer life [23]. Within this paper a patent from the Enrev Corporation was cited when referencing the charging device [34]. This patent did not go into detail on the parameters of the charging method, however another patent from the same author had listed certain parameters for pulse charging a NiCd cell [35], shown in Table 2.

Table 2: Parameters for Pulse Charging 1.25V NiCd Cell (nom. 500 mAh) [35]

I_{charge}	1.2 A
t_{charge}	700 ms
$I_{discharge}$	6 A
$t_{discharge}$	2 ms
t_{rest}	7-10 ms
Total Charge Time (0.2 to 1 SoC)	20 minutes

These parameters were not applicable for the Panasonic 18650B cells, which have a nominal capacity of 3400 mAh and a nominal voltage of 3.6 V, so they were used

as a starting guide and adjusted. To adjust, the discharge capacity and ratio of discharge to charge capacity values were held constant, these calculations are described in Eq. 52 and Eq. 53, and all other parameters were adjusted in order to maintain an average C-Rate of 1C. One factor which limited the parameter selection was the capabilities of the device, it was determined that 3 ms was the shortest possible pulse duration, but 5 ms was the first time for which more than just the transition voltage could be recorded and was therefore used for the first pulse plan. The parameters selection and equipment constraints are listed in the next section on experimentation.

From the other papers on this topic, additional constraints were considered when developing pulse plans, which were noted in Chapter 5. In order to maintain an equivalent charging current, the charging pulse current peak will need to be higher than the CCCV charge value which will result in a higher overpotential during the charge phase. Additionally, it was noted that it is important to consider the I_{rms} value because this term impacts ohmic heating and will be higher for pulse charging. From this, it was considered important to keep the charging phase current magnitude low, and the I_{rms} low, the latter also requiring a low discharge phase current.

Other terms which previous papers referenced as impacting pulsing were pulse frequency, pulse width, and charge to discharge capacity ratio. A higher pulse frequency was found to be preferred, but it was also noted if pulsing is too short any effect will be suppressed by the cell impedance. In the study by Jongh et al, they determined the millisecond range was too fast for pulsing and concentration effects were not noticed until the seconds range [11]. Additionally, in the paper by Li et al, they noted that it is important to optimize the discharge capacity and charge to discharge ratio. The reverse pulse should only discharge to the extent necessary to clear the ion build up at the surface and not overly discharge the cell during pulsing,

which would lower charge efficiency. For this reason, the ratio and discharge capacity were keep constant proportionally to the Enrev parameters.

Based on these considerations, a few initial pulse plans were developed which would test these parameters in an attempt to analyze pulse charging effectiveness, considering the charge capacity of each plan on single charge experiments and the impact of cycle life on lifetime experiments.

7.2 Experimentation

Before going into detail on the parametric experiments, it is first necessary to cover the way testing was conducted. As previously stated, a few conditions were put in place to create a fair comparison between CCCV and pulse testing. These are testing with a mean current of 1C C-Rate and, for the case of lifetime testing, 1 hour total charge time. The mean current condition was added to ensure an apples-to-apples charge comparison. Since rate of charge is known to affect aging, and will control the capacity charged in a defined time, it is necessary to ensure this is the same for each method of testing. The 1 hour limit was added to target the CC rate of interest. As stated, it is believed pulsing can improve charging by keeping the cell in the CC charging phase longer through lowering the overpotential in the cell and avoiding the 4.2 V cutoff, nevertheless a CV phase was added when necessary. The time of 1 hour was selected based off the 1C mean current condition, which is the magnitude necessary to charge the cell in 1 hour. Since part of this testing was based around fast charging, the experimentation was developed with the following idea, to what extent can each method charge the cell in one hour? This was chosen rather than simply cycling till the CC phase ended because during lifetime testing the time spent in CC will shrink as the cell ages, so to maintain a constant charge duration when cycling, 1 hour was selected. It was also necessary to limit the charge time, rather

than using a minimum current cutoff, to test the concept of rapid charge rather than simply charge capacity, as it is know that capacity lost during CC charging can be recovered during CV charging, at the expense of charge time. Additionally, in the case of lifetime testing, a constant discharge current of C/3.33 was used to ensure this did not impact aging, with discharge ending when a 2.5 V cutoff was reached. Between charge and discharge, and discharge and charge, a 30 minute pause was allowed for the cell to equilibrate. For the single charge experiments, cell aging was not an important consideration so testing simply ended when the CC stage was completed.

In addition to testing each profile, the single charge tests were also used to select the most promising testing methods for lifetime experiments. Lifetime testing requires weeks to complete and uses multiple cells, so fewer pulse plans could be analyzed.

7.2.1 Preparing the Device for Testing

These tests were conduct on battery cycling devices from BaSyTec. During testing, the cells were either placed within custom built holders or had connections added through spot welding in order to attach the wire to the cell and minimize ohmic losses. The cells were also placed within Voetsch VTL4006 temperature chambers in order to limit external factors on testing. These temperature chambers were set slightly above room temperature, generally around 24 °C. This was a shared testing environment, so the chamber temperature was selected as an appropriate level for a variety of cells, not specifically the Panasonic 18650B cell. A PT100 thermistor was placed on the surface, about halfway up the cell.

As previously stated, some literature claimed that pulsing was most effective at

high frequencies. In the paper by Chen et al. an optimal frequency of 998 Hz was used for testing [9]. In order to test these claims it was necessary to determine how quickly the battery cycling device was able to accurately and precisely apply and record pulses. The limit was believed to be 1ms, however after testing the ability to both apply and accurately record pulses, it was found to be 3 ms, with 5 ms being the first value more than one data point could be recorded. For this reason, 3 ms was used as the minimum value for high frequency test but for the majority of other tests a limit of 5ms was used.

To give a more clear understanding of what is meant by pulsing, discharge current, and resting; images of the voltage and current profile from a single pulse for the first proposed plan, pulse profile 2 (PP2), are shown in Fig. 17 and Fig. 18.

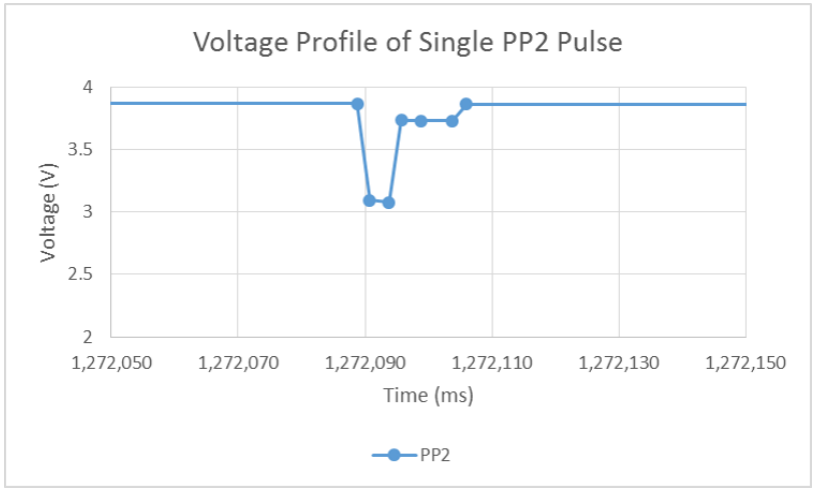

Figure 17: Snapshot of the PP2 voltage profile for a single pulse.

7.3 Single Charge Testing

The first testing completed was for single charge analysis, with the initial test being the modified version of the Enrev pulse profile, PP2. For consistency, all the pulse profiles used were titled pulse profile and then the number, abbreviated to PP and a number. The parameters which are necessary for the pulse profile are charge

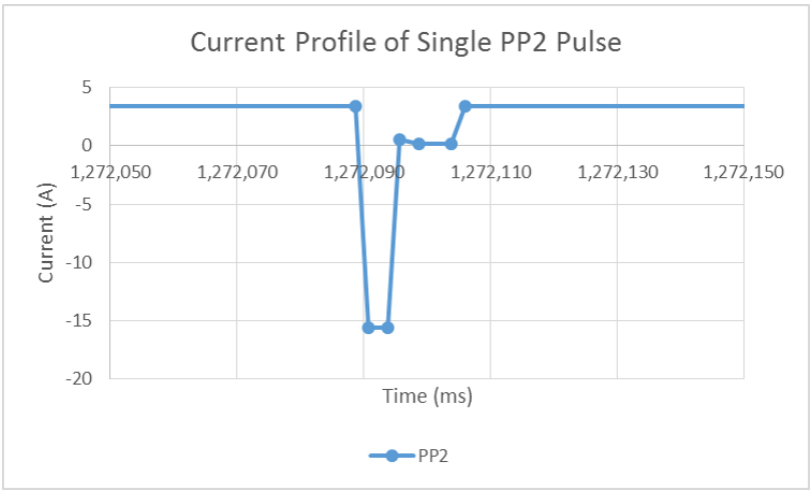

Figure 18: Snapshot of the PP2 current profile for a single pulse.

magnitude, I_{charge}, charge time, t_{charge}, discharge magnitude, $I_{discharge}$, discharge time, $t_{discharge}$, and rest time, t_{rest}. Additionally, the mean current, I_{mean}, discharge capacity, $C_{discharge}$, discharge capacity to charge capacity ratio, R, frequency, f, and current squared, I^2 are considered. As previously stated, for the first plan, the R and $C_{discharge}$ values were maintained from the Enrev patent and the I_{mean} value was held at 1 C.

7.3.1 Modified Enrev Profile: Pulse Profile 2

The values of the first plan tested, PP2, were determined as follows: first the Enrev discharge capacity and discharge to charge capacity ratio were calculated using the following equations:

$$C_{discharge,Enrev} = I_{discharge,Enrev} \cdot t_{discharge,Enrev} \tag{52}$$

$$R_{Enrev} = \frac{C_{discharge,Enrev}}{(I_{charge,Enrev} \cdot t_{charge,Enrev})}. \tag{53}$$

Discharge capacity and discharge current are both defined as positive in these equations. The discharge time for PP2 was set by the device capabilities

$$t_{discharge,PP2} = 5 \text{ ms}. \tag{54}$$

The discharge magnitude could then be determined from the condition that $C_{discharge,Enrev}$ is equal to $C_{discharge,PP2}$

$$I_{discharge,PP2} = \frac{C_{discharge,Enrev}}{t_{discharge,PP2}}. \tag{55}$$

The rest time was set to 2 times the discharge pulse time

$$t_{rest,PP2} = t_{discharge,PP2} \cdot 2. \tag{56}$$

The charge time and charge magnitude are then determined based on the condition of 1C mean current and the discharge ratio of the Enrev plan:

$$R_{Enrev} = \frac{C_{discharge,PP2}}{C_{charge,PP2}} \tag{57}$$

$$C_{charge,PP2} = \frac{C_{discharge,PP2}}{R_{Enrev}} \tag{58}$$

$$I_{mean} = \frac{C_{charge,PP2} - C_{discharge,PP2}}{t_{discharge,PP2} + t_{charge,PP2} + t_{rest,PP2}}. \tag{59}$$

By rearranging Eq. 58 and Eq. 59 the charge time can be calculated

$$t_{charge,PP2} = \frac{\frac{C_{discharge,PP2}}{R_{Enrev}} - C_{discharge,PP2}}{I_{mean}} - t_{discharge,PP2} - t_{rest,PP2}. \tag{60}$$

Now, with $t_{charge,PP2}$, $t_{discharge,PP2}$, $t_{rest,PP2}$, and $I_{discharge,PP2}$ known, by again rearraging Eq. 59 the $I_{charge,PP2}$ can be determined

$$I_{charge,PP2} = \frac{I_{mean} \cdot (t_{discharge,PP2} + t_{charge,PP2} + t_{rest,PP2}) + C_{discharge,PP2}}{t_{charge,PP2}}. \tag{61}$$

The pulsing parameters for PP2 are shown in Table 3 and the parameters that were targeted as being most influential on the effectiveness of pulse charging are shown in Table 4.

It is also important to describe how the I^2 value was calculated. This value has the same relevance as I_{rms} which was described previously, but is left in the I^2 form to emphasis its role in Ohmic heating

Table 3: Parameters for Pulse Profile 2 (PP2)

I_{charge}	1.024C (3.430 A)
t_{charge}	1641 ms
$I_{discharge}$	4.8C (16.08 A)
$t_{discharge}$	5 ms
t_{rest}	10 ms

$$I^2 = \frac{I_{charge}^2 \cdot t_{charge} + I_{discharge}^2 \cdot t_{discharge}}{t_{charge} + t_{discharge} + t_{rest}}. \tag{62}$$

The frequency is simply the inverse of the total time to complete a pulse

$$f = \frac{1}{t_{charge} + t_{discharge} + t_{rest}}. \tag{63}$$

Table 4: Targeted Parameters for Pulse Profile 2 (PP2)

f	0.6 [Hz]
I^2	12.4 $[A^2]$
$C_{discharge}$	80.4 [Ams]
R	0.014

The results from the test of PP2 are shown in Fig. 19 and Fig. 20 which compares the voltage profile of PP2 to a cell charged at 1C under CCCV conditions. First, it is important to clarify what is being shown in the voltage profile for pulse charging in Fig. 19; it appears that there are three distinct voltage profiles which are all identified with blue dots to represent PP2. These three lines actually correspond to the three phases of pulsing; the highest voltage is data recorded while charging, the middle line is data recorded while no current is applied (rest), and the lowest voltage line is data recorded during the discharge pulse.

From these results it can be seen that the charging voltage is consistently higher

than the CCCV charging voltage. This increase in voltage is attributed to the additional overpotential cause by the higher current required to maintain the mean 1C current during pulsing. The large gap in voltage magnitude between the discharge voltage and rest voltage when compared to the difference between the rest and charging voltage is also a result of the strong influence of Ohmic resistance. The discharge rate is about 4.8 times the charging current and as a result the Ohmic overpotential during discharge is much larger than the overpotential caused by charging. The main conclusion made from this voltage plot is that under these pulsing conditions, the pulsing was ineffective at extending the CC charge time, and was actually detrimental to charging due to the additional Ohmic overpotential causing the 4.2 V cutoff to be reached prematurely. Since the upper voltage limit was reached earlier for pulsing than for CCCV charging, the charge capacity under pulsing was also lower.

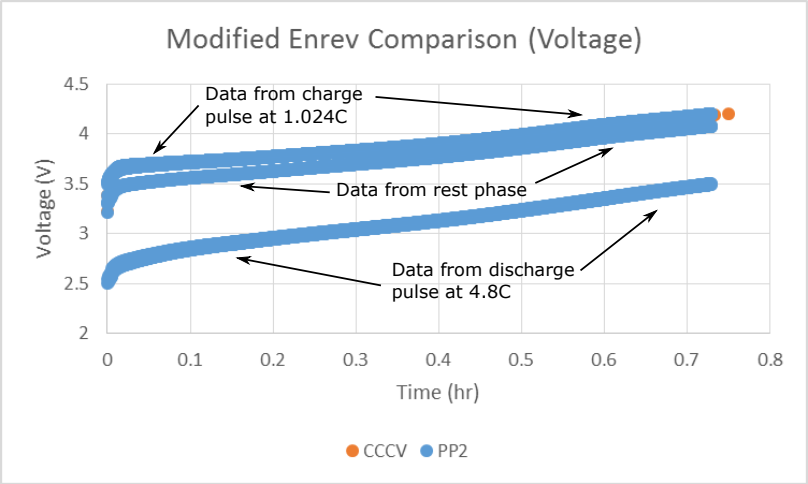

Figure 19: PP2 voltage profile compared against a CCCV voltage profile.

From the temperature profile, the main takeaway is again that the pulse profile had a detrimental effect causing a higher temperature increase than what was experienced during CCCV charging. This is attributed to the higher I^2 value causing additional heating.

From these tests it is clear that PP2 was ineffective at producing a faster or more efficient charge than what was experienced during CCCV, and to a small extent was

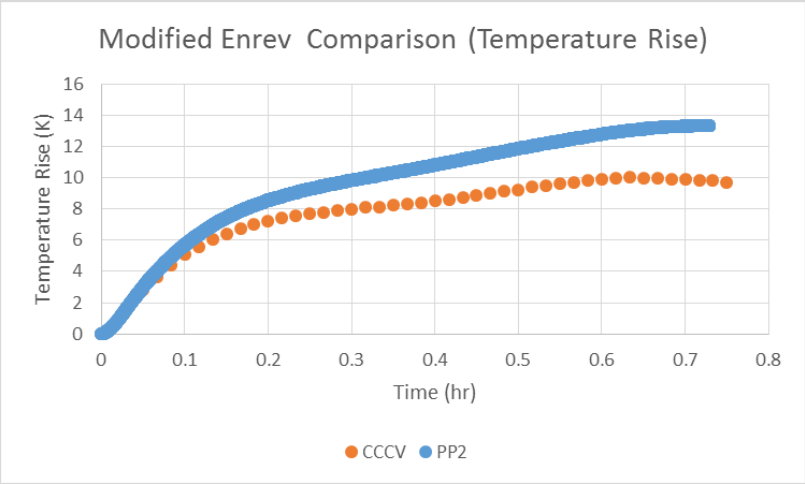

Figure 20: PP2 temperature profile compared against a CCCV temperature profile.

detrimental, most likely a result of the higher current required to maintain a mean 1C current.

7.3.2 Short Pulses: Pulse Profiles 3 and 6.

From PP2 alterations were made to analyze other factors suspected of influencing pulsing, PP3 and PP6 were designed to test the effect of shorter, more frequent pulses which were proposed to be more effective than longer pulses. The parameters are shown in Table 5 and Table 6. The voltage and temperature profiles for these are shown in Fig. 21 and Fig. 22.

Table 5: Parameters for Pulse Profiles 3 and 6 (PP3 and PP6)

Pulse Profile	PP3	PP6
I_{charge}	1.02C	1.2C
t_{charge}	600 ms	60 ms
$I_{discharge}$	1C	1C
$t_{discharge}$	3 ms	3 ms
t_{rest}	6 ms	6 ms

These plots largely produce the same results as what is seen from PP2. Notably, PP6 is a worse plan than PP3 both in terms of charge capacity in the CC phase and

Table 6: Targeted Parameters for Pulse Profile 3 and 6 (PP3 and PP6)

Pulse Profile	PP3	PP6
f	1.642 [Hz]	14.4 [Hz]
I^2	11.56 [A^2]	14.54 [A^2]
$C_{discharge}$	10.05 [Ams]	10.05 [Ams]
R	0.005	0.042

maximum temperature rise. This is suspected to be mainly a result of the higher current, 1.2 C against 1.02 C, and higher I^2 value, 14.54 A^2 against 11.56 A^2.

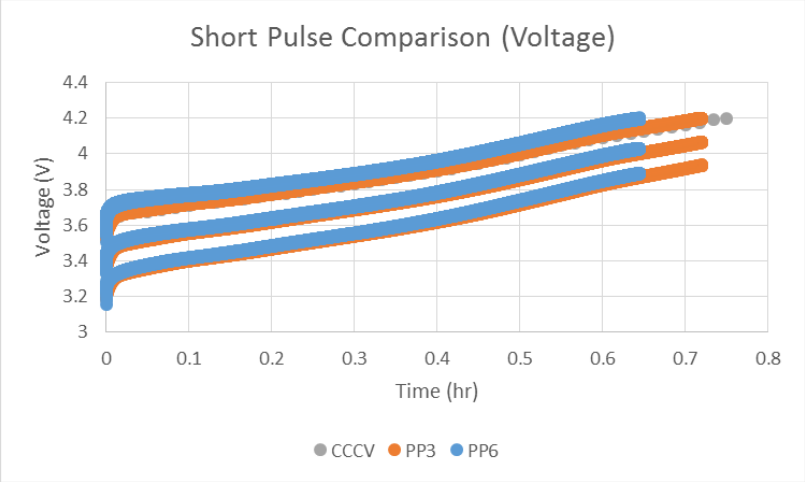

Figure 21: PP3 and PP6 voltage profiles compared against a CCCV voltage profile.

From this data, the temperature profile of PP3 is actually slightly lower than the CCCV data, however the difference is less than a degree Celsius and within the experimental error range as temperature will be dependent on the cell and testing environment.

These plots suggest increasing the frequency of pulsing does not produce an improved charge when compared to CCCV and, again, results seem most affected by I_{charge} and I^2. PP3 had a similar temperature rise to the CCCV method because the I^2 values were comparable, with the value for CCCV being 11.22 A^2

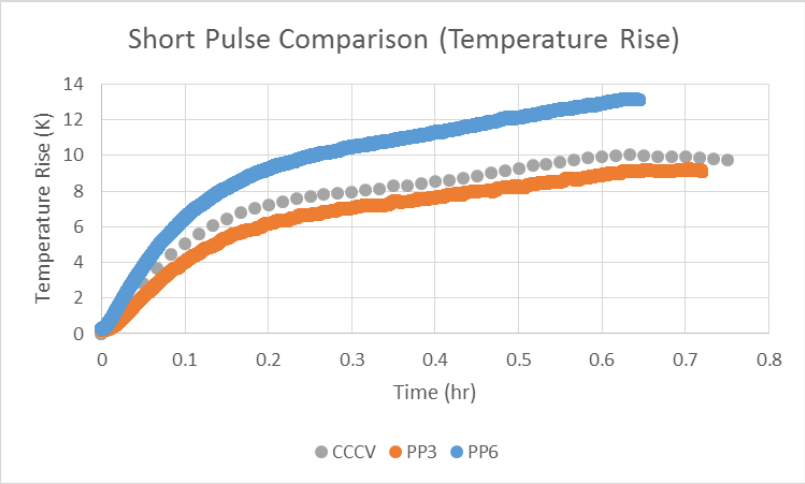

Figure 22: PP3 and PP6 temperature profiles compared against a CCCV temperature profile.

7.3.3 Intermediate Pulses: Pulse Profiles 9 and 17.

Since past literature has suggested a high frequency is preferred, but also that too fast of a pulse may miss any impact on concentration, a few different time scales were established for the discharge pulse and rest times. Two profiles were considered for the intermediate range of pulse length, in which the combined rest and discharge times are about an order of magnitude greater than for the short pulse plans. The parameters are shown in Table 7 and Table 8. One additional change for PP17 is no discharge pulse was included, resulting in a much longer rest period.

Table 7: Parameters for Pulse Profiles 9 and 17 (PP9 and PP17)

Pulse Profile	PP9	PP17
I_{charge}	1.07C	1.1C
t_{charge}	1000 ms	1000 ms
$I_{discharge}$	4C	0
$t_{discharge}$	10 ms	0
t_{rest}	20 ms	100 ms

One curious point of this data is that the capacity of PP9 was less than PP17, even though PP17 had a higher current, which based on previous data was unexpected.

Table 8: Targeted Parameters for Pulse Profile 9 and 17 (PP9 and PP17)

Pulse Profile	PP9	PP17
f	0.97 [Hz]	0.91 [Hz]
I^2	14.22 $[A^2]$	12.34 $[A^2]$
$C_{discharge}$	134 [Ams]	0
R	0.037	0

However, this is a cell dependent result. The cell which was used to test the profile for PP9 was also used for PP11 and PP16, all of which produced lower than expected capacity, including a CCCV test run on the cell. The percentage of capacity PP9 was able to achieve when compared to the CCCV test conducted on the same cell was 97.3 percent, compared with 96.8 percent for PP17. Otherwise, as with other results the pulsing was detrimental to charge capacity and resulted in a slight temperature increase when compared to CCCV, as can be seen in Fig. 23 and Fig. 24. In PP17, removing the discharge pulse from the test plan did not seem to result in a noticeable improvement or detriment to temperature or charge capacity.

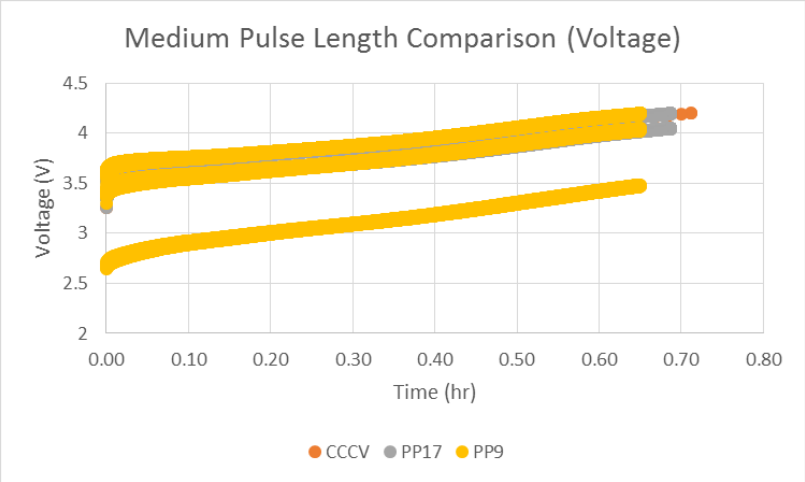

Figure 23: PP9 and PP17 voltage profiles compared against a CCCV voltage profile.

7.3.4 Long Pulses: Pulse Profiles 7 and 8.

Two profiles were also used to assess the effect of extending the pulses. These pulses increased the discharge pulse duration to 20 ms and had much longer charge periods

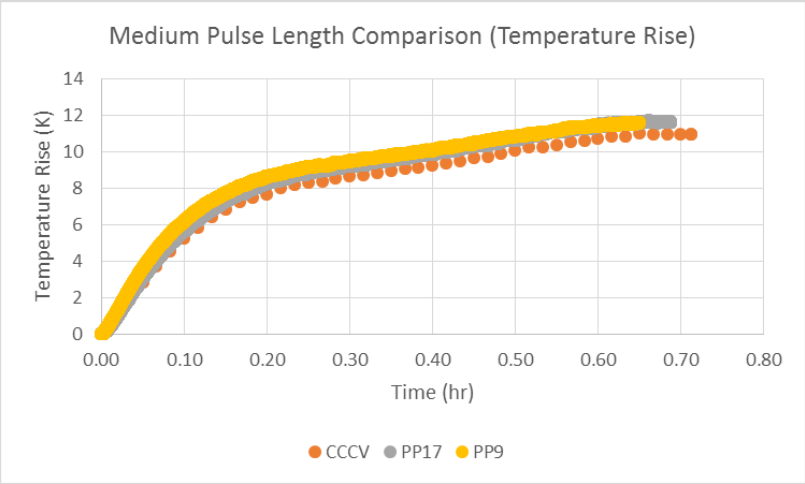

Figure 24: PP9 and PP17 temperature profiles compared against a CCCV temperature profile.

to lower the I^2 value. The parameters for these plans are shown in Table 9 and Table 10.

Table 9: Parameters for Pulse Profiles 7 and 8 (PP7 and PP8)

Pulse Profile	PP7	PP8
I_{charge}	1.02C	1.03C
t_{charge}	4000 ms	2000 ms
$I_{discharge}$	1C	1C
$t_{discharge}$	20 ms	20 ms
t_{rest}	40 ms	20 ms

The results of these plans are shown in Fig. 25 and Fig. 26. These results were still unable to produce any positive results, however, they were also much less detrimental than any of the other pulse profiles. This is however, also likely a result of lower I_{charge} and I^2 values.

7.3.5 High Discharge Capacity Ratio: Pulse Profiles 10, 14, and 15.

Three plans were also made to analyze the effect of discharge capacity. To do this the ratio of discharge to charge capacity for these profiles was increased. It is desirable to keep this value low to avoid unnecessary discharge, however the capacity required

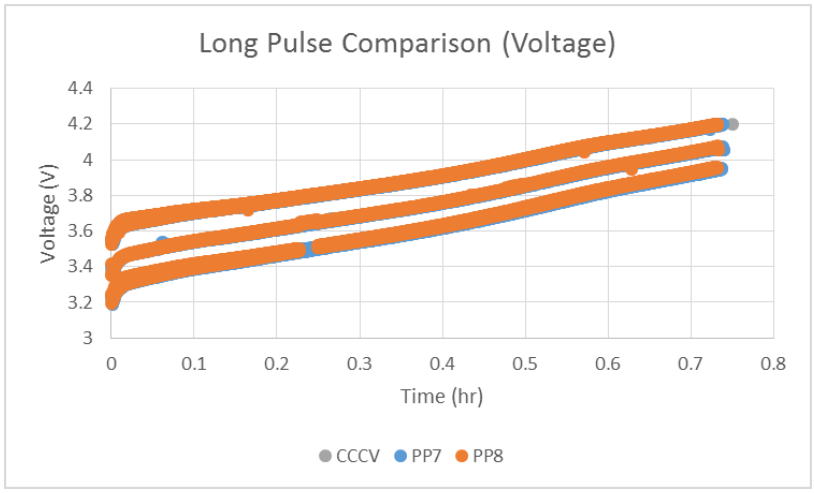

Figure 25: PP7 and PP8 voltage profiles compared against a CCCV voltage profile.

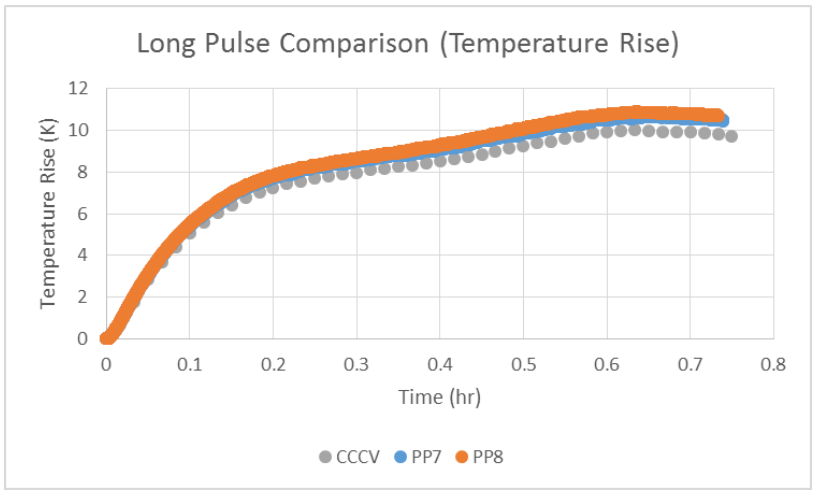

Figure 26: PP7 and PP8 temperature profiles compared against a CCCV temperature profile.

Table 10: Targeted Parameters for Pulse Profile 7 and 8 (PP7 and PP8)

Pulse Profile	PP7	PP8
f	0.246 [Hz]	0.49 [Hz]
I^2	11.56 [A^2]	11.78 [A^2]
$C_{discharge}$	67 [Ams]	67 [Ams]
R	0.005	0.010

to effect the concentration gradient is unknown. To increase the ratio, the discharge current was increased so the frequency of the pulses would remain high, however, as a result the I^2 value was also increased. The parameters for these plans are shown in Table 11 and Table 12.

Table 11: Parameters for Pulse Profile 10, 14, and 15 (PP10, PP14, PP15)

Pulse Profile	PP10	PP14	PP15
I_{charge}	1.15 C	1.625 C	1.6 C
t_{charge}	400 ms	400 ms	100 ms
$I_{discharge}$	4C	4C	4C
$t_{discharge}$	10 ms	10 ms	10 ms
t_{rest}	10 ms	200 ms	10 ms

Table 12: Targeted Parameters for Pulse Profile 10, 14, and 15 (PP10, PP14, PP15)

Pulse Profile	PP10	PP14	PP15
f	2.38 [Hz]	1.64 [Hz]	8.33 [Hz]
I^2	18.4 [A^2]	22.4 [A^2]	38.9 [A^2]
$C_{discharge}$	134 [Ams]	134 [Ams]	134 [Ams]
R	0.087	0.062	0.25

These plans are again evidence that the I^2 and I_{charge} values are the most critical factors. The I^2 values for these plans are the largest in the testing range conducted here and also produce the highest temperatures. Additionally, the charge capacities were very low, with PP14 producing the worst capacity and having the highest I_{charge} value followed closely by PP15.

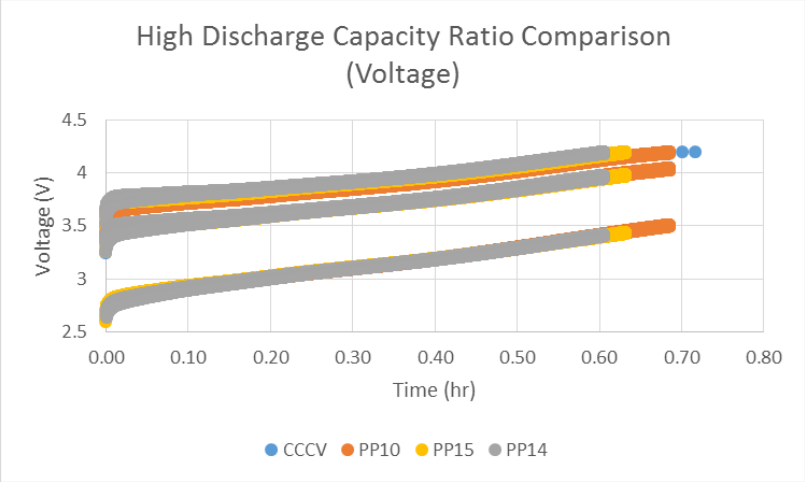

Figure 27: PP10, PP14 and PP15 voltage profile compared against a CCCV voltage profile.

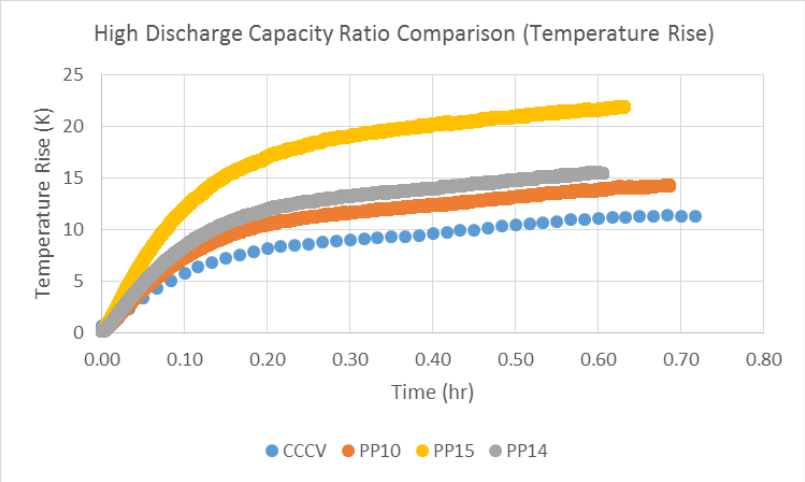

Figure 28: PP10, PP14 and PP15 temperature profile compared against a CCCV temperature profile.

Overall, increasing the discharge capacity ratio was not effective at producing a superior charge. The especially high currents dominated the effects, particular for the temperature which resulted in the highest recorded values of any plan.

7.3.6 Long Discharge Pulse: Pulse Profiles 11, 16.

Similarly to the previous profiles, the following plans were designed with the objective of analyzing the effectiveness the discharge capacity. However, in this case, the pulses were allowed to occur for much longer in order to keep the charge current at a lower value. The parameters are shown in Table 13 and Table 14.

Table 13: Parameters for Pulse Profile 11, 16 (PP11, PP16)

Pulse Profile	PP11	PP16
I_{charge}	1.06 C	1.017 C
t_{charge}	60,000 ms	30,000 ms
$I_{discharge}$	1C	1C
$t_{discharge}$	500 ms	250 ms
t_{rest}	26,000 ms	20 ms

Table 14: Targeted Parameters for Pulse Profile 11, and 16 (PP11, PP16)

Pulse Profile	PP11	PP16
f	0.0158 [Hz]	0.033 [Hz]
I^2	12.08 $[A^2]$	11.604 $[A^2]$
$C_{discharge}$	1675 [Ams]	837.5 [Ams]
R	0.0079	0.0082

These two profiles produce very similar results to CCCV, particularly PP16 which only has an I_{charge} value of 1.017C. There is also very little difference in the temperature profiles due to the small I^2 values, as seen in Fig. 30. However, again neither was able to successfully increase the capacity during the CC phase. As mentioned when discussing PP9, these capacities were lower than other capacities, however, as can be seen from Fig. 29 the CCCV capacity for this cell was also lower, reflecting the lower capacity of the cell.

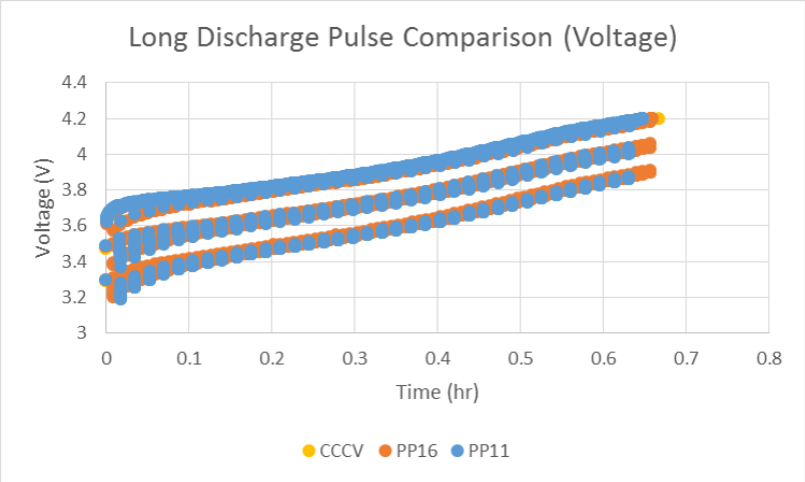

Figure 29: PP11 and PP16 voltage profile compared against a CCCV voltage profile.

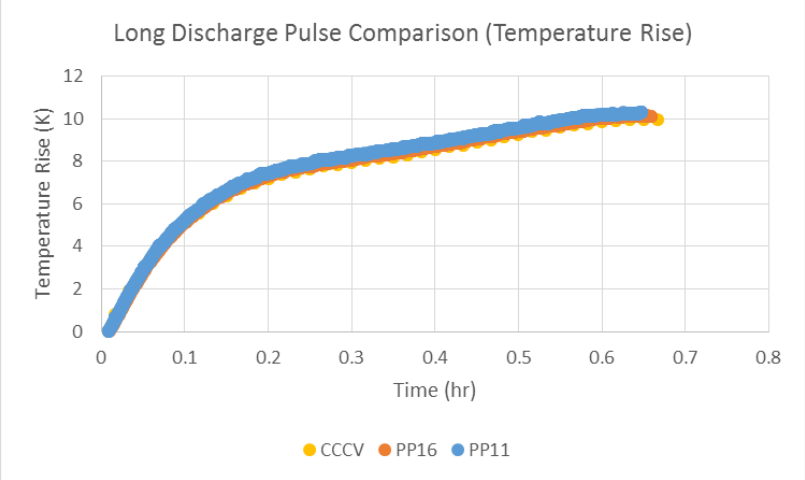

Figure 30: PP11 and PP16 temperature profile compared against a CCCV temperature profile.

7.3.7 High Frequency Pulse: Pulse Profile 4.

PP 4 was designed to analyze the effect of a very high frequency, as one potential reason proposed for the effectiveness of pulsing was from minimizing cell impedance through charging at an optimal frequency. The paper which proposed this found the optimal frequency to be nearly 1000 Hz, while the highest achievable frequency from the BasyTec system was 167 Hz. The parameters for this test are shown in Table 15 and Table 16.

Table 15: Parameters for Pulse Profile 4 (PP4)

Pulse Profile	PP4
I_{charge}	2 C
t_{charge}	3 ms
$I_{discharge}$	0
$t_{discharge}$	0
t_{rest}	3 ms

Table 16: Targeted Parameters for Pulse Profile 4 (PP4)

Pulse Profile	PP4
f	167 [Hz]
I^2	22.45 $[A^2]$
$C_{discharge}$	0
R	0

This plan produced interesting results, while unable to effectively charge the cell to a higher capacity, in fact being quite detrimental in capacity, the temperature was much lower than the I^2 value would suggest. The I^2 value is 22.45 A^2 and the temperature rise was only around 12 °C compared to 16 °C and 15 °C for the temperature rise of PP14 and PP10 which had I^2 values of 22.4 A^2 and 18.4 A^2 respectively, suggesting there was a positive effect from the high frequency on the temperature rise. This is shown in Fig. 31 and Fig. 32.

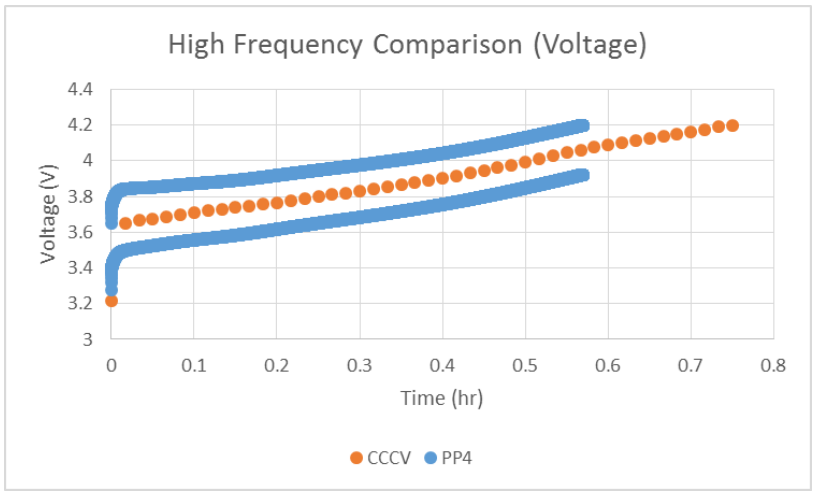

Figure 31: PP4 voltage profile compared against a CCCV voltage profile.

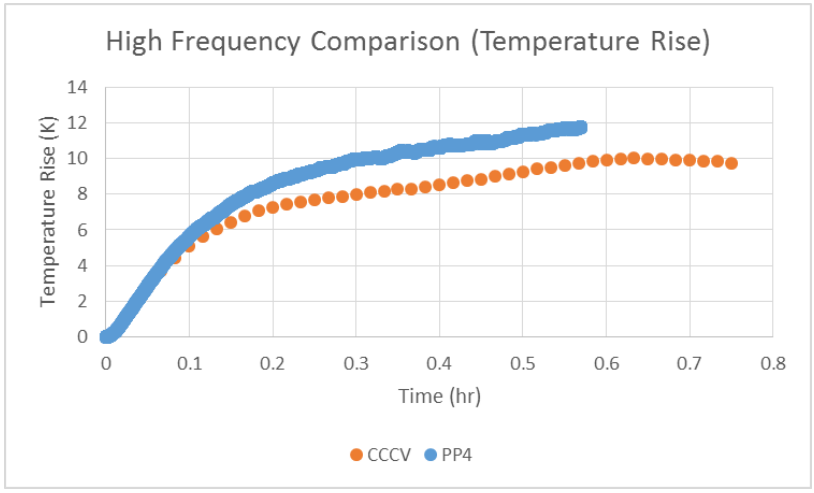

Figure 32: PP4 temperature profile compared against a CCCV temperature profile.

7.3.8 Summary of Single Pulse Tests

From the single pulse experiments no profile was found to effectively extend the CC charging phase to achieve a higher CC capacity. Many different tests were conducted to analyze the different factors which were proposed to effect pulse charging, however I^2 and I_{charge} were found to be the most dominate effects. This is expanded upon in Fig. 33 which shows a near linear increase between I^2 and temperature due to the increase in Ohmic heating. One test point which violates this is the very high frequency PP4. There is also some scatter in the lower values, however this is mainly attributed to the small differences in the environmental conditions and individual effects of the cell.

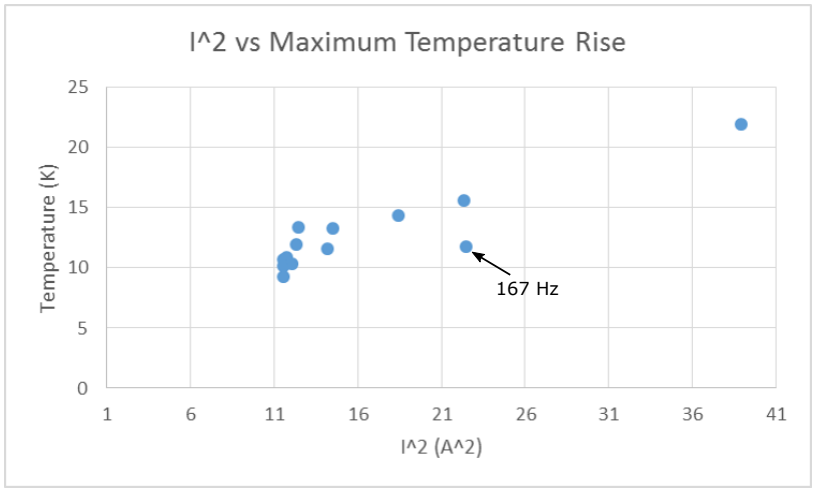

Figure 33: Effect of I^2 on temperature. The one notable standout point is from the 167 Hz PP4.

The effect of I_{charge} on capacity is shown in Fig. 34. As the peak current increases the capacity charged during the CC phase decreases linearly, which is attributed to the increase in Ohmic potential causing the 4.2 V cutoff limit to be reached early.

7.4 Lifetime Testing

In addition to the single charge testing, lifetime tests were conducted. The objective of these tests were to see if any of the proposed aging benefits from pulse charging

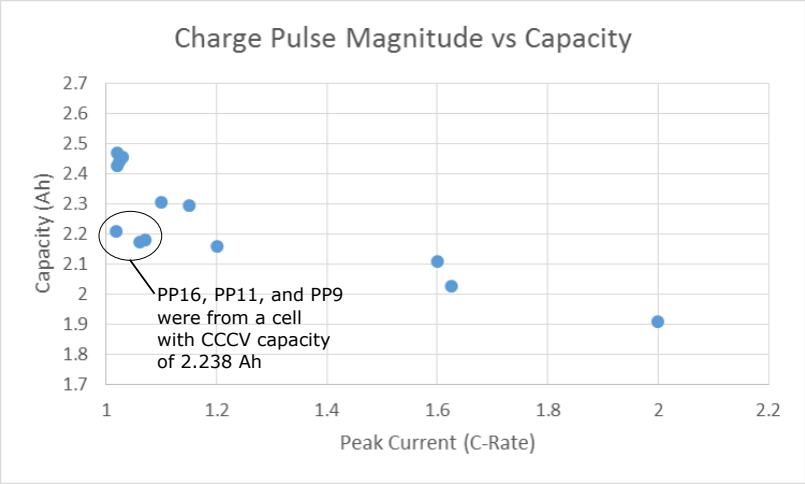

Figure 34: Effect of I_{charge} on capacity. There are three unexpectedly low capacity points which belong to PP9, PP11, and PP16, which were tested on a cell which had lower capacity.

could be realized. The lifetime tests were conducted through continuously cycling the cells between 2.5 V and 4.2 V until the initial capacity, which was about 2.87 Ah after 1 hour of charging, had dropped to 2.3 Ah (80 percent the initial value). This cutoff point was selected because it is known that beyond 80 percent, the cell will begin losing capacity at a very fast rate, which is even evident before the 80 percent value. During cycling, the cell will be charged at a mean 1C rate, then sits for one half hour to allow the cell to cool and equilibrate before being discharged. The discharge occurs at a C/3.33 rate (1 A) and then rests for one half hour again before the next charging takes place. It is important that the discharge value remain the same for all testing, as this is also a known source of aging.

To prepare the cells and check that each reacts similarly to charging; before testing each cell is cycled multiple times at a C/3.33 rate. From this, the capacity is checked to ensure it is near the nominal value claimed and the temperature rise is compared between cells. Additionally, this cycling ensures the SEI layer, which develops in the very early stages of cycling, has been fully formed before testing takes place. The

aging rate at C/3.33 is minimal, so these early cycles are not counted as part of the cycle life. After this the pulsed cycling begins charging at a mean 1C current continuously, until 30 full charges and discharges have been completed at which point cycling is stopped and a C/3 charge and discharge takes place to estimate the new cell capacity, and make an estimate of the internal resistance of the cell. After this, cycling will begin again for 30 cycles, continuing until the 80 percent cutoff limit is reached.

PP2 and PP7 were selected based off the results of the single pulse tests. The effect of cycling on capacity and maximum charge temperature is shown in Fig. 35 and Fig. 36. These figures show the results of lifetime testing which was conducted by using two cells for each pulse method plan and CCCV charging.

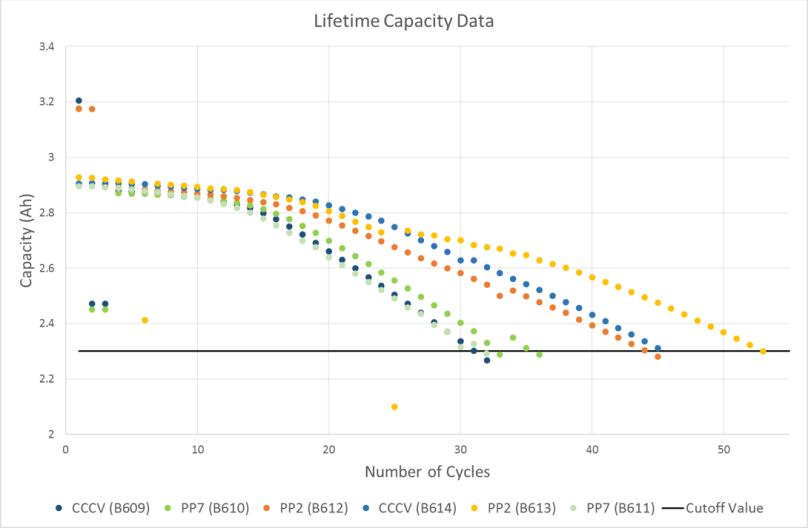

Figure 35: Effect of cycling on capacity.

From this it can be seen that there does not appear to be any substantial difference in aging, either detrimentally or positively. Due to the spread in results it is difficult to make definitive statements, the average life of PP2 is higher than with CCCV but not substantial enough to make a claim of its effectiveness. Due to the limited number of cells and channel availability only 6 cells total were able to be tested, which makes

it difficult to determine reasonable average values. From the graph, pulse method PP7 had both cells end after slightly over 30 cycles, producing the worst lifetime. The two cells cycled under CCCV method had one cell end at slightly over 30 cycles, similar to the PP7 cells, but the other cell lasted about 45 cycles, about were the PP2 ended. Cell B613 had the longest life, lasting about 53 cycles, but cell B612 also using PP2 only lasted about 44 cycles. An important note about cell B613, the capacity fade profile appeared to be on track to end about the same time as cell B612, but it produced an unusually small capacity which caused the cycling to stop. This was determined to be a machine error, as the CV phase of charging was skipped in one cycle, producing a false capacity measurement and triggering the 80 percent capacity termination condition. Before being able to restart the cell, it had sat for a few days. In restarting the lifetime test, the cell first underwent three C/3.33 charge cycles to estimate the cell resistance and ensure an expected voltage profile and capacity would be produced and check that it was not a cell issue that caused the unusual termination. It is unclear exactly why this changed the aging routine, particularly as in doing so there did not appear to be any recovery in capacity, however it is possible the C/3.33 charging allowed for greater use of the active material, and in producing a greater charge and discharge capacity than the 1C, 1 hour tests could, released some lithium which had become inactive. However, if this were the case, a larger increase in capacity on proceeding 1C pulsing tests would have been expected.

The temperature plots do not make a clear statement either. Again, the PP2 cells average a lower maximum charging temperature, about 2 °C lower than the average for CCCV, however cell B614, charged under CCCV method, produced a much higher temperature rise than what was generally seen during the single charge testing and makes the CCCV average temperature higher than expected. As expected, PP7 had a lower maximum temperature rise than PP2 which was also seen in the single charge

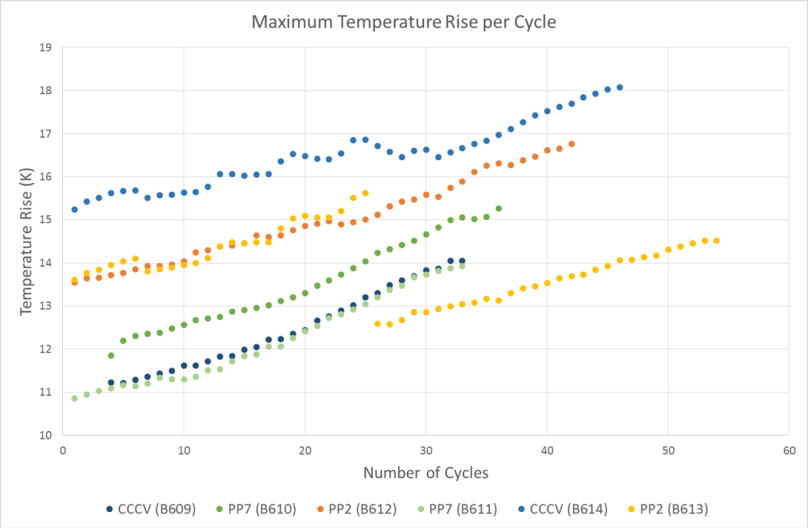

Figure 36: Effect of cycling on maximum charging temperature.

tests previously. B613 also produced a strange alteration in the temperature measurement after it was restarted. This may have been the case that the thermoresistor had partially separated from the surface. It is unlikely this resulted from the C/3.33 cycling, because even if this recovered some lithium, the highly aged cell should still have prodcued a higher temperature than the temperature rise recorded by the fresh cell.

In addition to the temperature and capacity measurements, estimates of the resistance were made by two short discharge pulses of different current on a fully charged cell at 0 cycles, 30 cycles, and at the end of life. This was used to estimate the causes of cell aging. This estimate was made by applying short discharge pulses to a fully charged cell, in this case a 0.5 A pulse for 10 seconds and a 2.0 A pulse for 3 seconds, and dividing the measured voltage drop by the current. The two calculated resistances were then averaged to make the corresponging DC resistance estimate. These values are shown in Table 17.

Since there was considerable scatter in the capacity results of the previous tests, a second batch of cells was purchased from another distributer, to ensure all cells were

Table 17: The cells resistance was estimated at 0 cycles, 30 cycles, and in the case of B613 and B614, the final cycle. Internal resistance increased with cycling, as expected.

Cell	0 Cycles	30 Cycles	Last Cycle
B609	0.052 Ω	0.066 Ω	N/A
B610	0.051 Ω	0.064 Ω	N/A
B611	0.049 Ω	0.061 Ω	N/A
B612	0.051 Ω	0.059 Ω	N/A
B613	0.050 Ω	0.063 Ω	0.093 Ω
B614	0.047 Ω	0.058 Ω	0.087 Ω

from the same production lot. This data is shown in Fig. 37 and Fig. 38. The results were much more consistent than with the previous lifetime tests, with the exception of cell S3_C14, all of the cells lasted between 25 and 35 cycles. From this, it is more clear that very little distinction can be made between the PP2 and CCCV charging. It appears that PP2 was not able to charge the cells to as high a capacity as CCCV, which would agree with the single charge test results. In this data, PP7 was replaced with a type of charging profile called Boost, in which the charge pulse amplitude starts high, but decreases as testing continues. This method is explained in greater detail later in the chapter. From these results, the Boost profile is shown to have produced the highest charge capacity and maintained this high charge capacity for a longer time, while then also experiencing a much faster capacity fade once significant fade began. This method had some conflicting results however, while the cell S3_C5 showed the improved results just mentioned, cell S3_C14 began capacity fade almost immediately. Both cells charged with Boost reached a higher capacity. Unfortunately, due to time and limited tool availability, these tests were unable to be further analyzed or rerun for confirmation.

The temperature results from this test were not as consistent as the capacity data, cells S3_C1 and S3_C7 produced unusually low results. Part of this may have been a result of the temperature chamber, due to a lack of space these two cells were tested in

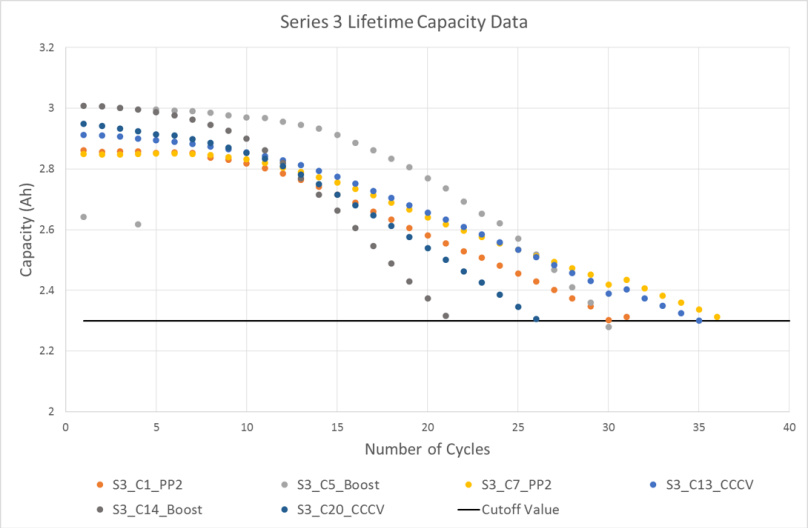

Figure 37: Effect of cycling on capacity from the second set of cells used in lifetime testing.

a different chamber which tended to be about 1 to 2 °C higher than the environment the other cells were run in. As expected, the Boost charged cells experienced the highest average temperature rise, however this occurred at low SoC when the current was very high, as oppossed to the other pulse methods and CCCV charging when the highest temperature occurs at the end of charge. The Boost charged cells experienced especially high temperature rises during the period of increased capacity fading near the end of life. For the final cycles of S3_C5, the temperature rise was reaching above 20 °C, which would correspond to an actual temperature of over 40 °C. At this temperature aging is expected to be enhanced, which could explain the much faster capacity fade that is experienced by the cell. Cell S3_C14 did not experience the same temperature rises, being on the same level as cells S3_C13 and S3_C20 which were charged with CCCV technique. The two cells charged with the CCCV method had temperature rises of around 10 to 12 °C which was the expected value and that increased by about 4 °C during the course of aging which was similar to the results seen in the previous lifetime test.

Additionally, the resistance measurements were made with the second set of tested

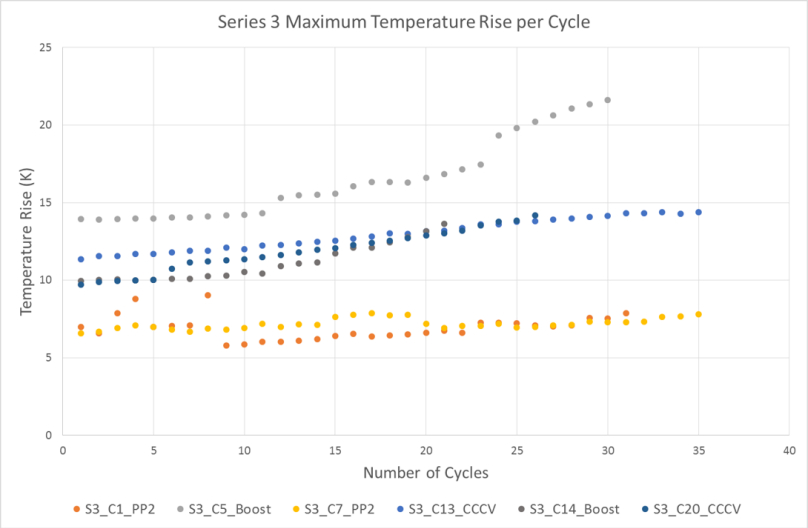

Figure 38: Effect of cycling on maximum charging temperature from the second set of cells used in lifetime testing.

cells, shown in Table 18. Similar results were produced as with the previous test, the initial DC resistance was nearly doubled between the initial estimate and the estimate made when the cell was at 80 percent capacity. The resistance at 30 cycles was slightly higher for these cells, however this is not surprising as 30 cycles was generally the end of life in this second set of cycling while the previous set of cells tended to last longer.

Table 18: The resistance of the cells from the second batch of lifetime measurements was estimated at 0 cycles, 30 cycles, and the end of life. As expected, internal resistance increased with cycling.

Cell	0 Cycles	30 Cycles	Last Cycle
S3_C1	0.051 Ω	0.074 Ω	0.076 Ω (32 cycles)
S3_C5	0.044 Ω	0.064 Ω	0.064 Ω (30 cycles)
S3_C7	0.048 Ω	0.071 Ω	0.077 Ω (38 cycles)
S3_C13	0.049 Ω	0.072 Ω	0.076 Ω (36 cycles)
S3_C14	0.048 Ω	N/A	0.068 Ω (21 cycles)
S3_C20	0.048 Ω	N/A	0.072 Ω (27 cycles)

7.5 Mathematical Modeling Analysis

The effectiveness of the math model was limited in analyzing pulse charging. One of the key issues in using the model was the time to solve, running a simulation of a single charge would take a few days, when the same test could be completed in a few hours testing a particular charge plan on a cell. However, it was still used to analyze the internal dynamics that were occurring during testing. Similarly to the experimental results, no benefit was realized through pulsing. To analyze the internal operation of the cell, the liquid phase concentration distribution and liquid phase voltage across the three domains of the 1D geometry were plotted at various times to assess if the pulsing had any benefit on the gradients, as seen in Fig. 39 and Fig. 40. Additionally, the solid phase potential in the electrode domains of the 1D geometry were plotted, as seen in Fig. 41 and Fig. 42, for the negative and positive electrode respectively. This was also done for the concentration profiles in the 2D electrode domains, as seen in Fig. 43a to Fig. 43d. In all of these figures, very little difference is noticed between the two charging methods. Focusing particularly on the ion concentration, for the liquid phase graph the two distributions line up exactly on each other. The solid phase concentration is more difficult to directly compare due to the graphing method, however again no significant improvement is noticed.

In addition to the evaluation methods mentioned above, concentration data was collected at specific points on the surface of the electrode to analyze how this value changed with time. Here the affects of pulsing are more evident, shown in Fig 44. This figure is a zoomed in view towards the end of charging, to make the pulsing effects visible. At the negative electrode, the pulsing has the opposite of the intended effect, developing a slightly greater concentration gradient over the length of the electrode, which expands over time. This is not directly evident from Fig 44, here it can be seen that the concentration is higher, with a similar view at 33.3 μm the concentration is

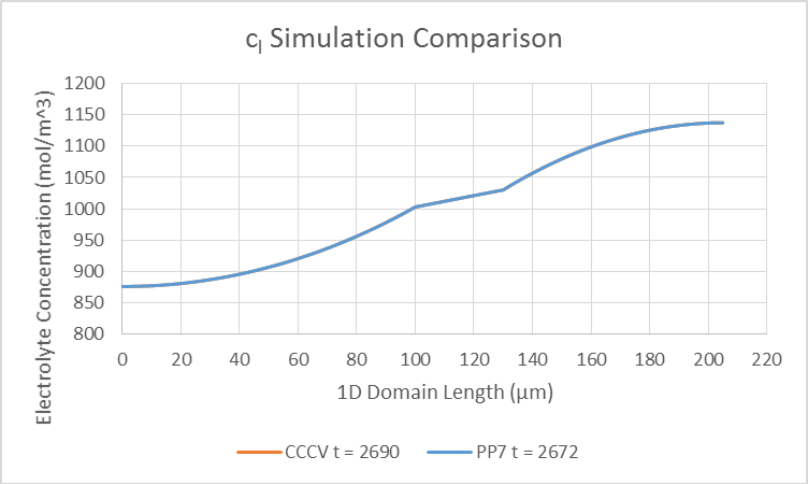

Figure 39: End of charge concentration distribution in the electrolyte, produced by the simulation of a CCCV and PP7 charge.

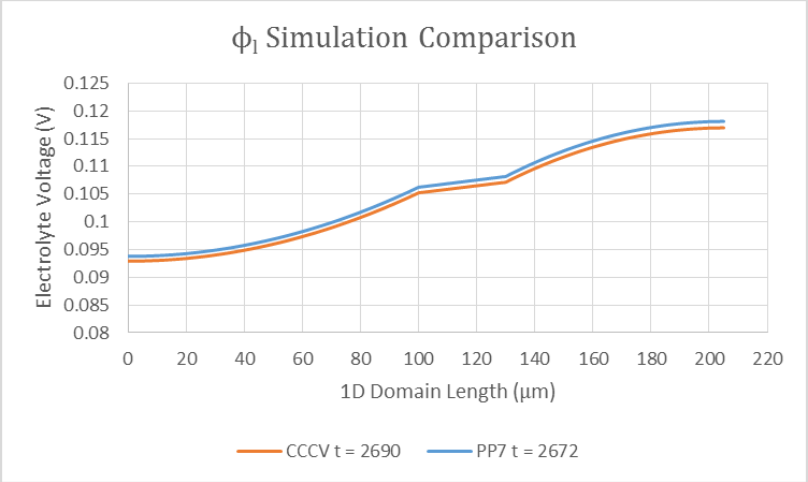

Figure 40: End of charge potential distribution in the electrolyte, produced by the simulation of a CCCV and PP7 charge.

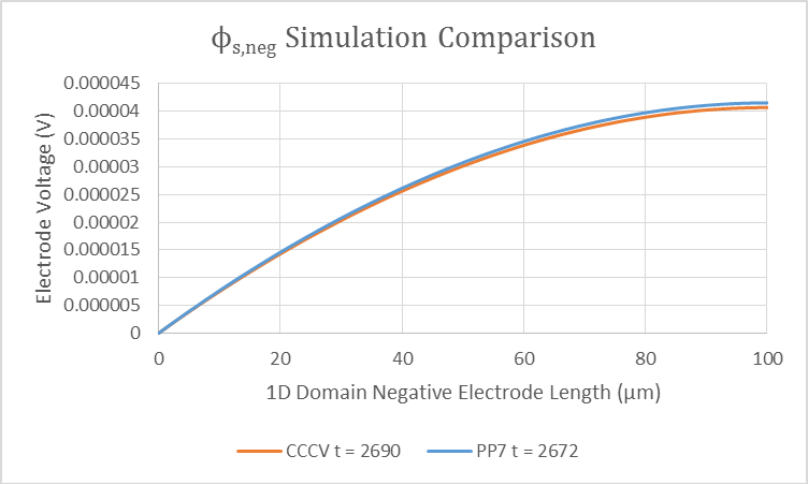

Figure 41: End of charge solid phase potential distribution for the negative electrode, produced by the simulation of a CCCV and PP7 charge.

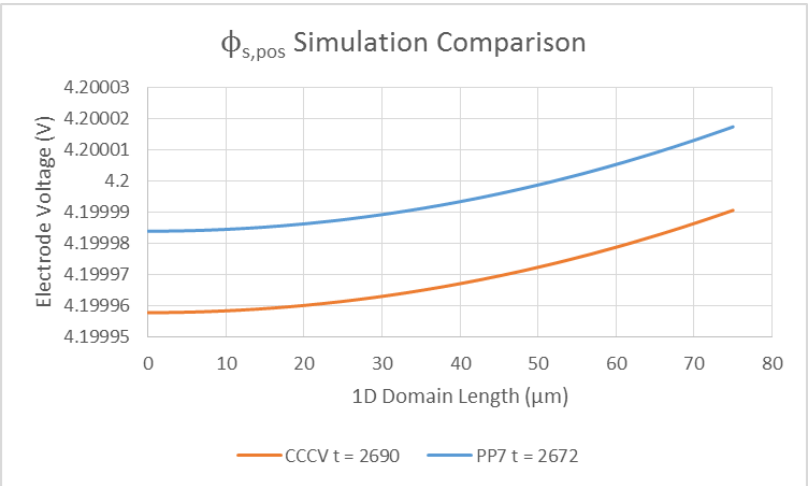

Figure 42: End of charge solid phase potential distribution for the positive electrode, produced by the simulation of a CCCV and PP7 charge.

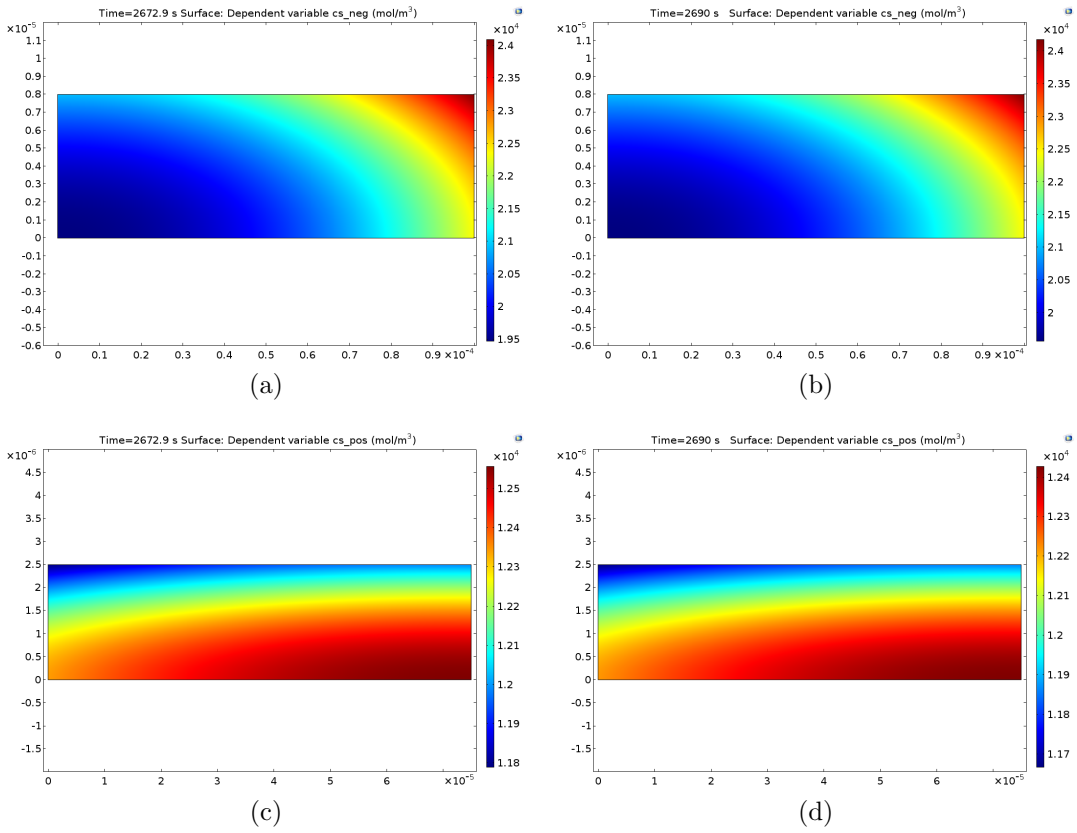

Figure 43: End of charge concentration distribution in the electrode for a) PP7 simulation of the negative electrode b) CCCV simulation of the negative electrode c) PP7 simulation of the positive electrode d) CCCV simulation of the positive electrode.

lower.

The principle take away from these figures is that, while the pulsing does impact the concentration and produces a measurable effects on the internal dynamics, no improvement is realized when these pulses are averaged over time. As was seen in the experimental testing, the higher applied current density causes a slightly higher potential, causing the cell to reach the 4.2 V cutoff prematurely.

7.6 Boost Charging

7.6.1 Introduction to Boost Charging

An alternative technique of pulse charging was also attempted after no positive results were found with the initial style of constant amplitude and constant pulse

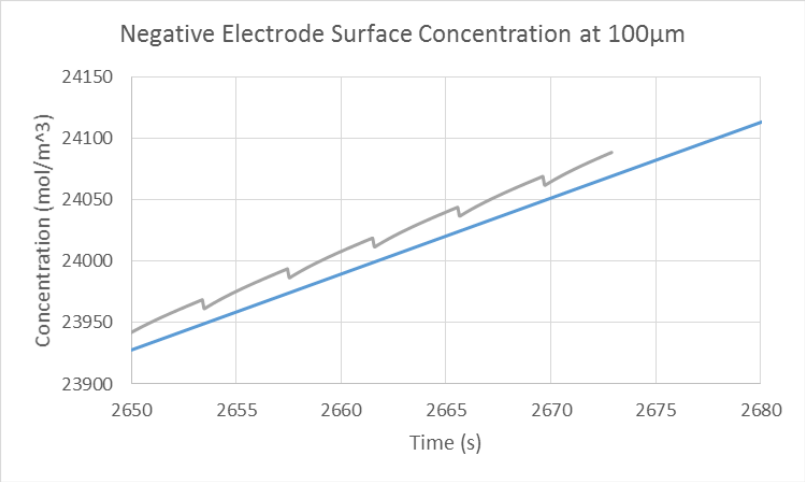

Figure 44: Concentration of lithium at the negative electrode surface near the electrode/separator interface.

duration was attempted. This technique was found effective through modeling by Purushothaman et al and also suggested by Notten et al, although in the latter case without pulse [37] [31]. The Notten paper used the term "Boost Charging" to describe this process, which will continue to be used here. In this technique, a constant duration pulse is applied, while the charge current continuously drops as testing proceeds. In all boost charging methods done here, the pulse only consists of a charge and rest phase. The logic of this type of charging is two-fold, first it has been proposed that a high current in the early stages is not going to impact the cell significantly in terms of aging, and as a result the first half of charging can be conducted at a much faster rate. The second idea, proposed by Purushothaman is that this technique will result in a near saturation level ion concentration at the particle surface which will improve diffusion into the negative electrode, considered the rate limiting process, and the concentration overpotential will be lowered during the rest periods. At low SoC, few ions are in the negative electrode particles, so the high concentration of ions that will build up on the surface of the particles due to high current can be mitigated by the very high concentration gradient which drives diffusion. Then, as the particles fill and the concentration gradient lowers, the current building up the concentration of

ions at the surface will lower with it.

A few different pulse profiles using the boost charging technique were applied here, the results shown in Fig. 45 and Fig. 46, with the boost charging parameters given Table 19.

Table 19: Parameters for boost charging methods. PP13 consisted of two sections listed as phase 1 and phase 2. All methods consisted of a pulsing cycle made up of charge and rest phases only.

Plan (Runtime)	I_{init}	δI	I_{on}	I_{off}
PP13 Phase 1 (1080 s)	6.6598 A	-0.0154 A every 10 s	9 s	1 s
PP13 Phase 2 (Till 4.2 V)	5.4404 A	-0.0209 A every 10 s	9 s	1 s
PP18 (Till 4.2 V)	5.134 A	-0.3935 A every 361 s	360 s	1 s
Boost Method (Till 4.2 V)	5.6474	-0.5 A every 363 s	9 s	1 s

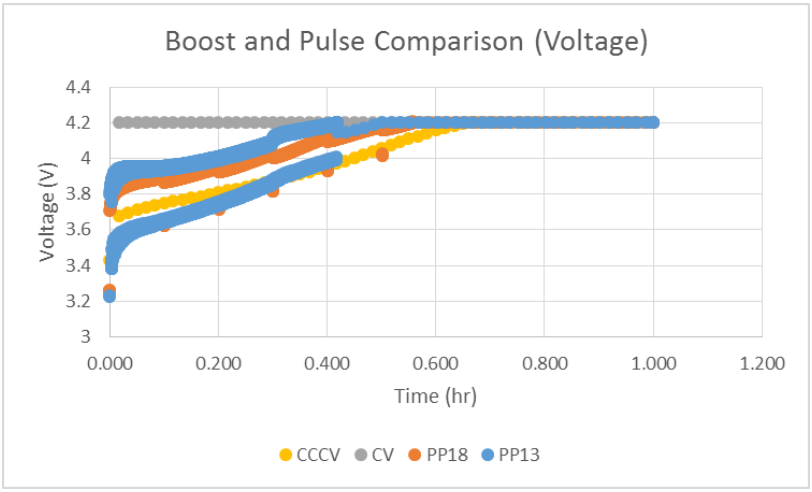

Figure 45: Voltage profiles of cells experiencing boost charging compared to CCCV.

Boost charging is similar to a pure CV charge method, also tested here, in which the cell is held at the upper voltage limit and the current continuously drops. The concerns with this is that very high currents are produced and potentially excessive temperatures, which during the CV charge in Fig.46 can be seen rising 30 °C. Boost charging differs from CV by limiting the upper current and lowering the current in a preplanned manner, in an attempt to mitigate the concerns of CV charging. It can be

seen that with PP13 and PP18 the temperature at the beginning of charge does not end up much higher than what is experienced during CCCV charging, particularly for PP18.

One challenge with this type of charging was maintaining the 1C mean current value, which requires the profile to end exactly when intended, however for both cases tested here the 4.2 V cutoff was reached before the plan was suppose to terminate, resulting in a mean current above 1C. Including the CV portion of the charge, after an hour the boost charging methods were able to produce a higher capacity, with PP14 resulting in 2.994 Ah, PP18 with 2.93 Ah, and CCCV with 2.8 Ah. The capacity profiles are shown in Fig. 47.

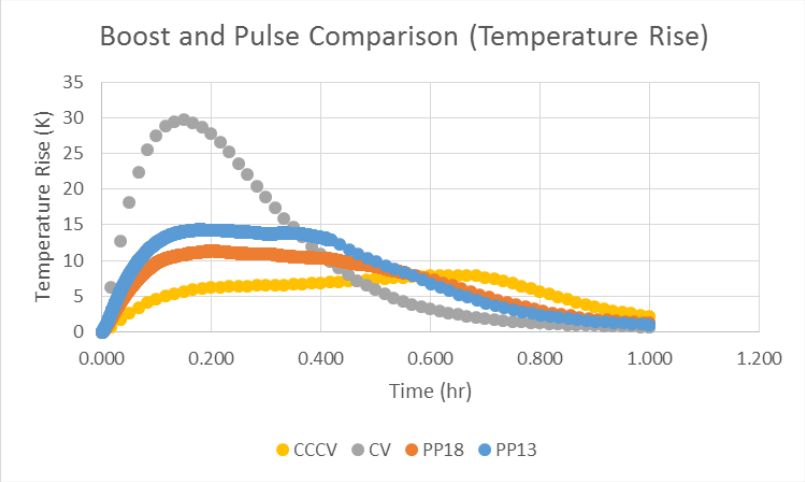

Figure 46: Temperature profiles of cells experiencing boost charging compared to CCCV.

7.6.2 Analysis of the Boost Method in Lifetime Testing

The lifetime testing of the plan entitled "Boost Method" was considered after the standard method of pulsing was shown to be ineffective, so the ability to experiment was limited. As shown in Fig. 37, the Boost method was able to produce a higher capacity in the 1 hour range, without a significant additional loss of capacity, and in the

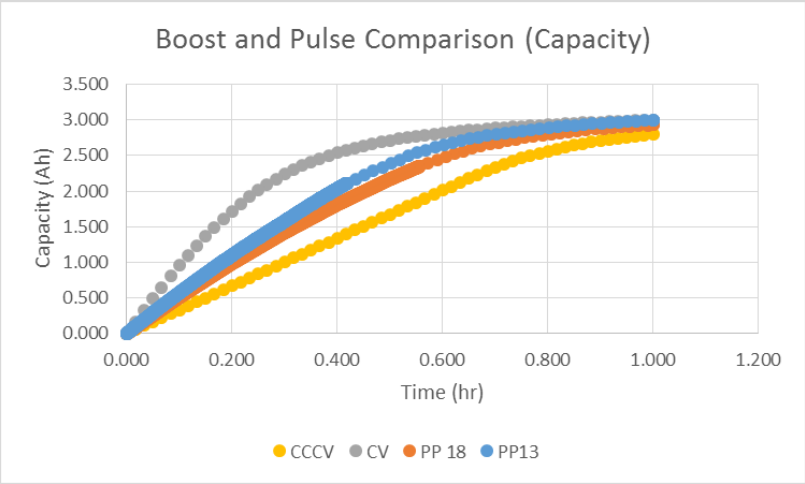

Figure 47: Capacity profiles of cells experiencing boost charging compared to CCCV.

case of one cell actually appear to have a delayed capacity fade, which was eventually overcome by a faster capacity fade, after about 20 cycles. The most promising results are shown in Table 20. Here, it can be seen that both cells charge by Boost were able to achieve about 3.94 percent greater capacity before the CV phase was reached than the average CCCV and about 3.1 percent greater capacity at the 1 hour cutoff. From this, it appears this method of charging is more effective at the fast charge routine and, if the lifetime testing could confirm that this higher capacity is maintained longer with little or no detriment to total cycle life, this would be a very promising form of charging. Unfortunately, due to the time constraints, no postmortem analysis of these cells were able to be conducted. From the past literature review and analysis of Fig. 37, it can be speculated that for cell S3_C5 the SEI layer developed at the same rate as the other methods, since the first region of capacity fade appears fairly similar to other charging methods, but that the deterioration of the positive electrode may have been delayed, since the first region of aging is longer for the Boost cell. The greater rate of capacity loss during the second region of fading could be a result of the slightly higher temperature or that the cell is held at a higher voltage longer, reaching 4 V after only 0.346 hours against 0.517 hours for CCCV charge, as it was suggested high voltage will cause electrode deterioration. However, any speculation

is difficult without further analysis.

Table 20: Capacity from the first cycle of each cell during the lifetime test.

Cell	Charge Method	Capacity at CC cutoff	Capacity at 1 hr
S3_C1	PP2	2.38 Ah	2.86 Ah
S3_C5	Boost	2.64 Ah	2.64 Ah
S3_C7	PP2	2.39 Ah	2.87 Ah
S3_C13	CCCV	2.51 Ah	2.91 Ah
S3_C14	Boost	2.64 Ah	3.01 Ah
S3_C20	CCCV	2.57 Ah	2.94 Ah

The model was also used to analyze the effects of boost charging. This required the simulation to leave the validated current range, as a result the voltage plot was less accurate than for charging at 1C, shown in Fig. 48, ending after 0.67 hours compared with the experimental results of 0.7 hours. The temperature was also less accurate, as shown in Fig. 49. Although the results are less likely to reflect the exact internal kinetics due to the wide current range, some analysis of the simulation data can still be done to analyze the concept of boost charging.

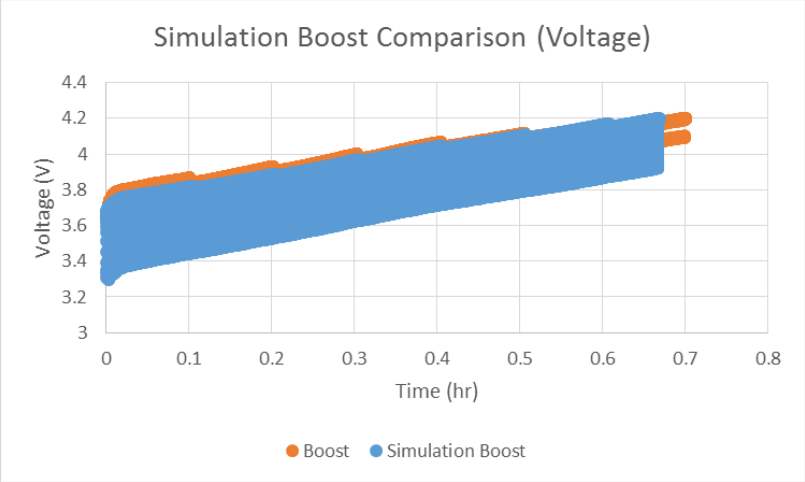

Figure 48: Comparison of simulation voltage data to the experimental data for the Boost charging profile.

Looking at the surface concentration comparisons for the positive and negative electrodes, shown in Fig. 50 and Fig. 51 respectively, the results are as expected.

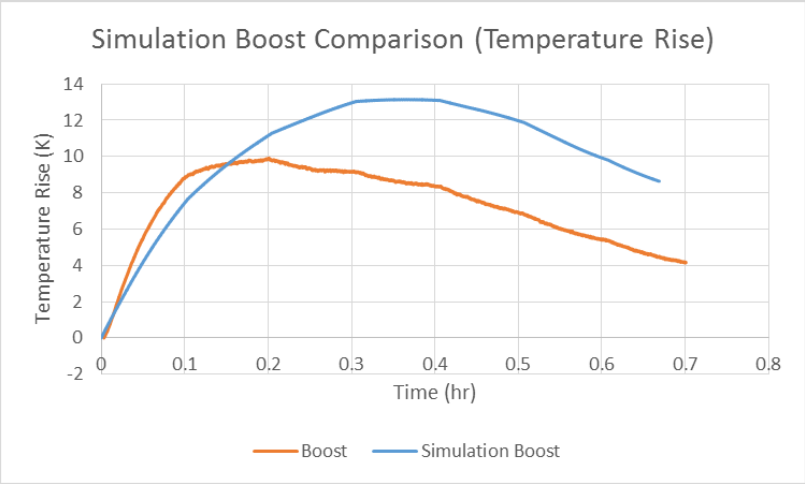

Figure 49: Comparison of simulation temperature data to the experimental data for the Boost charging profile.

The concentration of the positive electrode for the Boost simulation initially falls much faster than the CCCV charge as the current starts higher but this drop begins to plateau at the end of charge when the Boost method is producing a very low current. The same is true for the negative electrode, except that in this case the ions are filling the electrode rather than exiting. The most telling aspect from these graphs is, the negative received more ions and the positive expelled more for Boost charging than for CCCV charging, showing the Boost method charged the cell to a greater capacity before the 4.2 V cutoff, in agreement with experimental results. Another point that can be assessed from the simulation data is analyzing the difference between the concentration difference on the surface of the electrodes. As can be seen in Fig. 52, the difference in concentration at the positive electrode is lower at the end of charge, suggesting the electrode was more uniformly utilized. The negative electrode shows the opposite to be true, as seen in Fig. 53, but this difference appears to have plateaued while it was still increasing for CCCV charging. Since the cell was able to charge longer, this suggests a decrease in overpotential, which could be a result of the more uniform electrode utilization. Since boost charging ends on a lower current, the ohmic overpotential will also be lower at the end of charge.

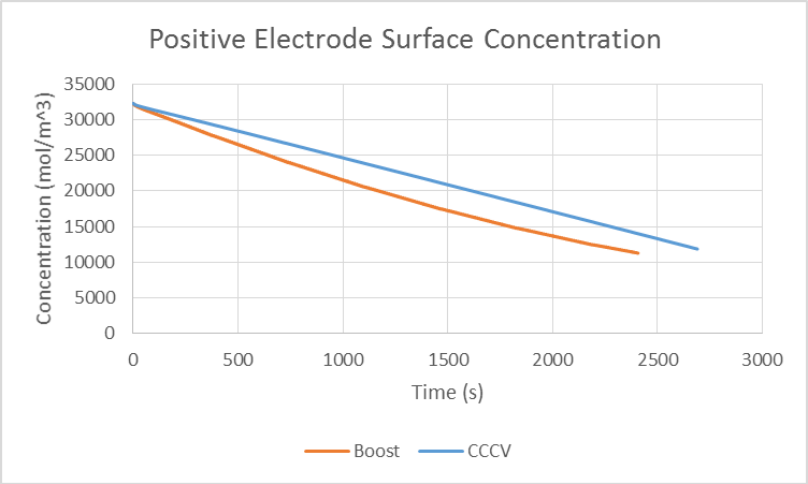

Figure 50: Comparison of the surface concentration at the end of the positive electrode between the Boost simulation and CCCV simulation data.

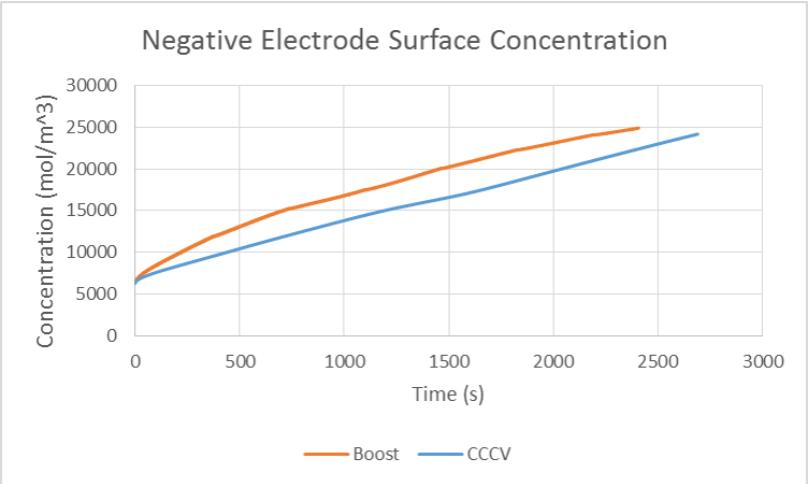

Figure 51: Comparison of the surface concentration at the end of the negative electrode between the Boost simulation and CCCV simulation data.

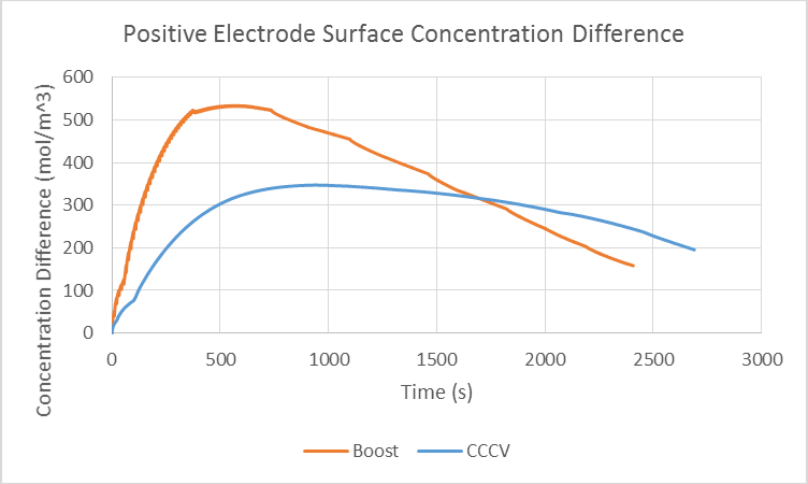

Figure 52: Comparison of the difference in surface concentration between the end of the positive electrode and the positive electrode at the separator boundary, for the Boost simulation and CCCV simulation data.

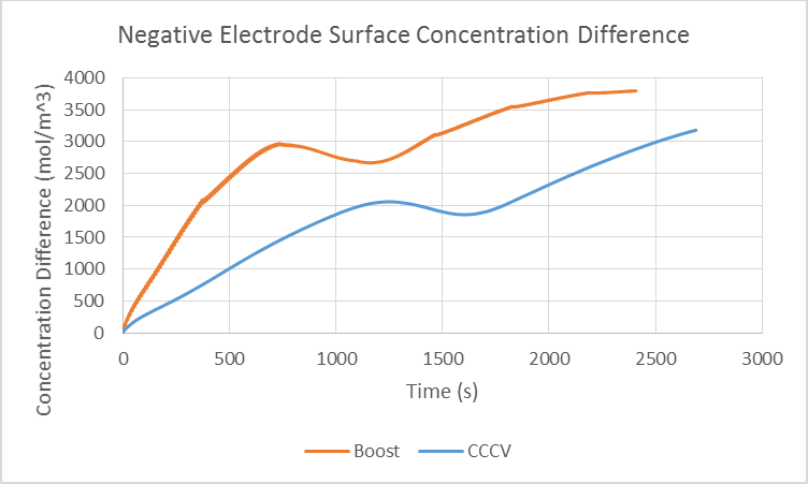

Figure 53: Comparison of the difference in surface concentration between the negative electrode at the separator boundary and the start of the negative electrode, for the Boost simulation and CCCV simulation data.

The 2D representation of the concentration in the electrodes are shown in Fig. 54a and Fig. 54c for the negative and positive electrodes under Boost charge respectively, and Fig. 54b and Fig. 54d for the negative and positive electrodes under CCCV charging respectively. From these it can be seen that the Boost method was better able to fill the negative electrode and extract from the positive electrode. The concentration range for the positive electrode under Boost is 1.11E4 to 1.17E4 $^{mol}/_{m^3}$ compared to 1.17E4 to 1.24E4 $^{mol}/_{m^3}$ for CCCV charging. For the positive electrode, only a small improvement can be seen in the color gradient. The concentration in the negative electrode is 2E4 to 2.5E4 $^{mol}/_{m^3}$ and 1.95E4 to 2.45E4 $^{mol}/_{m^3}$ for Boost and CCCV respectively. For this electrode, the color gradient shows a much greater impact on the distribution, showing the Boost method resulted in a much lower gradient within the radial direction. This also suggests the electrode was more fully utilized. This is thought to be beneficial, as it could lower the stress on the electrode from volume changes, preventing electrode deterioration, and could lower the concentration gradient within the cell, lowering the overpotential.

In addition to the concentration of ions in the solid electrode, the concentration in the electrolyte was analyzed, shown in Fig. 55. At the end of charge this is also a significantly lower gradient in all three domains. The same is true for the potential difference at the end of charge in the solid and liquid phase, shown in Fig. 56 and Fig. 57 respectively. This is largely a result of the lower current, particularly the voltage difference which has a nearly instantaneous response to current change, but is relevant because heat generation is directly dependent on the gradients of potential and concentration. This shows that the heat generation in the cell will be lower at higher SoC for the boost charging method. This could be very important as past literature has suggested that aging is enhanced at high temperature, high voltage, and high SoC. By using this Boost method, the temperature profile is flipped from CCCV charging, being lower at the high voltage and SoC values, as seen in Fig. 46,

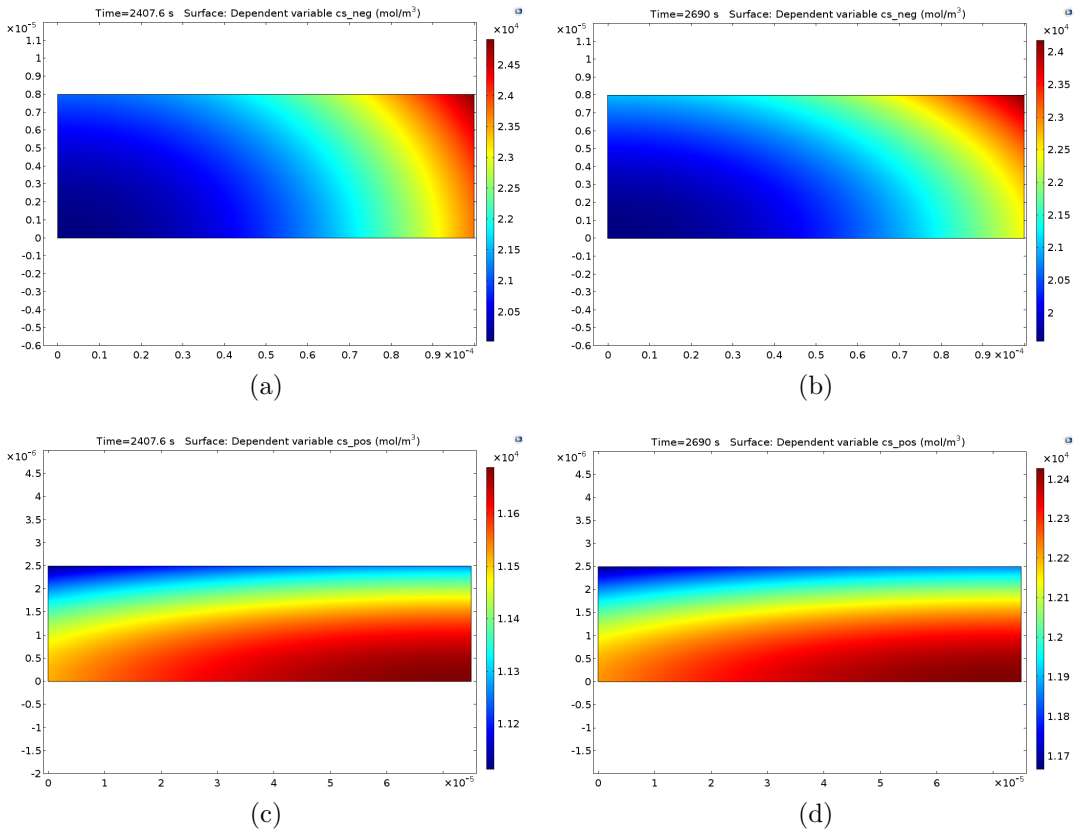

Figure 54: End of charge concentration distribution in the electrode for a) Boost simulation of the negative electrode b) CCCV simulation of the negative electrode c) Boost simulation of the positive electrode d) CCCV simulation of the positive electrode.

which could be beneficial to electrode stability and battery life.

7.6.3 Summary of Boost Charging Tests

Due to time constraints, the model was unable to be improved to better represent the entire current range and only a limited sample of data was able to be collected, and as a result the conclusions that can be made from the results are limited. However, both simulation and experimental results have shown that boost charging is capable of producing a greater capacity during the CC phase of charging. The effects on lifetime are much more difficult to make a definitive conclusion on due to the spread in results. Using the model to analyze the Boost Method showed that at the end of the CC phase, the concentration gradient in both electrodes were less than

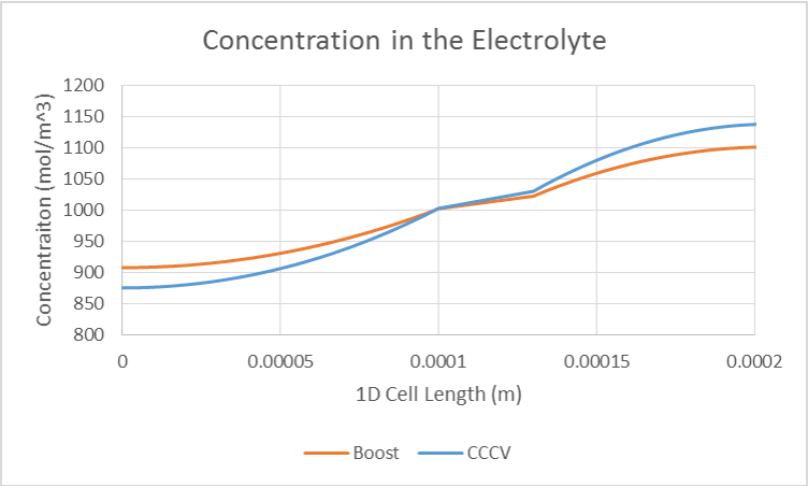

Figure 55: Concentration of lithium ions in the electrolyte liquid phase at the end of charging.

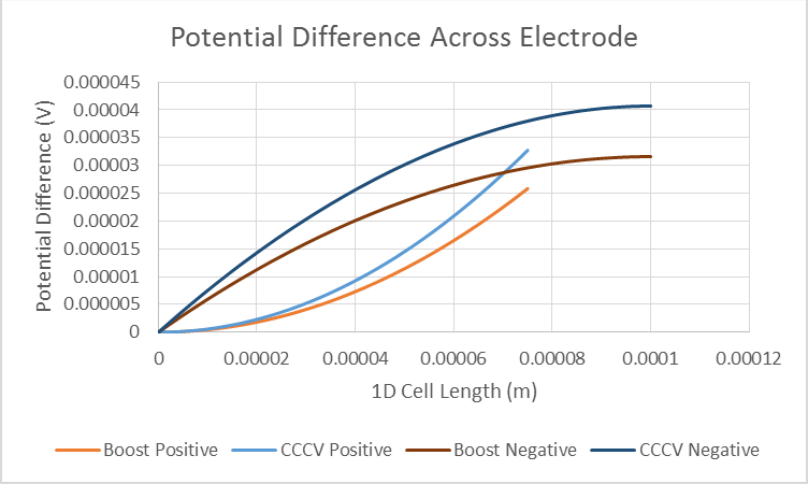

Figure 56: Voltage difference in the electrode solid phase at the end of charging.

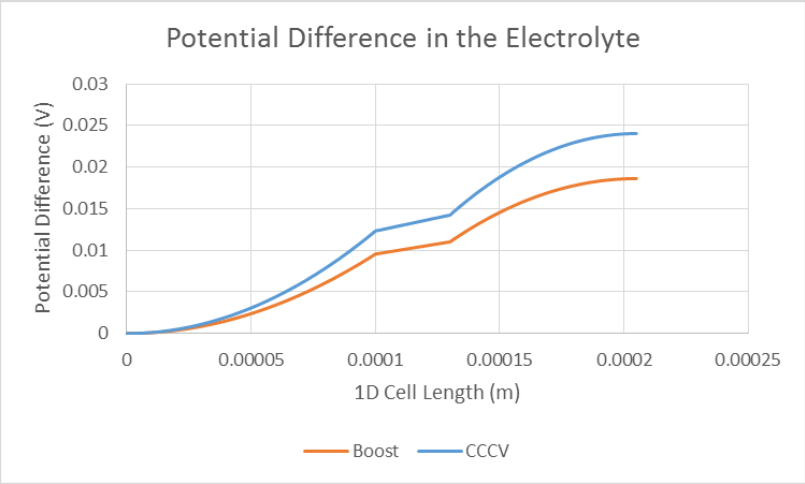

Figure 57: Voltage difference in the electrolyte liquid phase at the end of charging.

when compared to the CCCV method, particularly in the negative electrode, which could be indicative of better aging as well. Moving forward, this method of charging should be considered further. The same parameters which were tested in the pulsing method should be considered for their role on boost charging, as well as whether these results are improved from pulsing, or simply from the decreasing current. Additionally, methods to optimize the rate current decreases with SoC to achieve the highest capacity within the CC phase should be considered. However, different equivalence conditions will need to be developed for comparison to CCCV charging, as producing a 1C mean current with boost charging is very difficult to maintain.

CHAPTER VIII

SUMMARY

8.1 Conclusion

This thesis examined the concept of pulse charging and tested its effectiveness as a method to improve the rate of charge and lifetime of lithium ion cells. A model was developed in order to examine the internal kinetics of the lithium ion cell, determine, in the case of pulsing, what is different from CCCV charging, and develop an optimized pulse plan. A literature review was conducted which analyzed different possibilities for modeling, the sources of aging in lithium ion cells, and the previous research into pulse charging. For modeling, a pseudo-2D electrochemical model was found to have the best combination of computational complexity and ability to fully describe the cell kinetics under pulsing. From the literature review on aging and pulsing, it became apparent that one of the challenges with this type of research is the significant differences that exist between the different types of battery chemistries, even amongst lithium ion cells. The main sources of aging are thought to be destruction of the positive electrode from volume and phase changes, decomposition of the electrode from operating at high voltages, and formation of an SEI layer on the negative electrode. The review of pulse charging papers suggested that these aging mechanisms could be improve through more effective use of the active material and that faster charging could be achieved through lowering the concentration gradient, and as a result the overpotential, extending CC charging.

Numerous pulse plans were tested in single charge experiments which analyzed the parameters determined to be most influential on pulse charging effectiveness. These

were frequency, I^2 value, discharge capacity, and the ratio of charge to discharge. A range of these values were tested, however none was able to more effectively charge the cell than the CCCV method. Upon analyzing this data it became clear that the most influential factors were the I^2 value and total charge current magnitude. When comparing capacity to charge current magnitude, the capacity that was achieved during the CC phase of charging decreased with increasing charge phase current amplitude. None of the other factors which were suggested were able to lower the voltage to mitigate the increased overpotential from the higher current required for pulsing. The I^2 value had a more influential role on heat generation and produced a near linear increase in temperature with increasing I^2. This is attributed to the Ohmic heating, and again, none of the other suggested pulsing benefits were able to offset this increase.

In addition to the single pulse testing, a couple of pulse plans were selected to analyze their effectiveness on cell lifetime. Here the results were less clear, however it appeared unlikely that any benefit was realized, nor did it appear that the pulsing was in anyway detrimental. The total capacity appeared about the same, as any capacity that was lost from the pulse profile exiting the CC phase prematurely was quickly recovered during the CV phase.

Additionally, little positive information was able to be achieved from the modeling of the cells. Achieving a very accurate model was difficult as the exact cell parameters were unknown, however it was still used to analyze the concept, knowing that the results will differ slightly from experimental operation of this particular cell. No improvement in cell operation was realized from simulations. One objective of this thesis was to analyze if any additional concepts needed to be implemented into the model to appropriately reflect pulsed charging operation, but since very little difference was realized between pulsing and CCCV charging, no additional elements

were incorporated into the model. However, with some confidence it can be claimed that after these three types of testing, pulsing with a constant current magnitude and duration does not produce any positive results, which is in agreement with some of the reviewed literature.

8.2 Future Work

A couple of areas were this work could be continued were determined. Analysis of boost charging was also attempted and appeared to have some positive results, however due to limited time these results were unable to be further explored. The boost charging method used here was a slightly altered method of the charging techniques suggested by Purushothaman and Landau [37], in which the charge was pulsed and the amplitude of charge was dropped each cycle, with the intention of charging the cell fully in 0.85 hours. In the boost charging method used here, the objective was to charge to as high a capacity as possible while maintaining the comparitive testing condition of a mean 1C current and 1 hour of charge. This was very difficult to maintain as it would require knowing exactly when the CC phase would reach the voltage limit, which was made more difficult by the fact that in lifetime testing this point would change with age. Higher capacities were achieved within the 1 hour limit and in the case of one of the lifetime cells, this higher capacity appear to have been more stable than the CCCV method in the early stages of lifetime testing, although experiencing greater capacity fade once fading began. The boost charging methods were also seen to have higher CC phase capacity, more indicative of an improve charging method because CC phase testing won't be improved by the slightly higher mean current. Due to limited time, the results that were recorded were unable to be rerun to ensure repeatability, but this would be an area of potential optimization and improvement of parameters in the future. Additionally, this is also an area were the

modeling developed could be effective at aiding in parameter selection and analyzing what is occurring within the cell. The model was used to analyze the Boost method tested here, and showed a lower concentration gradient in the radial direction of negative, and to a lesser extend the positive electrodes. Additionally, it showed lower overpotential at the end of charge, although this was dominated by the lower ending current, and it showed lower temperature at high SoC, all of which are considered to be beneficial to charge rate and aging.

A second area of potential future work would be very high frequency pulsing. Due to equipment limitations, the frequency which was used here was relatively low compared to the value used for optimal charge frequency. No charging benefit was realized at the frequencies used in this thesis, however some data suggested the higher frequency was producing lower than expected temperatures for the I^2 values used, which could suggest that using a device that could reach the optimal frequency may produce greater benefit.

APPENDIX A

APPENDIX

A.1 Model Parameters

Table 21: Input Parameters for Mathematical Model of 3.4 Ah NCA cell

Parameter	Cathode	Separator Electrolyte	Anode
Particle Radius, r_{p} [μm]	2.5[e]		8.0[e]
Electrode Length, L_i [μm]	75[f]	30[f]	100[f]
Init. Electroylte Conc., $c_{\mathrm{l},0}$ $^{\mathrm{mol}}/_{\mathrm{m}^3}$	1000[d]	1000[d]	1000[d]
Electrolyte Diffusion Coefficient, D_e $^{\mathrm{m}^2}/_{\mathrm{s}}$	3x10^{-10}[d]	3x10^{-10}[d]	3x10^{-10}[d]
Transference Number, t_+^0	0.363[d]	0.363[d]	0.363[d]
Charge Transfer Coefficient, $\alpha_{\mathrm{a,c}}$	0.5,0.5[a]		0.5,0.5[c]
Init. Conc. in Solid, c_{s_0} $^{\mathrm{mol}}/_{\mathrm{m}^3}$	32292[e]		6314[e]
Min. Conc. in Solid, $c_{\mathrm{s}_{\mathrm{min}}}$ $^{\mathrm{mol}}/_{\mathrm{m}^3}$	10187[e]		0[e]
Max. Conc. in Solid, $c_{\mathrm{s}_{\mathrm{max}}}$ $^{\mathrm{mol}}/_{\mathrm{m}^3}$	33956[d]		31570[d]
Electrode Diffusion Coefficient, $D_{\mathrm{s},i}$ $^{\mathrm{m}^2}/_{\mathrm{s}}$	1.4x10^{-14}[a]		3.9x10^{-14}[c]
Electrolyte Phase Volume Fraction, ϵ_l	0.3382[a]	0.724[c]	0.357[c]
Filler Volume Fraction, ϵ_f	0.1942[a]		0.172[c]
Solid Phase Volume Fraction, ϵ_s	0.4676[a]	0.276[c]	0.471[c]
Electrode Conductivity, σ $^{\mathrm{S}}/_{\mathrm{m}}$	91[d]		100[c]
Reaction Rate Coefficient, k $^{\mathrm{m}}/_{\mathrm{s}}$	1.25x10^{-12}[e]		1.25x10^{-12}[e]
Heat Capacity, c_p $^{\mathrm{kJ}}/_{\mathrm{kg-K}}$	1150[b]	1978[c]	1437[c]
Thermal Conductivity, λ $^{\mathrm{W}}/_{\mathrm{m*K}}$	1[e]	0.3344[c]	1.04[c]
Density, ρ $^{\mathrm{kg}}/_{\mathrm{m}^3}$	4740[d]	1009[c]	1347[c]
Heat Transfer Coefficient, h $^{\mathrm{W}}/_{\mathrm{m}^2}$	0.45[e]		0.45[e]
Double Layer Capacity, C_{dl} $^{\mathrm{F}}/_{\mathrm{m}^2}$	0.08		0.2
Applied C-Rate	1.14		
Est. Applied Current, 1C i_{1C}, $^{\mathrm{A}}/_{\mathrm{m}^2}$	22.341		

a = Bernadi [6] b = Shadman Rad [42] c = Saw [40] d = Comsol e = Estimate f = Measured

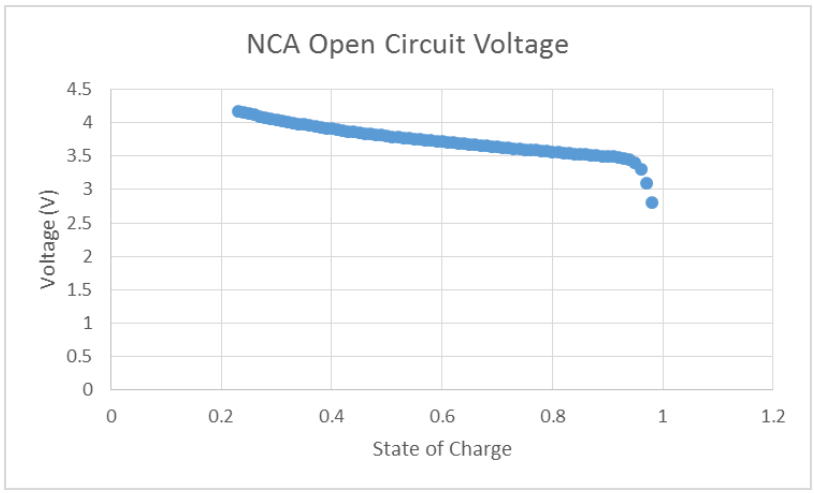

Figure 58: Positive Electrode OCV, take from Comsol materials library for NCA chemistry.

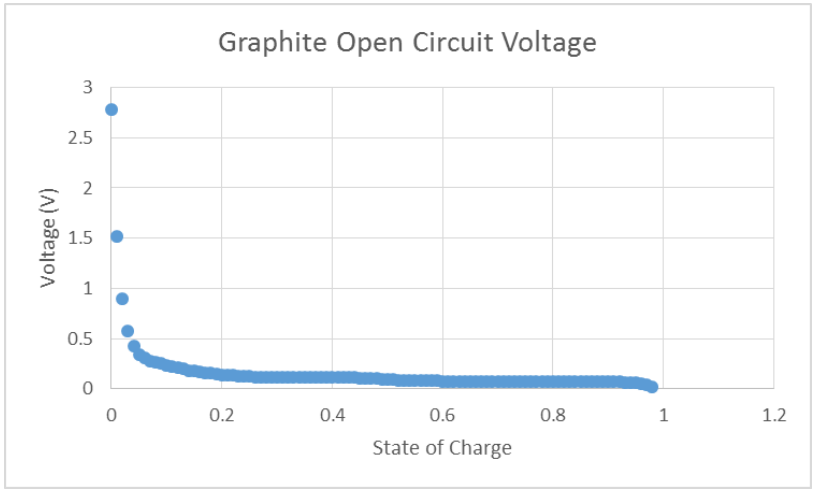

Figure 59: Negative Electrode OCV, take from Comsol materials library for Graphite Li_xC_6 chemistry.

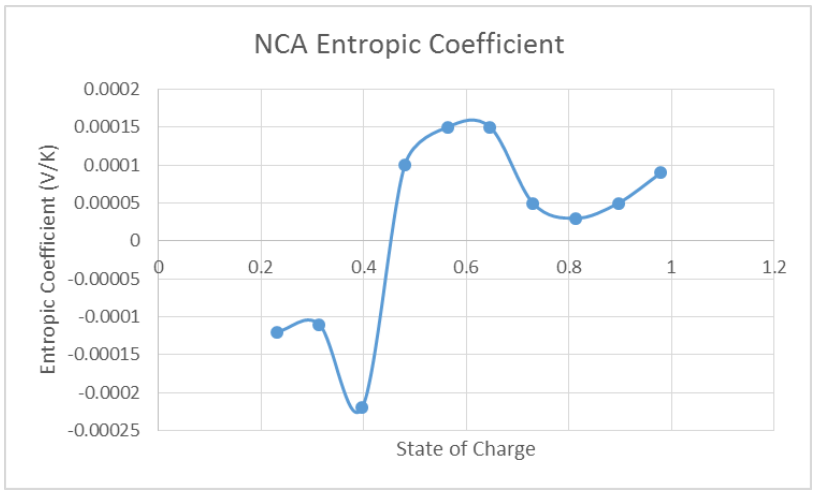

Figure 60: Positive Electrode Entropic Coefficient, take from research by Shadman Rad et al. [42]

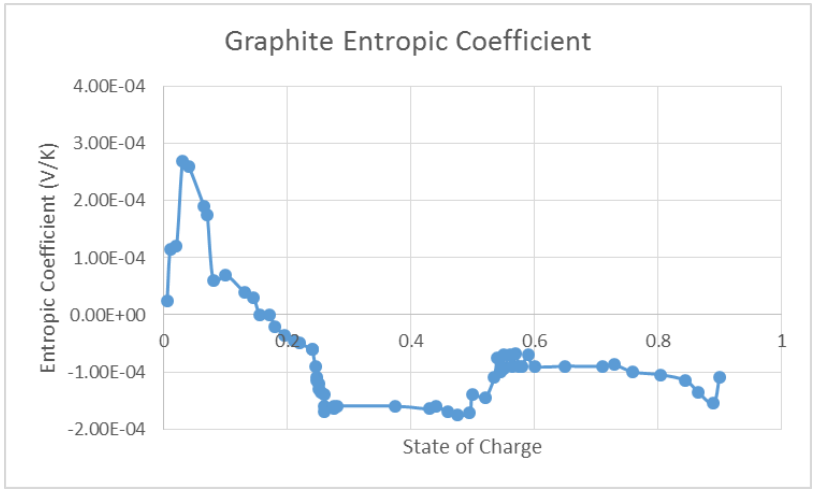

Figure 61: Negative Electrode Entropic Coefficient, take from Comsol materials library for Graphite Li_xC_6 chemistry.

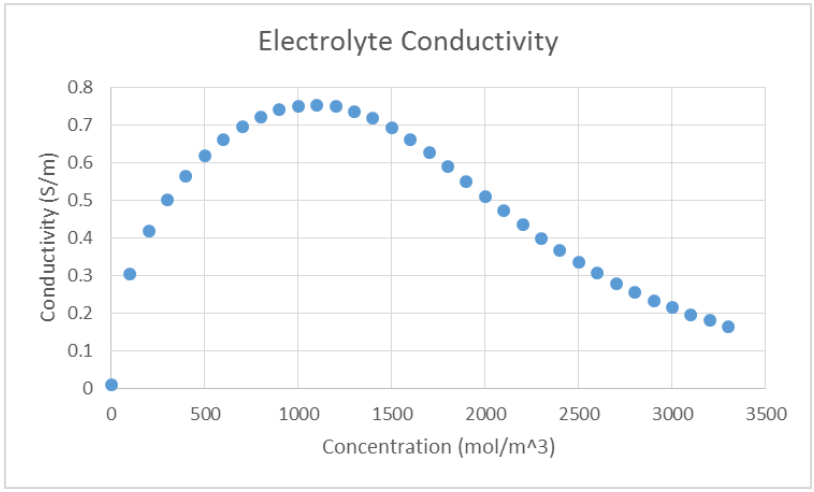

Figure 62: Electrolyte conductivity with dependence on SoC, take from Comsol materials library for $LiPF_6$ electrolyte.

REFERENCES

[1] Anwar, S., Zou, C., and Manzie, C., "Distributed Thermal-Electrochemical Modeling of a Lithium-Ion Battery to Study the Effect of High Charging Rate," *IFAC Proceedings Volumes*, vol. 47, pp. 6258–6263, 2014.

[2] Aryanfar, A., Brooks, D., Merinov, B., Goddard III, W., Colussi, A., and Hoffmann, M., "Dynamics of Lithium Dendrite Growth and Inhibition: Pulse Charging Experiments and Monte Carlo Calculations," *The Journal of Physical Chemistry Letters*, vol. 5, pp. 1721–1726, 2014.

[3] Bagotsky, V., *Fundamentals of Electrochemistry*. John Wiley and Sons, USA, 2006.

[4] Bandhauer, T., Garimella, S., and Fuller, T., "A critical review of thermal issues in lithium-ion batteries," *Journal of the Electrochemical Society*, vol. 158, pp. R1–R25, 2011.

[5] Bernardi, D., Pawlikowski, E., and Newman, J., "A General Energy Balance for Battery Systems," *Journal of the Electrochemical Society*, vol. 132, pp. 5–12, 1985.

[6] Bernardi, D. and Go, J., "Analysis of pulse and relaxation behavior in lithium-ion batteries," *Journal of Power Sources*, vol. 196, pp. 412–427, 2011.

[7] Broussely, M., Biensan, P., Bonhommme, F., Blanchard, P., Herreyre, S., Nechev, K., and Staniewicz, R., "Main aging mechanisms in li ion batteries," *Journal of Power Sources*, vol. 146, pp. 90–96, 2005.

[8] Cai, L. and White, R., "Mathematical modeling of a lithium ion battery with thermal effects in COMSOL Inc. Multiphysics (MP) software," *Journal of Power Sources*, vol. 196, pp. 5985–5989, 2011.

[9] Chen, L., Wu, S., Shieh, D., and Chen, T., "Sinusoidal-Ripple-Current Charging Strategy and Optimal Charging Frequency Study for Li-Ion Batteries," *IEEE Transactions on Industrial Electronics*, vol. 60, pp. 88–97, 2013.

[10] Dai, H., Wei, X., Sun, Z., Wang, J., and Gu, W., "Online cell SOC estimation of Li-ion battery packs using a dual time-scale Kalman filtering for EV applications," *Applied Energy*, vol. 95, pp. 227–237, 2012.

[11] de Jongh, P. and Notten, P., "Effect of current pulses on lithium intercalation batteries," *Solid State Ionics*, vol. 148, pp. 259–268, 2002.

[12] Dokko, K., Horikoshi, S., Itoh, T., Nishizawa, M., Mohamedi, M., and Uchida, I., "Microvoltammetry for cathode materials at elevated temperature: electrochemical stability of single particles," *Battery Conference on Applications and Advances, 2000. The Fifteenth Annual*, vol. 90, pp. 109–115, 2000.

[13] Doyle, C., *Design and simulation of lithium rechargeable batteries*. PhD thesis, University of California at Berkley, 1995.

[14] Doyle, M., Fuller, T., and Newman, J., "Modeling of galvanostatic charge and discharge of the lthium/polymer/insertion cell," *Journal of the Electrochemical Society*, vol. 140, pp. 1526–1533, 1993.

[15] Forgez, C., Do, D., Friedrich, G., Morcrette, M., and C, D., "Thermal modeling of a cylindrical lifepo$_4$/graphite lithium-ion battery," *Journal of Power Sources*, vol. 195, pp. 2961–2968, 2010.

[16] Gu, W. and CY, W., "Thermal-electrochemical modeling of battery systems," *Journal of the Electrochemical Society*, vol. 147, pp. 2910–2922, 2000.

[17] Guo, M., Sikha, G., and White, R., "Single Particle Model for a Lithium-Ion Cell: Thermal Behavior," *Journal of the Electrochemical Society*, vol. 158, pp. A122–A132, 2011.

[18] Hasan, M., Chen, C., Shaffer, C., and Mukherjee, P., "Aalysis of the Implications of Rapid Charging on Lithium-Ion Battery Performance," *Journal of Electrochemical Society*, vol. 162, pp. A1382–A1395, 2015.

[19] Hoon, L. C., "iii. Reaction Kinetics Lecture.13: Butler-Volmer equation." MIT OpenCourseWare, 2014.

[20] Howard, W. and Spotnitz, R., "Theoretical evaluation of high-energy lithium metal phosphate cathode materials in li-ion batteries," *Journal of Power Sources*, vol. 165, pp. 887–891, 2007.

[21] Kuhn, E., Forgez, C., Lagonotte, P., and Friedrich, G., "Modeling Ni-mH battery using Cauer and Foster structures," *Journal of Power Sources*, vol. 158, pp. 1490–1497, 2006.

[22] Li, J., Murphy, E., Winnick, J., and Kohl, P., "Studies on the cycle life of commercial lithium ion batteries during rapid charge-discharge cycling," *Journal of Power Sources*, vol. 102, pp. 294–301, 2001.

[23] Li, J., Murphy, E., Winnick, J., and Kohl, P., "The effects of pulse charging on cycling characteristics of commercial lithium-ion batteries," *Journal of Power Sources*, vol. 102, pp. 302–309, 2001.

[24] Liaw, B., Nagasubramanian, G., Jungst, R., and Doughty, D., "Modeling of lithium ion cells - A simple equivalent-circuit model approach," *Solid State Ionics*, vol. 175, pp. 835–839, 2004.

[25] Linden, D. and Reddy, T., *Handbook of batteries*. McGraw-Hill companies, Inc., 2002.

[26] Linden, D. and Reddy, T., *Linden's Handbook of Batteries*. McGraw-Hill companies, Inc., 2010.

[27] Luo, W., Lyu, C., Wang, L., and Zhang, L., "A new extensino of physics-based single particle model for higher charge-discharge rates," *Journal of Power Science*, vol. 241, pp. 295–310, 2013.

[28] Martinsen, O. and Grimnes, S., *Bioimpedance and Bioelectricity Basics*. Academic Press, USA, 2007.

[29] Narula, A., "Modeling of ageing of lithium-ion battery at low temperatures," Master's thesis, Chalmers University of Technology, 2014.

[30] NISSANUSA.

[31] Notten, P., Op het Veld, J., and van Beek, J., "Boostcharging Li-Ion batteries: A challenging new charging concept," *Journal of Power Sources*, vol. 145, pp. 89–94, 2005.

[32] Ong, I. and Newman, J., "Double-Layer Capacity in a Dual Lithium Ion Insertion Cell," *Journal of the Electrochemical Society*, vol. 146, pp. 4360–4365, 1999.

[33] Panasonic, "Overview of lithium-ion batteries," 2007.

[34] Podrazhansky, Y., Podrazhansky, M., and Golod, M., "US Patent No. 5504415 Method and apparatus for automatic equalization of series-connected batteries," 1996.

[35] Podrazhansky, Y. and Popp, P., "US Patent No. 4829225 Rapid battery charger, discharger and conditioner," 1989.

[36] Popov, B., Durairajan, A., Podrazhansky, R., and Cope, R., "Capacity Fade of Li-ion Cells: Comparison of DC and ENREV Charging Protocals," *Battery Conference on Applications and Advances, 2000. The Fifteenth Annual*, pp. 185–191, 2000.

[37] Purushothaman, B. and Landau, U., "Rapid Charging of Lithium-Ion Batteries Using Pulsed Currents," *Journal of the Electrochemical Society*, vol. 153, pp. A533–A542, 2006.

[38] R, S., "Simulation of capacity fade in lithium-ion batteries," *Journal of Power Sources*, vol. 113, pp. 72–80, 2003.

[39] Savoye, F., Venet, P., Millet, M., and Groot, J., "Impact of Periodic Current Pulses on Li-Ion Battery Performance," *IEEE Transactions on Industrial Electronics*, vol. 59, pp. 3481–3488, 2012.

[40] Saw, L., Yonghuang, Y., and Tay, A., "Electrochemical-thermal analysis of 18650 Lithium Iron Phosphate cell," *Energy Conversion and Management*, vol. 75, pp. 162–174, 2013.

[41] Scrosati, B., Abraham, K., van Schalkwijk, W., and Hassoun, J., *Lithium Batteries: advance technologies and applications*. John Wiley and Sons, Inc., 2013.

[42] Shadman Rad, M., Danilov, D., Baghalha, M., Kazemeini, M., and Notten, P., "Adaptive thermal modeling of li-ion batteries," *Electrochimica Acta*, vol. 102, pp. 183–195, 2013.

[43] Smtih, K. and Wang, P., "Power and thermal characterization of a lithium-ion battery pack for hybrid-electric vehicles," *Journal of Power Sources*, vol. 160, pp. 662–673, 2006.

[44] Vetter, J., Novak, P., Wagner, M., Veit, C., Möller KC, Besenhard, J., Winter, M., Wohlfahrt-Mehrens, M., Volger, C., and Hammouche, A., "Ageing mechanisms in lithium-ion batteries," *Journal of Power Sources*, vol. 147, pp. 269–281, 2005.

[45] Wohlfahrt-Mehrens, M., Vogler, C., and Garche, J., "Aging mechanisms of lithium cathode materials," *Journal of Power Sources*, vol. 127, pp. 58–64, 2004.

[46] Yang, N., Zhang, X., Li, G., and Hua, D., "Assessment of the forces air-cooling performance for cylindrical lithium ion battery packs: A comparative analysis between aligned and staggered cell arrangements," *Applied Thermal Engineering*, vol. 80, pp. 55–65, 2015.